POLY (PROPYLENE FUMARATE) – VINYL PHOSPHONIC ACID BASED DRUG RELEASE SYSTEMS

by
Bahadır Başkaya

Submitted to Graduate School of Natural and Applied Sciences
in Partial Fulfillment of the Requirements
for the Degree of Master of Science in
Chemical Engineering

Yeditepe University
2022

POLY (PROPYLENE FUMARATE) – VINYL PHOSPHONIC ACID BASED DRUG RELEASE SYSTEMS

APPROVED BY:

Assoc. Prof. Dr. Erde Can Şafak ……
(Thesis Supervisor)
(Yeditepe University)

Assist. Prof. Dr. Cem Levent Altan ……
(Yeditepe University)

Prof. Dr. Rana Sanyal ...……
(Boğaziçi University)

DATE OF APPROVAL: ..../..../20..

I hereby declare that this thesis is my own work and that all information in this thesis has been obtained and presented in accordance with academic rules and ethical conduct. I have fully cited and referenced all material and results as required by these rules and conduct, and this thesis study does not contain any plagiarism. If any material used in the thesis requires copyright, the necessary permissions have been obtained. No material from this thesis has been used for the award of another degree.

I accept all kinds of legal liability that may arise in case contrary to these situations.

Name, Last name Bahadır Başkaya

Signature …..…….……..

ACKNOWLEDGMENTS

Firstly, I would like to express my special thanks to my thesis supervisor Assoc. Prof. Dr. Erde Can for both helping and for encouraging me. She was especially helpful about trying to move forward, improving my skills, solving all kinds of problems, and encouraging me to do more. Without her guidance, encouragement, and help, this thesis would not be this delightful.

Furthermore, I gained wonderful friendships along this graduate road, I would like to thank all of them, especially to Çağla Albayrak, Yasin Can Pişiren, Alp Tunga Keskin, Yaşar Kaan Kepekçi.

Also, I would like to give my deepest appreciation to my family for their love and endless support. I will be grateful forever for their support in every decision I make.

ABSTRACT

POLY (PROPYLENE FUMARATE) - VINYL PHOSPHONIC ACID BASED DRUG RELEASE SYSTEMS

Poly (propylene fumarate) (PPF) and vinyl phosphonic acid (VPA) based nanoparticles were developed as drug delivery vehicles within the scope of this study. In addition, studies on folic acid conjugation to PPF and the preparation of PPF-FA and VPA based nanoparticles were also carried out due to folic acid's known specificity against cancer cells. Thus, the first PPF pre-polymer was synthesized polycondensation of fumaric acid and an excess of propylene glycol then PPF was copolymerized with VPA in 70/30 weight ratio via UV mini-emulsion polymerization to produce PPF/VPA nanoparticles. The highest gel content of 87.6 percent and particle formation in the 500 nm to 2000 nm size range were achieved under the optimized reaction conditions using 3 weight percent BAPO initiator, 0.04 weight percent TAA co-catalyst with 9 weight percent SDS surfactant applying 2 hours of UV cure with 10 minutes of homogenization time at 1000 rpm. The completion of the cure reaction was confirmed via DSC analysis. Degradation profiles of the PPF/VPA particles in PBS buffer solution (pH=7.4) showed that 88 to 98 percent of the particles degraded in 84 days depending on the homogenization time, whereas the pH dropped from 7.4 to 2.9 to 3.3 at the end of 89 days. PPF/VPA nanoparticles were also prepared in the presence of the model anti-cancer drug Paclitaxel. Paclitaxel release from the PPF/VPA particles resulted the in the linear and prolonged release which was degradation controlled. PPF-Folic Acid (PPF-FA) conjugate was synthesized via the addition of FA to PPF pre-polymer in the presence of dehydrant: dicyclo hexyl carbodiimide (DCC) and catalyst. 4-dimethyl amino pyridine (DMAP). The PPF-FA pre-polymer was characterized via FT-IR and ^{1}H-NMR spectroscopy. UV mini emulsion polymerization of PPF-FA with VPA resulted in microplate morphology with nanoparticles which showed variation with surfactant concentration.

ÖZET

POLİ (PROPİLEN FUMARAT) - VİNİL FOSFONİK ASİT BAZLI İLAÇ SALIM SİSTEMLERİ

Bu çalışma kapsamında poli (propilen fumarat) (PPF) ve vinil fosfonik asit (VPA) bazlı nanopartiküller geliştirilmiştir. Ayrıca folik asidin kanser hücrelerine karşı seçiciliğine istinaden folik asidin PPF polimerine konjugasyonu ve PPF-FA ve VPA bazlı nanopartiküllerin geliştirilmesi çalışmaları da gerçekleştirilmiştir. Bu kapsamda, öncelikle PPF pre-polimeri fumarik asit ve propilen glikolün fazlasının polikondenzasyon reaksiyonu ile sentezlenmiş, sonrasında PPF/VPA nanopartiküllerini elde etmek üzere PPF polimeri VPA ile 70/30 ağırlık oranında UV mini-emülsiyon polimerizasyonu ile kopolimerize edilmiştir. En yüksek yüzde 86,7 jel oranı ve 500 ila 2000 nanometre aralığındaki boyutlarda partikül oluşumu, ağırlık olarak yüzde 3 BAPO radikal başlatıcısı, yüzde 0,04 ko-katalizör TAA ve yüzde 9 SDS yüzey aktif madde kullanımı ile 1000 rpm hızda 10 dakika homojenizasyon ve 2 saat UV kür uygulanarak elde edilmiştir. Kür reaksiyonun tamamlanmış olduğu DSC analizi ile konfirme edilmiştir. PPF/VPA partiküllerinin, PBS tampon çözeltisindeki (pH=7.4) bozunma profilleri, uygulanan homojenizasyon sürelerine bağlı olarak partiküllerin yüzde 88 ila 98'nin 84 gün içinde bozunduğunu, pH'ın ise 89 gün içerisinde 7.4'ten 2.9 ila 3.3 arasına düştüğünü göstermiştir. PPF/VPA nanopartikülleri aynı zamanda model anti-kanser ilacı Paclitaxel varlığında da hazırlanmıştır. PPF/VPA partiküllerinden Paclitaxel ilaç salımı lineer, zamana yayılmış şekilde ve polimer bozunması kontrolünde gerçekleşmiştir. Folik asit konjuge PPF (PPF-FA) sentezi, folik asidin PPF pre-polimerine dehidrant: disiklo heksil karbodiimid (DCC) ve katalizör: 4-dimetil amino piridin (DMAP) varlığında katılımı ile gerçekleştirilmiş olup, ürün FT-IR ve ^{1}H-NMR spektroskopisi ile karakterize edilmiştir. PPF-FA'nın VPA ile UV mini emülsiyon polimerizasyonu yüzey aktif madde konsentrasyonu ile etkilenen nanopartiküller ile beraber mikro tabakaların oluşumu ile sonuçlanmıştır.

TABLE OF CONTENTS

LIST OF FIGURES

LIST OF TABLES

LIST OF SYMBOLS / ABBREVIATIONS

UV	Ultraviolet
μ	Micro
PVA	Poly (vinyl alcohol)
PC	Polycarbonate
PEEK	Poly (ether ether ketone)
LED	Light-emitting diode
PGA	Poly (glycolic acid)
fmDA	Furan-maleimide Diels-Alder (A variation of DART)
PLA	Poly (lactic acid)
PCL	Poly (ε-capro lactone)
PBT	Poly (butylene terephthalate)
PTMC	Poly (trimethylene carbonate)
PEG	Poly (ethylene glycol)
PETA	Pentaerythritol triacrylate
HYP	Hydroxyproline
GAG	Glycoamine glycan
DMA	Dynamic mechanical analysis
HEMA	(Hydroxyethyl)methacrylate
SMC	Smooth muscle cells
VIC	Aortic valve leaflet interstitial cells
NIPAAm	N-isopropylacrylamide
AAm	Acrylamide
PEO	Poly (Ethylene Oxide)
HPMA	(N-(2-hydroxypropyl) methacrylamide)
PDI	Polydispersity Index
PLGA	Poly (lactic-co-glycolic acid)
Wt.	Weight
MRI	Magnetic resonance imaging
FT-IR	Fourier transform infrared spectroscopy

1. INTRODUCTION

Upcoming sections consist of theoretical information on polymers, a brief history of drug delivery systems, and nanoparticle drug delivery systems.

1.1. POLYMERS

Polymers are types of compounds that consist of monomers. Monomers get chained together to form a polymer. This reaction is called polymerization. Polymerization can happen through chemical reactions. Various parameters at polymerization affect the polymer chain length and reactivity which can cause different responses in different media. This property of polymers found a lot of usage in pharmacology, oncology, and medical fields.

Polymers, due to their flexible chain length and their copolymerization ability with a variety of monomers found a lot of use in medical fields. Biodegradability, flexibility, and bonding capability make polymers a great candidate for medical agents. Polymers can be bonded to other compounds which gives different responses to different media. These compounds can have an affinity for specific areas of human cells.

1.2. THE HISTORY OF DRUG DELIVERY SYSTEMS

Modern drug delivery methods try to deliver drugs to particular cells. While drugs get more potent, selectivity becomes important. To protect healthy cells from apoptosis, drug formulations have to be developed with selectivity. This selectivity can originate from external conditions of cell media such as temperature [1], pH [2] or genetic ligands ,[3] and ultrasound [4].

Modern drug delivery technology is only 60 years old [5]. Hee Yun et al. divided the drug delivery history into two generations which first one is from 1950 to 1980 and the second one from 1980 to 2010 as presented in Figure 1.1.

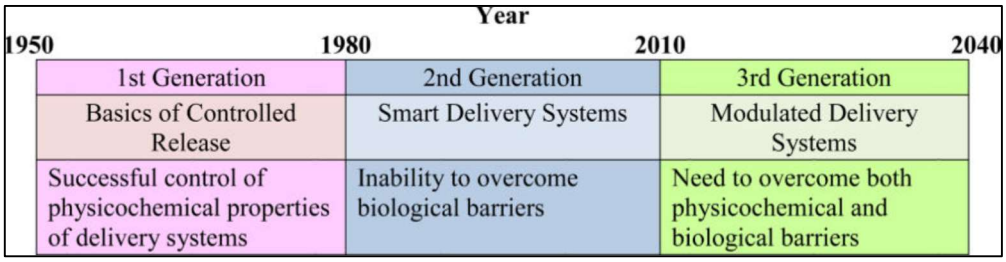

Figure 1.1. Hee Yun et al. drug delivery generations [5]

Before 1950, all drugs had been administered orally, made to pill, or capsule formulations. These drugs released their product in immediate contact with water. In 1952, Smith Klein Beecham et al. introduced sustained release drug delivery that was able to control drug release kinetics for 12 hours [6]. There were two different control techniques, which were diffusion-controlled and dissolution-controlled.

A second-generation phase, researchers could not become successful mostly, as measured by the number of clinical products produced. Very difficult formulations with different approaches to delivery caused this. At the last periods of second generation, researchers focused on tumor-targeted drug delivery using nanoparticles which is also investigated in this thesis. Administration of drugs locally than systematically is a common way to increase treatment's impact while decreasing side effects and drug toxicity. Some medications must be given systematically to achieve greater impact; especially in cancer drugs which selectivity has been an issue [7].

Table 1.1. Routes of drug administration [8]

Routes of drug administration
Anal Route
Oral Route
Transdermal Route
Parenteral Route
Topical Route (Skin or mucous membranes)

While drug delivery systems can change through the chemical formulation of drugs, several methods are used. Medications can be taken in by swallowing, intravenous injection, inhalation, and absorption through the skin. Different routes of drug administration are presented in Table 1.1. Drugs work by interacting with receptors on the surface of cells or enzymes. To reach the target site, drugs mostly travel the blood stream. This causes toxicity and side effects to humans [9], [10]. Every medication cannot be used with all delivery methods. Current delivery method improvement and designing new methods can improve the quality and variety of existing medications. For example, microneedles can be fabricated to contain medicine, which is composed of arrays each far thinner than 90 μm, with higher surface area [11]. Microneedles and their differences are presented in Figure 1.2.

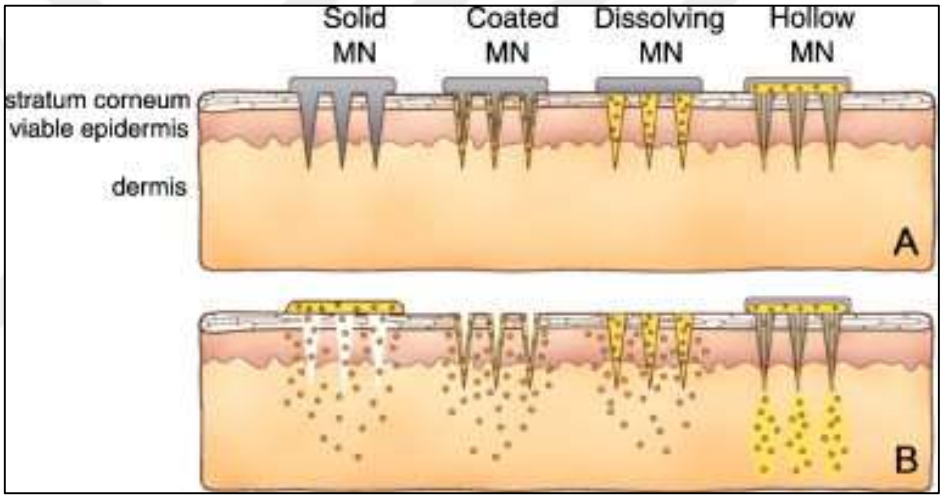

Figure 1.2. Microneedles and their differences [12]

It can be said that drug formulation that can release its drug when it comes to targeting site is the main goal of cancer research. There are several drugs that efficiently kill cancer cells along with healthy cells (*e.*g., doxorubicin, paclitaxel) [2], [13]. In order to achieve selectivity, most used technique is micro-nanoparticle delivery. These particles are very sensitive to external conditions which make them great candidates for targeted delivery.

A search in the Web of Science using “drug delivery nanoparticle” results in 17090 results during 1991-2019. Among these, 6090 of them are about targeted drug delivery. Tumor targeted drug delivery is the main research among them. With the flexibility, shape changing and controllability of nanoparticles, research wended to usage in targeted drug delivery. Many of these systems showed good results *in vitro* and *in vivo* studies [10], [14]–[16].

Targeting occurs as nanoparticles circulate through the blood stream and by the external conditions, they become active and release the drugs. Toxicity and side effects' decrease are advantages of nanoparticle drug delivery. Drug penetration can also be visualized with various florescence agents (such as Riboflavin, Rhodamine) [3]. An example of a nanoparticle mediated drug delivery is presented in Figure 1.3.

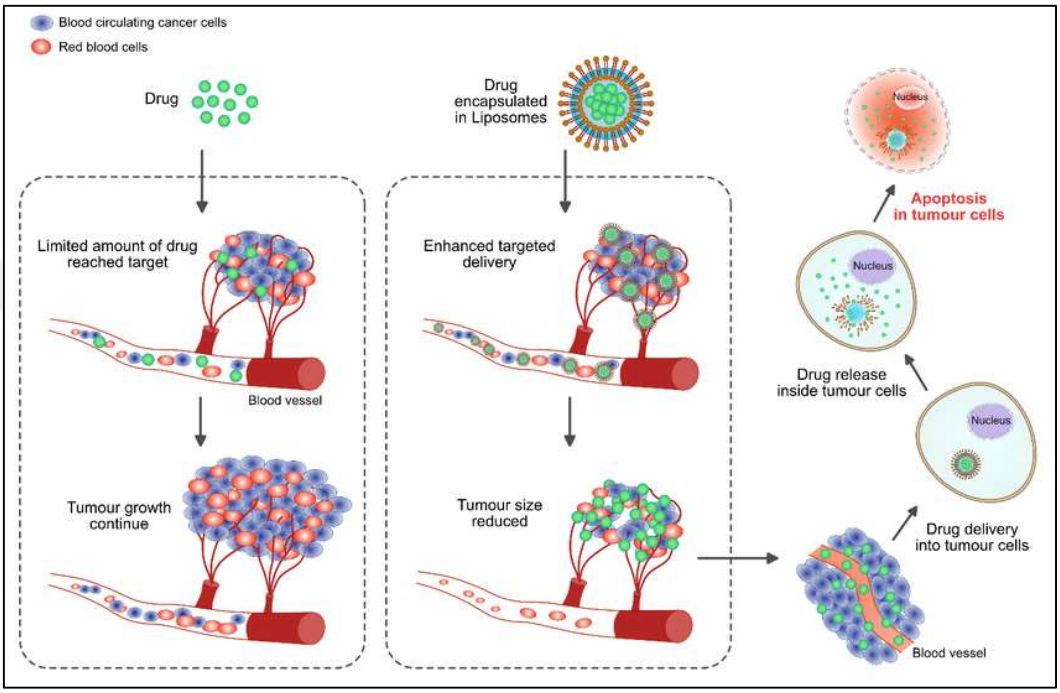

Figure 1.3. Example of nanoparticle mediated drug delivery [17]

Nanoparticle based drug delivery systems are only in trial stage. For example, human's tumors have likely to be less in size than mice. These scale differences need to be considered when animal models are used in analysis.

Nanoparticles can also be synthesized with different processes such as Stöber process [18], emulsion polymerization [19]–[22] or precipitation method [23][24][25]. Emulsion polymerization can also be used for both copolymerization and nanoparticle formation. Emulsion polymerization usually consists of hydrophobic polymers which generally forms nanoparticles because of decreased surface tension between water-polymer surface. Stöber process is a chemical process that prepares silica particles of controllable and uniform size. Modified Stober process can be used for the preparation of Fe_3O_4 nanoparticles conjugated with the Rhodamine B [18].

Small scale drug delivery systems include liposomes, other lipid- based carriers such as micelles, lipid emulsions and lipid-drug complexes. These can be used to improve efficiency and selectivity of conventional drugs. Basic structure of liposomes is presented in Figure 1.4.

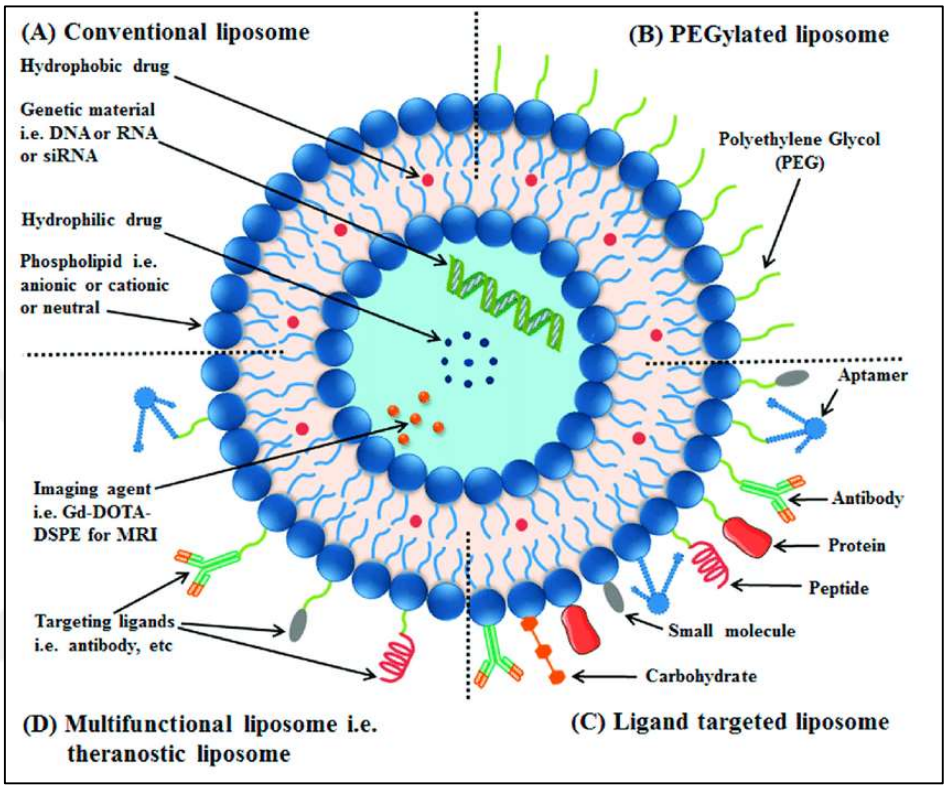

Figure 1.4. Basic structure of liposomes PEGylated liposomes contains a layer of polyethylene glycol (A), targeted liposomes contain specific target ligand (B), (C) multifunctional such as theragnostic liposomes which can be used for solid tumors (D) [26]

1.3. NANOPARTICLE DRUG DELIVERY SYSTEMS

Last century was the birth of Nanotechnology. “Nanotechnology” was first introduced by Richard P. Feynman: a Nobel laureate during his famous lecture in 1959 ‘‘There’s Plenty of Room at the Bottom”. There have been various groundbreaking developments in the field of nanotechnology since then [27]. Nanotechnology had been an area which was exclusively investigated in literature in 1981, with the development of Scanning Electron Microscope. Nanotechnology was then used extensively to develop cancer drugs and their efficiency. There can be liposome-based nanoparticles and polymer-based particles as drug carriers. In

this study, poly (propylene fumarate)-based nanoparticles were investigated for their potential use as anti-cancer drug delivery agents. Due to poly (propylene fumarate)'s hydrophobic and biocompatible nature, high drug encapsulating and drug delivery efficiency in human body can be achieved.

Transcutaneous drug delivery is limited to patient's skin or other surface tissue administration. In this way, delivery is relatively inefficient because of non-selective administration [28]. Additionally, drug can be picked up by capillaries and carried beyond the diseased or damaged area. Because of these reasons, transcutaneous drug delivery is not always appropriate when especially drug is very toxic or burdensomely expensive. Oral administration, injection, and intravenous administration are systemic, which means that these methods use blood stream to effect damaged or diseased area. These methods have lots of shortcomings. The main reason is that the systemic drug delivery fails to concentrate drug on the damaged area, it has no selectivity. Drug also effects areas that do not need medication. As a result, drug dosage is increased adding expense to treatment and causing harmful side effects. So, there is a need of selective drug delivery systems which can be used especially with very toxic drugs. Different type of nanoparticles is presented in Figure 1.5.

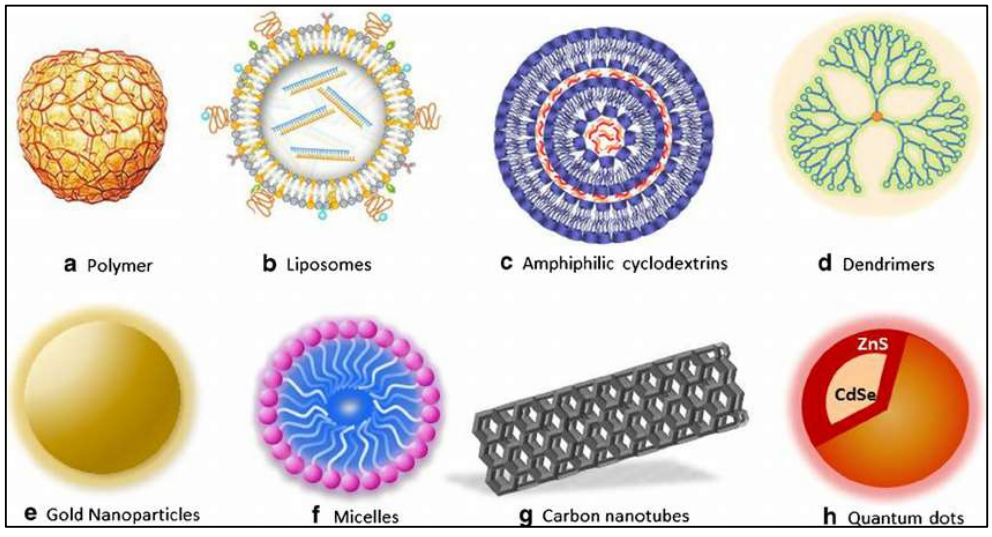

Figure 1.5. Nanoparticle Types [29]

Nanoparticles have the ability of reducing toxicity and side effects of potent drugs. With the targeting ability and flexibility, it is a great candidate for the tumor targeting and drug delivery. For example, polysaccharide (starch or dextran)-coated iron oxide nanoparticles

have been employed in biomedicine for decades as agents for parenteral anemia therapy, magnetic resonance contrast, cancer hyperthermia, medication administration, and, most recently, triggering ferroptosis in cancer cells. [30]. Nanoparticles can unload their drugs with various external conditions. External factors such as magnetism, pH, temperature can affect the nanoparticle to release its drugs (Figure 2).

Controllable and precise synthesis of nanoparticle assemblies can be achieved with tuning interparticle interactions and modifying assembly strategies [31]. In polymer nanoparticles, especially with copolymers, interactions and assembly are mostly determined by stoichiometry of the polymers. Polymer composition can affect the viscosity and nanoparticle formation. Polymers are in use for the nanoparticle synthesis because of these properties. In this study, PPF prepolymer will be copolymerized with VPA (that may behave differently in different pH mediums) and Folic acid conjugated PPF will also be copolymerized with VPA to produce nanoparticles that are expected to be selective towards cancer and tumor cells.

Nanoparticles can also be directed to the needed place in a variety of ways. As listed below [31];

- Electrically powered motion
- Magnetism driven motion
- External force-driven motion
- Photoinduced motion
- Shape memory-induced motion
- Self-healing properties
- Self-replication properties

A description of magnetic nanoparticle drug delivery is presented in Figure 1.6.

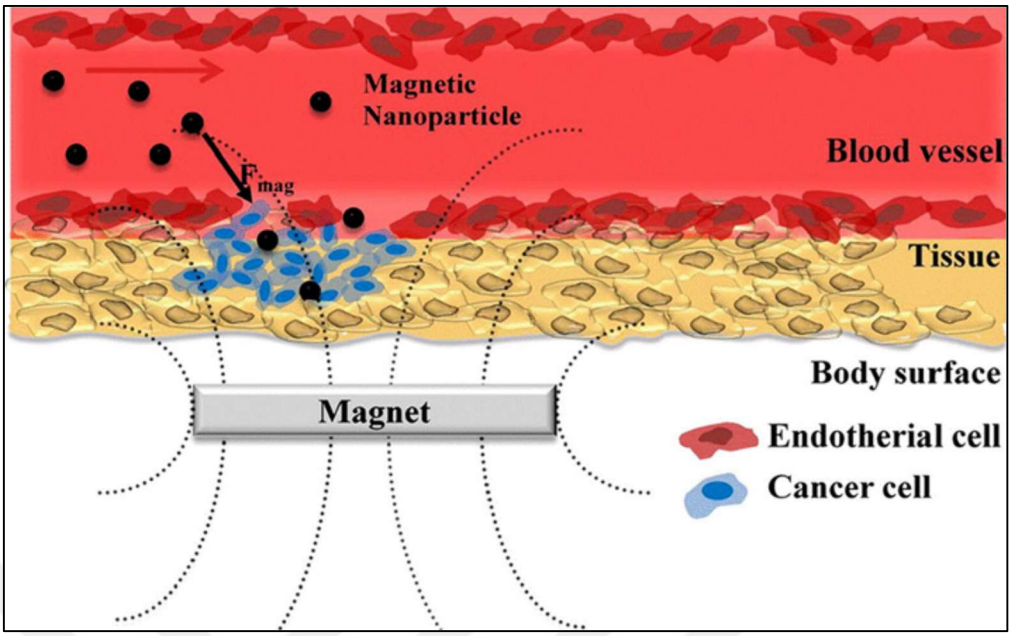

Figure 1.6. Magnetic nanoparticle drug delivery [32]

Nanoparticles can also be dynamic. They can explode, break, form bonds, and reform under the influence of other external stimuli. These are called living nanoparticles. They can reform their bonds, because of their reversible bonds or interaction ability [31].

1.3.1. Ligands for Tumors

Tumor cells are investigated for cell targeting. There are many developed ligands for tumors, including aptamers, folic acid, antibodies, and peptides [33] [34]. Folic acid is a great candidate for targeting because of high folate intake of cancer cells. Folic acid enters cells by attaching to folic acid receptors on the cellular membrane, which are overexpressed in human cancer cells. In Figure 1.7, mechanism of folic acid intake of cancer cells can be seen.

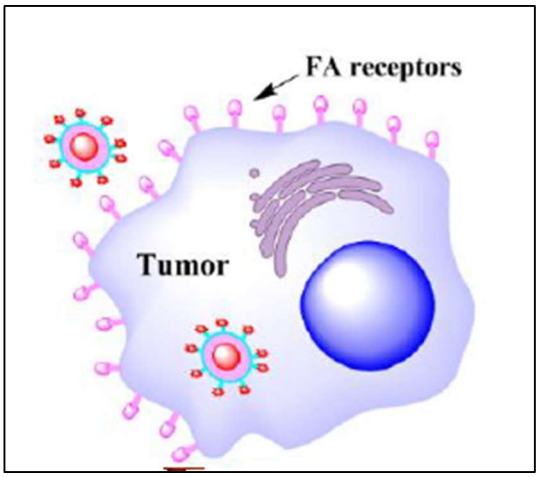

Figure 1.7. Visual representation of tumor cells folate intake [3]

Folic acid deficiency can be linked to megaloblastic anemia, neural tube defects in the neonate and heart disease. There are two principal mechanisms whereby folate is thought to modulate DNA stability and cancer.

Folic acid can be used in order to release drugs in specific media. In this study, folic acid is used for appealing tumor cells because of higher folate intake. As shown in Figure 1.7, tumor cells have higher concentration of folate ligands. It can be said that this mechanism can be used in order to get past cancer cell's wall. With drug activation, cancer cells can get to apoptosis phase. Due to this property, folic acid is used extensively for tumor cell research [10], [13]–[15], [35]. Venkatasubba et al. [36]designed and produced folic acid conjugated PEG nanoparticles [36]. Venkatasubba et al. characterized the folic acid conjugation with UV-visible spectroscopy, which a red shift in the spectra is enough for the characterization of bonding. The hydroxyl groups in the PEG are ideal candidate for the bonding to the folic acid. Also, the drug loading capacity and mixing time relationship was investigated. Drug loading capacity increased as the mixing time increased. At the case of PEG nanoparticles, maximum drug loading of 50 percent for 3 hours' mixing time which stayed constant was achieved.

1.3.2. Anti-cancer Drugs

In cancer treatments, Paclitaxel and Doxorubicin are two drugs that are commonly used. In this study, Paclitaxel was used as a model anti-cancer drug. It causes apoptosis in cells by

promoting tubulin dimer polymerization to create microtubules and stabilizing microtubules by blocking depolymerization. Initially, hypersensitivity reactions were a concern with Paclitaxel administration, but modern dosing regimens have lowered the occurrence of these events to less than 5 percent. Paclitaxel's major dose-limiting side effects include leucopenia (neutropenia) and peripheral neuropathy. In order to prevent hypersensitivity and side effects of the drugs, time delayed and controlled release can be crucial, thus PPF/VPA nanoparticles which biodegrade over time to nontoxic species were prepared and investigated as Paclitaxel delivery agents. In addition, preliminary studies on folic acid conjugated PPF/VPA nanoparticles synthesis were also carried out. Although several aspects of Paclitaxel use remain to be clarified, including optimal dosage and infusion time, release from polymeric nanoparticles can provide a stable and selective release. The chemical structure of Paclitaxel is presented in Figure 1.8.

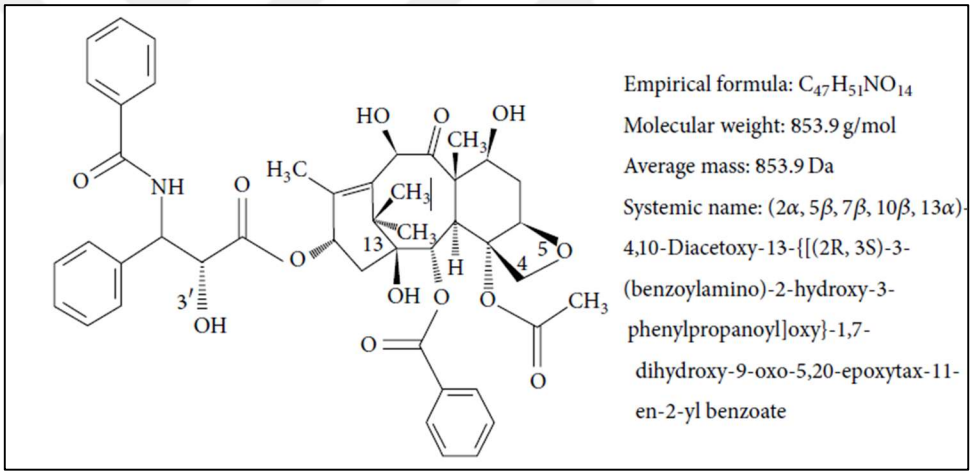

Figure 1.8. Paclitaxel chemical structure [19]

1.3.3. Encapsulation Effectivity

Nanoparticles must encapsulate the matter inside it effectively to ensure that no accidental leakages happen. Encapsulation of a drug generally expressed as percent drug loading capacity; weight percent of drug loaded per unit weight of drug delivery system. For most carrier systems, the drug loading capacity fluctuates between 5 percent-25 percent [37]. However, it can be changed with the solution and formulation.

According to reports, high capacities range from 10% to 60% [38]. The amine functionality of doxorubicin was coupled with the carboxylic acid functioning of PEG, and the amine functionality of the PEG was coupled with a targeted folic acid moiety by NHS/DCC coupling in a similar study [38]. Micellar assembly is enabled by the hydrophilic-lipophilic balance of this system.

There is a misconception that micelles and particles are the same concept. Micelles are amphiphilic colloidal structures which contain both hydrophilic and lipophilic properties, while nanoparticles are tiny particles which can be formed via both hydrophobic and lipophobic chemicals.

1.4. POLYMERIC DRUG DELIVERY SYSTEMS

Polymers are used in the drug delivery systems [11], [38], [39] due to their different characteristics. Poly(Propylene Fumarate) [38], [40], [41] and Poly(Lactic-co-Glycolic Acid) [39], [42], [43], Poly (Lactic Acid) [40], [44], [45], Poly (Ethylene Glycol) [3], [46]–[48], Poly (Caprolactone) [46], [49], [50] are the most used polymers in the drug delivery systems because of their biodegradability and biocompatibility. Poly (Caprolactone) used for fast degradation profile [51], tissue engineering scaffolds [50] and controlled release [52]. Poly (Lactic Acid) (PLA) used for parenteral administration [44], ophthalmic drug delivery [53] and for treatment of liver cancer [54] and PLA have many other applications. Poly (Ethylene Glycol) have been used for selective drug delivery [47], for multi-targeting [55] and orthopedic tissue engineering [56]. PPF used for bone filler [57], bone cement [58] and have other usage areas. Although, polymers usage areas were given as summary, polymers have many other usage areas.

Polymers have drug delivery advantages such as (Figure 1.9):

1. They are stable at high concentrations of surfactant. Since polymers and copolymers have higher molecular weight than other molecules, the dissociation with dilution usually takes longer time than other nanoparticles.
2. When their corona contains PEO (poly (ethylene oxide)) chains, the nanoparticles are able to circulate in blood stream without recognized or cleared.

3. The simple action of micelles allows hydrophobic medicines to be easily integrated into copolymeric micelles. Physical entrapment is a simple and effective method [4].

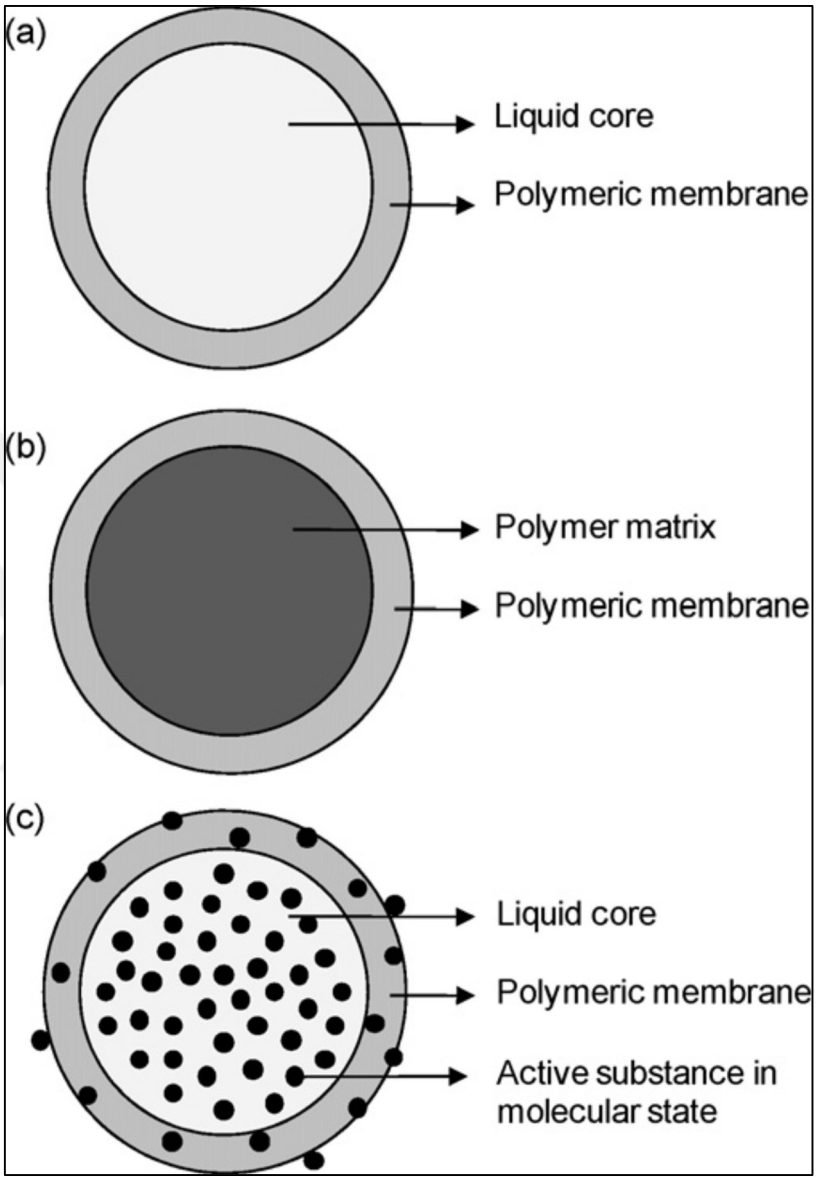

Figure 1.9. Different nano capsular structures A) Liquid core, B) Polymer matrix C) Active substance in molecular dispersion [59]

Polymers are especially used for nanoparticle formation with the drug substance [17], [53], [60]. Their subcellular size and different bonded compounds (such as Folic acid, riboflavin conjugates) can react with the cell ligands and create a selectivity towards particular cell types. Nanoparticles which generally have drug substance confined in a cavity consist of an

inner liquid core or polymer matrix and a polymeric membrane on the outer shell as depicted in Figure 1.9. Generally, there are 6 methods to produce nanoparticles.

- Nanoprecipitation
- Emulsion-Diffusion
- Double Emulsification
- Emulsion-Coacervation
- Emulsion-Polymerization
- Polymer-Coating
- Layer-by-layer

Composites of thermally sensitive hydrogels and optically active nanoparticles are widely used for drug delivery systems. Sershen et al. [61] produced N-isopropylacrylamide (NIPAAm) and acrylamide (AAm) copolymers conjugated with the gold-gold sulfide nano shells. Copolymer of NIPAAm-co-AAm exhibited critical solution temperature which was slightly above body temperature. When the temperature of shells exceeded the critical solution temperature, it collapsed and released its drugs to medium.

Pechar et al. [62] have created a biodegradable PEO (polyethylene oxide) block copolymer connected by oligopeptides with amino end groups. To react diamine with poly (ethylene glycol) bis, they employed an interfacial polycondensation process (succinimidyl carbonate). Doxorubicin (Dox) was connected to the drug carrier by a (Gly-Phe-Leu-Gly) tetrapeptide spacer, which was hydrolyzed by enzymes in the body. Dox that was polymer-bound was able to slow tumor development and lessen drug toxicity. However, their method included complicated synthesis stages, extensive purification procedures, and chemical (rather than ultrasonic) drug release at the target region [62].

Polymers that have one or more blocks of homopolymer which grafted as branches onto a main chain, called “Graft Polymers” [63]. Graft polymers can have both hydrophilic and hydrophobic character. Polymers such as poly (ethylene oxide) (PEO) and hydrophobic blocks of poly (propylene oxide) (PPO), poly (lactic acid) (PLA), or other biocompatible and hydrophobic polyethers or polyesters can be used in drug delivery, these polymers can be used in the form of diblock, triblock or are even more complex structures [64]. One of the most used copolymers is an ABA block copolymer, PEO-PPO-PEO structure with trade

names of Pluronic® and Poloxamer™. The chemical structure of Poloxamer is shown in Figure 1.10.

Finally, to sum up, schematic illustrations of various nanoparticles that may be used in enhanced drug delivery systems are presented in Figure 1.11.

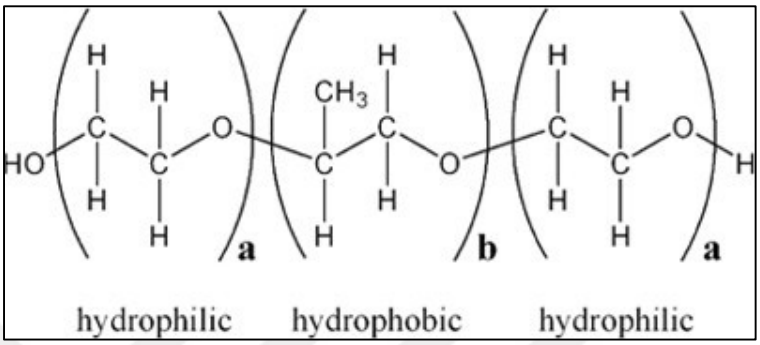

Figure 1.10. Poloxamer 188 structure [65]

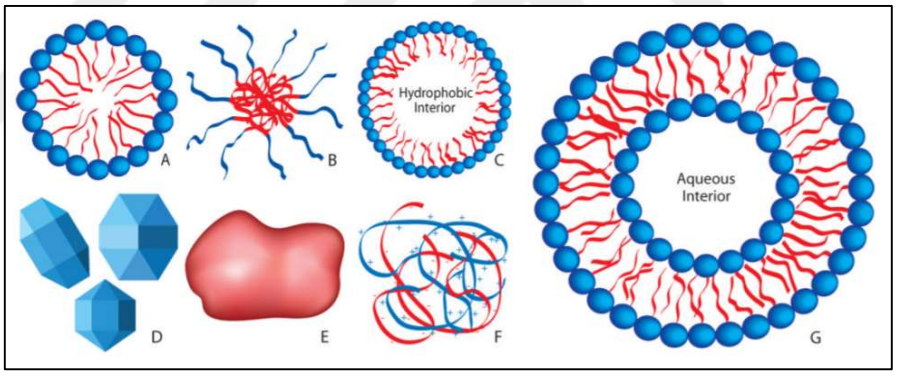

Figure 1.11. Illustrations of nanoparticles that could be utilized in a variety of medication delivery systems. (a) Non-polymeric micelle with amphiphilic surfactants. (b) Polymer micelle with amphiphilic block copolymers. (c) Nano emulsion with a hydrophobic liquid core which is stabilized by surfactant. (d) Nanoparticles in crystalline form (e) Amorphous polymer nanoparticle. (f) Condensed ionic oligomers (g) Liposome with an amphiphilic bilayer around an aqueous core [4]

2. THEORITICAL BACKGROUND

2.1. POLY (PROPYLENE FUMARATE), DRUG DELIVERY AND BONE TISSUE ENGINEERING APPLICATIONS

2.1.1. Drug Delivery

Due to its flexibility and copolymerization ability, PPF has attracted attention for drug delivery formulations. All polymers, especially with high molecular weight and biocompatibility have been used for many drug formulations for a long time [9], [11], [39], [60], [66], [67]. As in this study, PPF will be used to synthesize nanoparticles and the use of these particles as anti-cancer drug delivery agents will be explored, examples of works on PPF drug delivery systems will be presented under this section.

Anti-cancer drugs can be coated with the polymers for efficient apoptosis while recovering the healthy cells. PPF offers good release profile and strength under in vitro conditions. Also, its degradability can be controlled via adjusting the fabrication parameters such as photo initiator concentration. However, the direct incorporation of water-soluble drugs to PPF is challenging due to its hydrophobicity. Choi et al. [68] utilized the PPF nanoparticles with the coating of Doxorubicin, iron oxide which was used for imaging with Magnetic Resonance Imaging (MRI). Using of PPF resulted in a stable release profile of Doxorubicin after 2 hours. Figure 2.1 shows the Release Profile of DOX.

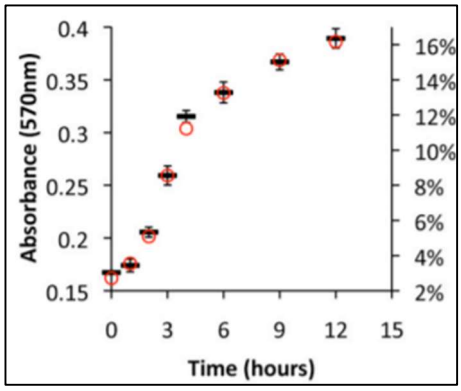

Figure 2.1. Release profile of DOX. Red circles indicate results of Magnetic Resonance Imaging (MRI), and black hyphen symbol means BSA assay [68]

In another study, Ueda et al. [69] synthesized fluocinolone acetonide loaded PPF matrix. The release profiles were investigated for 62 weeks. Figure 2.2 shows the release profiles which reach up to 100 percent release of the fluocinolone acetonide.

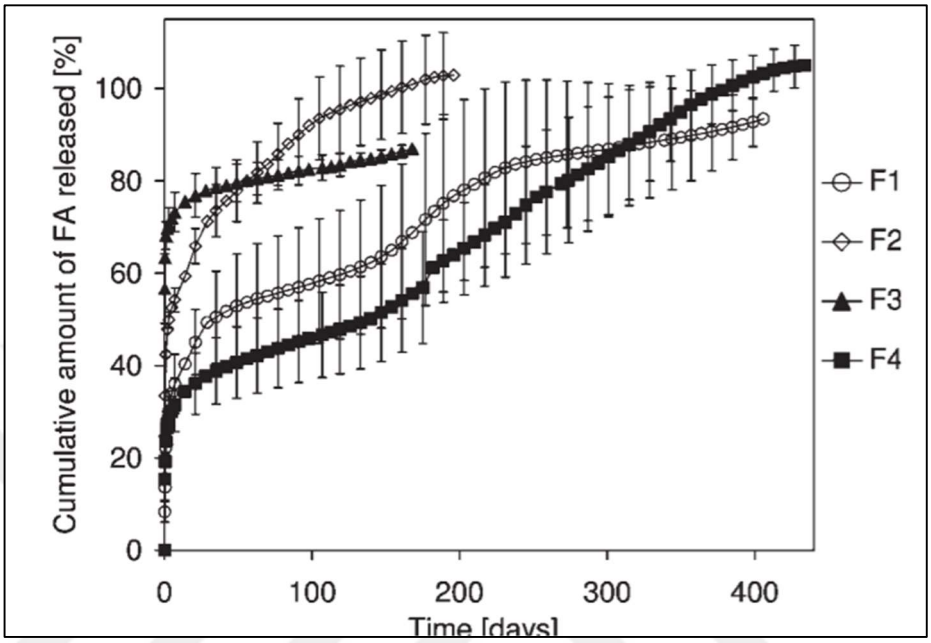

Figure 2.2. The release profiles of fluocinolone acetonide loaded PPF Matrix [69] (F1: (%w/w) 50 PPF, 5 Fluocinolone Acetonide, 45 N-Methyl-2-pyrrolidone. F2: (%w/w) 50 PPF, 2,5 Fluocinolone Acetonide, 47,5 N-Methyl-2-pyrrolidone. F3: (%w/w) 25 PPF, 2,5 Fluocinolone Acetonide, 72,5 N-Methyl-2-pyrrolidone. F4: (%w/w) 50 PPF, 5 Fluocinolone Acetonide, 44,5 N-Methyl-2-pyrrolidone, 0,5 BAPO)

Kempen at al. [42] synthesized poly (propylene fumarate)/poly (lactic-co-glycolic acid) (PPF/PLGA) blend microspheres were investigated for release kinetics by Texas Red Dextran (TRD). Figure 2.3 shows the TRD release from poly (propylene fumarate)/poly (lactic-co-glycolic acid) (PPF/PLGA) blend microspheres.

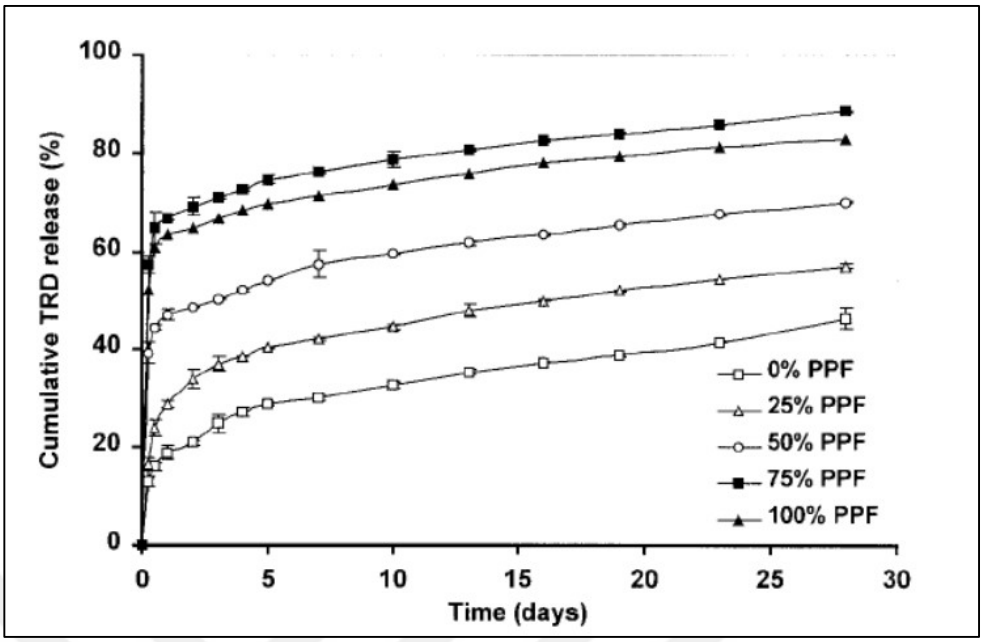

Figure 2.3. Cumulative TRD Release of poly (propylene fumarate)/poly (lactic-co-glycolic acid) (PPF/PLGA) blend microspheres

Array with 25 PPF microneedles were fabricated with multi-material micro stereolithography (μSL) by Lu et al. [70]. Lu et al. used Diethyl Fumarate in order to control the viscosity and improve the mechanical properties. In this study, VPA were used in order to create time delayed controlled drug release profile.

Hacker et al. [71] photo crosslinked the PPF/ poly (N-vinyl pyrrolidone) matrix for sustained ophthalmic 3 different drug delivery system. Drugs were different in molecular weight which greatly effects the release. PPF/ poly (N-vinyl pyrrolidone) matrix released the drugs with initial burst which became linear for an average of 250 days.

2.1.2. Bone Tissue Engineering Applications

PPF, due to its reduced toxicity, biocompatibility and biodegradability can be used for bone tissue engineering too [72].

The global incidence of bone illnesses and ailments has risen sharply in recent years and is anticipated to double by 2020, particularly in populations where aging is accompanied by

increased obesity and insufficient physical activity [73]. Limited supply of bone graft resulted in the research about engineered bone grafts and scaffolds. Bone tissue engineering aims to induce new functional, biocompatible, biodegradable materials for the scaffolding and supporting of the new bone formation. Bone scaffolds significantly reduce the time needed to recover whole bone. Scaffolds to bone tissue can be made with 3D printers, salt leaching etc. There are also chemical formulations and chemical reactions that can be used to prepare scaffolds.

Bone tissue engineering has numerous scaffolds [11]. Scaffolds are used for treating skeletal injuries, traumas, total joint arthroplasties, and trabecular voids. There are two different bone grafts: natural bone grafts (autographs) or allographs (from a donor). Autographs are preferred however, these are limited and collecting of it creates secondary wound site. Furthermore, allographs have the disadvantage of being rejected by the tissue. So, synthetic scaffolds can be used as an alternative. Metals, ceramics, and polymers can be used for scaffolds. SEM image of a polymeric scaffold is presented in Figure 2.4.

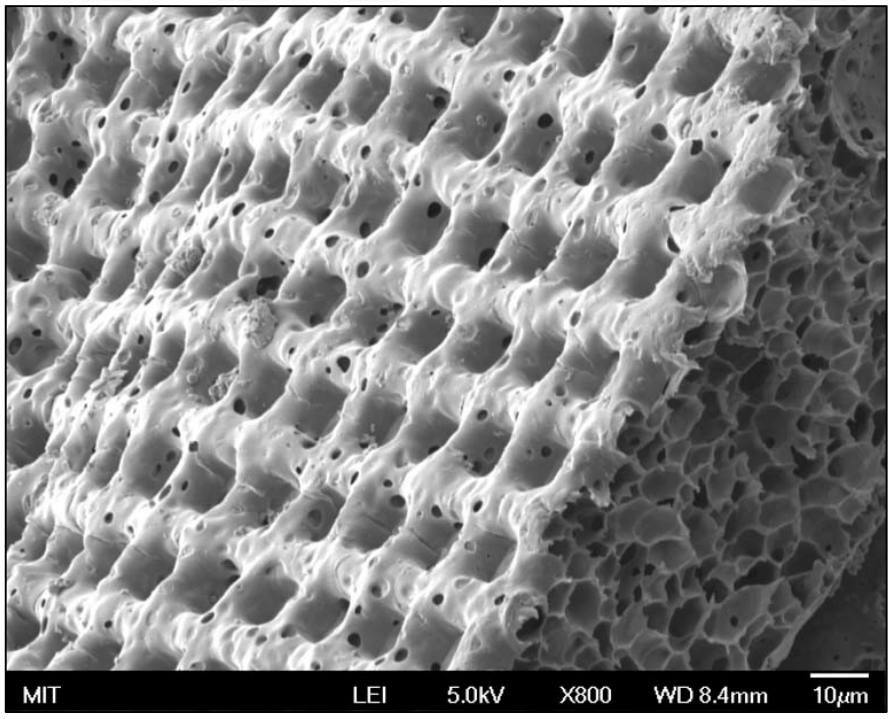

Figure 2.4. SEM image of a polymeric scaffold [74]

Scaffold material must be non-toxic, biodegradable and should cause minimal inflammation. Poly (propylene fumarate) (PPF) is a promising material for the engineering scaffolds. Biodegradation to its core compounds (fumaric acid and propylene glycol) is the main advantage of this polymer. Hydrolysis of the ester bond causes biodegradation with time [72]. Propylene glycol is quickly resorbed and eliminated by the human body, and fumaric acid is used during the Krebs cycle. In addition, PPF polymer can be cross-linked with various vinyl monomers to produce a network structure that can exhibit similar mechanical properties to those of bone [72].

2.2. MINI EMULSION POLYMERIZATION

Mini emulsion polymerization occurs with emulsification of hydrophobic polymer chain. When free radicals start to form by water or oil initiators, polymerization starts. Overall reaction rate is controlled from the rate determining step, which is radical polymerization step [21]. There are.

1. Conventional Emulsion Polymerization: in which a hydrophobic polymer chain is emulsified in water and polymerization is initiated with a water-soluble initiator.

2. Inverse Emulsion Polymerization: where organic solvents of very low polarity such as paraffin or xylene is used as a polymerization media to emulsify hydrophobic monomers.

3. Mini Emulsion Polymerization: this polymerization is characterized as monomers form droplets which have 50-1000 nm diameter. In this polymerization method, the critical micelle concentration is bigger than surfactant concentration. The mechanism of miniemulsion polymerization is presented in Figure 2.5.

4. Microemulsion Polymerization; this type of emulsion polymerization is characterized by smaller particles which have diameters of 10-50 nm.

Every polymerization type shows different reaction rates, reaction steps and kinetics [75], [76].

The main components of emulsion polymerization are monomers, dispersing medium, emulsifier, and water-soluble initiator. Radical polymerization occurs when a UV light is projected into solution of emulsion. There are three steps for this reaction.

- Initiation
- Propagation
- Termination

Initiation occurs when free radicals are formed with the UV light energy. Propagation is the repetitive operation in which polymer chain gets taller and branched or cross-linked. Finally, termination occurs when another free radical, left over from the original splitting of the initiator, meets the end of the growing chain which ends the polymerization process for that chain. There must be greater energy to start polymerization again [77].

In this study, to entrap Paclitaxel drug inside the PPF/VPA copolymer with a mainly hydrophobic PPF component (70wt%) to form nano-(micro-) particles, mini emulsion polymerization method was used. PPF prepolymer and VPA were used as the macromer and the monomer respectively in water as the dispersing medium, with sodium dodecyl sulfate (SDS) as the emulsifier, phenylbis(2,4,6-trimethylbenzoyl) phosphine oxide (BAPO) as the initiator and titanium acetyl acetonate as the catalyst. Preliminary studies on the mini-emulsion polymerization of PPF-FA with VPA were also performed under similar reaction conditions.

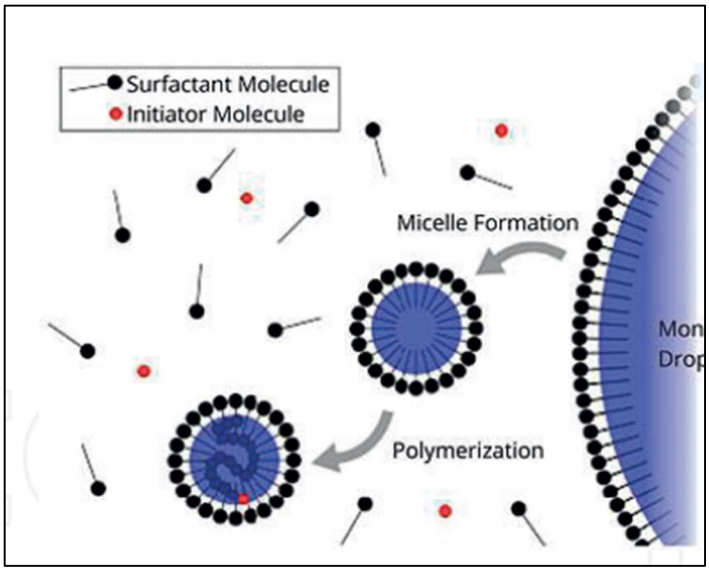

Figure 2.5. Mini emulsion polymerization mechanism [21]

2.2.1. Components of Emulsion Polymerization

2.2.1.1. Initiators

Initiators start to form radical compounds by thermal decomposition, UV radiation or redox reactions. There are two different initiators;

1. Water soluble initiators e.g. (2,2-Azobis(2-amidinopropane) dihydrochloride etc.)
2. Partially water-soluble peroxides e.g. (t-butyl hydroperoxide etc.)
3. Redox systems e.g. (persulfate with ferrous ion etc.)

2.2.1.2. Surfactants

Surfactants are type of compounds that have both hydrophobic and hydrophilic side. They act as a glue between different media by making bonds with them. The hydrophobic tail can be hydrocarbon, fluorocarbon, or siloxane.

Because the hydrophobic tails of surfactants are often similar, they are usually classed by their polar head. In the case of emulsion polymerization, they act by decreasing interfacial tension between monomer and aqueous phase, stabilize the micelles and particles. Particle number can be increased, and particle size can be decreased by surfactant concentration increment.

Surfactant concentration above which, micelles can be formed is called Critical Micelle Concentration (CMC). There are 3 types of surfactants which are classified according to their polar heads;

1. Anionic surfactants e.g. (fatty acid soaps (sodium or potassium stearate, laurate, palmitate), etc.)
2. Nonionic surfactants e.g. (poly (ethylene oxide), etc.)
3. Cationic surfactants e.g. (Cationic surfactants such as dodecyl ammonium chloride and cetyltrimethylammonium bromide)

Also, polymerizable surfactants can be used to produce micelles. The influence of the molecular structure on the characteristics and application of the end products has been studied using a variety of polymerizable surfactants, including cationic [41], anionic [42] and nonionic [43].

Kriwet et al. [78] fabricated Poly (Acrylic acid) nano and microparticles for hydrophilic drug entrapment. Poly (Acrylic acid) nano and microparticles were fabricated with the emulsion polymerization technique. Also, Abeylath et al. [79] prepared new and simple route for glycosylated polyacrylate nanoparticle synthesis. They achieved average particle size of 40 nm by radical-initiated emulsion polymerization.

2.2.1.3. Dispersion Medium

Water is frequently used for dispersion medium in emulsion polymerization.

2.2.1.4. Monomer

Monomers are type of compounds that form polymers when bonded together. Monomers can be reacted to form long chains of polymer. Depending on monomer solubility in aqueous phase, there are three categories which are;

1. Monomers that have high solubility [80]
2. Monomers that have medium solubility [81]
3. Monomers that is insoluble in aqueous phase [82].

3. MATERIALS AND METHODS

In this section, materials used in the synthesis of the PPF and PPF-FA pre-polymers and in preparation of PPF/VPA microparticles will be presented first and then brief theoretical information on the methods used in characterization of these polymers will be given.

3.1. MATERIALS

3.1.1. Materials used in PPF, PPF-FA and PPF Nanoparticle Synthesis

Materials used in PPF, PPF-FA synthesis and in PPF/VPA UV mini emulsion polymerization are listed in Table 3.1, Table 3.2 and Table 3.3 respectively.

Table 3.1. Materials used in PPF Synthesis

Material Name	**Chemical Formula**	**Purity**	**Supplier**
Propylene Glycol	$C_3H_8O_2$	≥99.5%	Sigma Aldrich
Fumaric Acid	$C_4H_4O_4$	≥99%	Sigma Aldrich
P-toluene Sulphonic Acid	$C_7H_8O_3S$	≥98.5%	Sigma Aldrich
Hydroquinone	$C_6H_6O_2$	≥99%	Sigma Aldrich
Methanol	CH_3OH	≥99.7%	Sigma Aldrich
Diethyl Ether	$(C_2H_5)_2O$	≥99.8%	Sigma Aldrich
Calcium Chloride	$CaCl_2$	≥99.5%	Sigma Aldrich

Table 3.2. Materials used in PPF–FA Synthesis

Material Name	**Chemical Formula**	**Purity**	**Supplier**
Folic Acid	$C_{19}H_{19}N_7O_6$	≥97%	Sigma Aldrich
N,N –dicyclohexyl carbodiimide	$C_{13}H_{22}N_2$	(DCC, >99%)	Sigma Aldrich
4-(dimethyl amino) pyridine	$C_7H_{10}N_2$	(DMAP, >99%)	Sigma Aldrich

Table 3.3. Materials used in PPF/VPA and PPF-FA/VPA UV mini emulsion polymerization

Material Name	**Chemical Formula**	**Purity**	**Supplier**
Vinyl Phosphonic Acid	$C_2H_5O_3P$	90%	MERCK
Titanium Acetyl Acetonate	$C_{20}H_{32}O_8Ti$	(Ti,9-10.5% gravimetric)	Sigma Aldrich
BAPO	$(CH_3)_3C_6H_2CO]_2P(O)C_6H_5$	97%	Sigma Aldrich
Sodium Dodecyl Sulfate	$NaC_{12}H_{25}SO_4$	<= 100 %	MERCK
Water	H_2O	100%	
Dichloromethane	CH_2Cl_2	≥99.8%	Sigma Aldrich
Paclitaxel	$C_{47}H_{51}NO_{14}$	≥99.8%	Sigma Aldrich

3.1.1.1. Vinyl Phosphonic Acid

Vinyl phosphonic acid (VPA) (Figure 3.1) is a colorless-yellow liquid which is odorless. It is soluble in water and most organic solvents such as acetonitrile, acetone, 2-butanone.

Due to the existence of both lipophilic and hydrophilic functions in one molecule, VPA's polymers and co-polymers have properties in a variety of applications, including emulsion

polymerization. These products are utilized in sectors such as coatings, corrosion prevention, lithography (printing plates, off-set printing), metal treatment, dental care, pigment dispersion, cement additives, flame retardants, and fuel cells to improve material qualities and surfaces. [83].

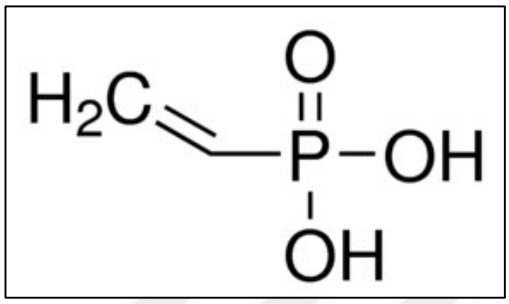

Figure 3.1. VPA chemical structure [84]

3.1.1.2. Phenyl-bis (2,4,6-trimethylbenzoyl) Phosphine Oxide (BAPO)

BAPO has the ability to produce radicals that can start polymerization at the exposure to Ultraviolet light. BAPO can be activated between 325-465 nm wavelength [85] which can penetrate deep into layers of coatings or polymers and produce radicals that start the polymerization. Figure 3.2 shows the BAPO chemical structure.

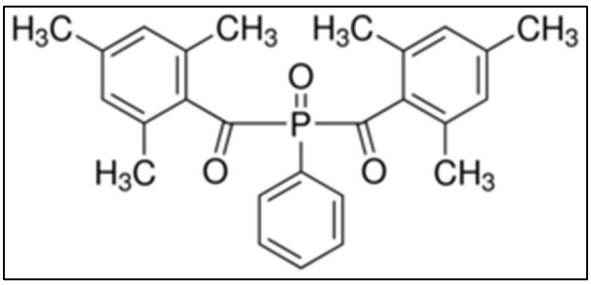

Figure 3.2. BAPO chemical structure [86]

3.1.1.3. Sodium Dodecyl Sulfate (SDS)

The molecule sodium dodecyl sulfate (Sodium laurate sulfate) has the chemical formula $CH_3(CH_2)_{11}SO_4Na$. An anionic surfactant, sodium dodecyl sulfate is widely found in cleaning solutions. The lengthy hydrocarbon tail attached to the polar head group of sodium

dodecyl sulfate affords the chemical amphiphilic characteristics. This feature allows it to be used in detergents.

SDS (or SLS) can be used as a surfactant for emulsion polymerization. It is a surfactant which decreases the surface tension between polymer and water interface, which helps the emulsion polymerization and formation of nanoparticles. In Figure 3.3 SDS chemical structure can be seen.

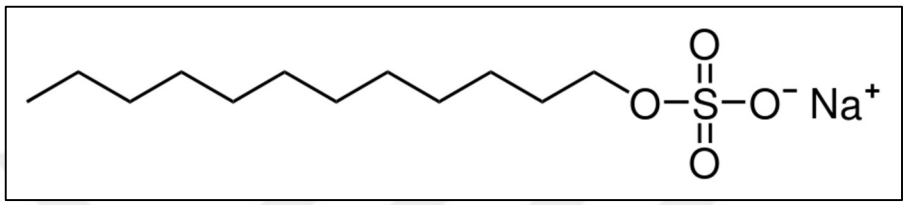

Figure 3.3. SDS chemical structure [87]

3.1.1.4. Paclitaxel

Paclitaxel is an anti-cancer (tumor) drug. Paclitaxel is classified as a "plant alkaloid," a "taxane" and an "antimicrotubular agent." [88]. Taxol is the brand name for it. Hair loss, bone marrow suppression, numbness, allergic responses, muscle pains, and diarrhea are all side effects of this parenteral medication. Microtubules are disrupted during cell division, which is how it operates [89].

It was first isolated from the Pacific Yew in 1971 and approved for medical use in 1993. Paclitaxel works as effecting the tubulin protein. Paclitaxel effected cells have defects in cell division. Paclitaxel prevents the microtubule polymer from disintegration by stabilizing it in the cell. Metaphase spindle conformation is not achieved by chromosomes. This stops mitosis from progressing, and prolonged activation of the mitotic checkpoint causes apoptosis. Figure 3.4 shows the Paclitaxel chemical structure and interaction with α and β microtubules.

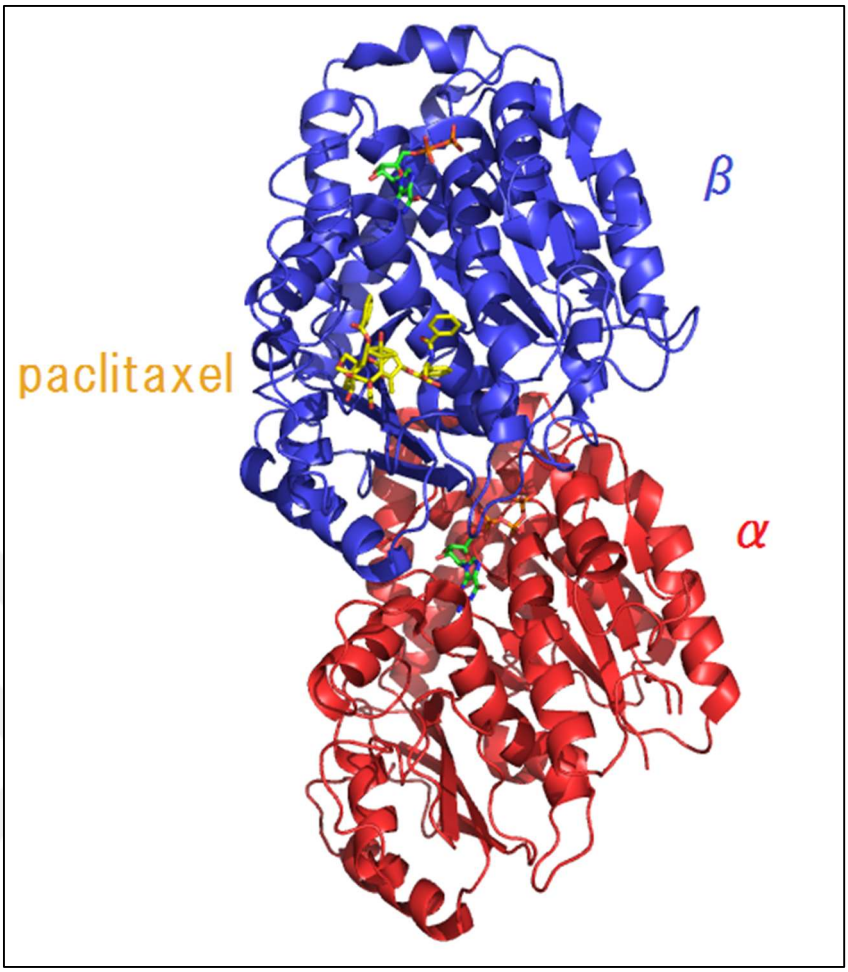

Figure 3.4. Paclitaxel between complexes of α, β tubulin subunits.

3.1.1.5. Folic Acid

Folic acid is a chemical that is in the class of Vitamin B. It is converted to the folate by the human metabolism [90]. Figure 3.5 shows the folic acid chemical structure. It is needed for the healthy development of fetus, nucleic acid synthesis and growth.

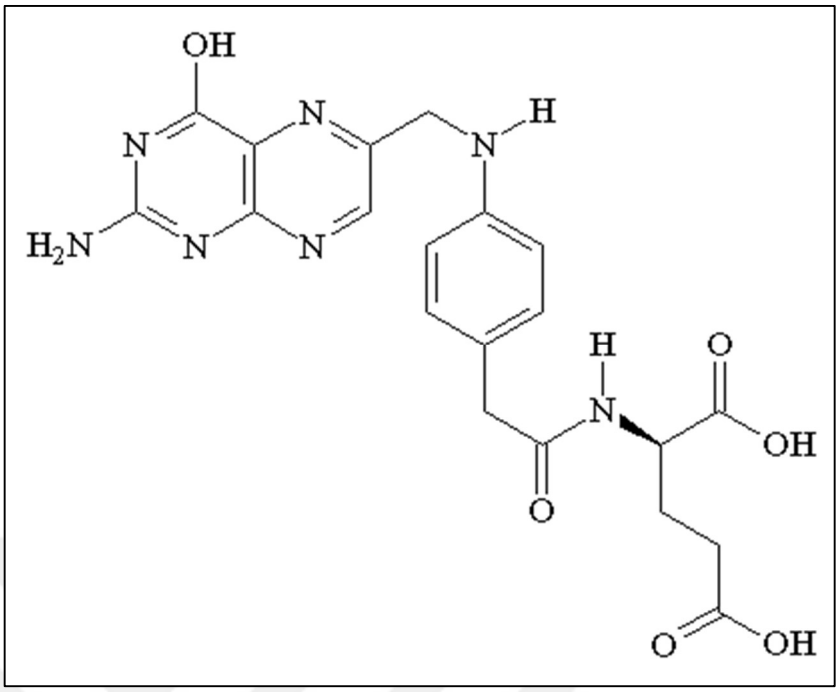

Figure 3.5. Folic acid chemical structure [90]

Folate receptors are overexpressed in tumor cells [91]. The receptor has been identified as a tumor marker, especially in ovarian carcinomas. Folic acid metabolizes to folate within the human body. Structure difference between folic acid and folate can be seen at Figure 3.7. In this study, folic acid was used for this property. The conjugation of folic acid to the drugs or drug carriers, can make drugs more potent and selective to tumoral cells. Thus, in this study, in addition to the preparation of PPF/VPA microparticles via UV miniemulsion polymerization as drug delivery agents, preliminary studies on conjugation of folic acid to the PPF-prepolymer and the UV-miniemulsion polymerization of the PPF-FA pre-polymer with VPA to produce microparticles were also carried out.

3.2. METHODS

3.2.1. Differential Scanning Calorimetry (DSC)

Enthalpy is measured using Differential Scanning Calorimetry (DSC) in relation to temperature and time. DSC is most commonly used to investigate phase transitions such as melting, glass transitions, and exothermic decompositions. These transitions necessitate

changes in energy or heat capacity, which may be measured with excellent sensitivity using DSC.

DSC works with a reference sample. Temperature difference between reference sample and real sample gives the thermogram, which can be interpreted as melting, crystallization, and other various phase transitions [92]. In Figure 3.6, the typical thermogram and working principle of DSC can be seen.

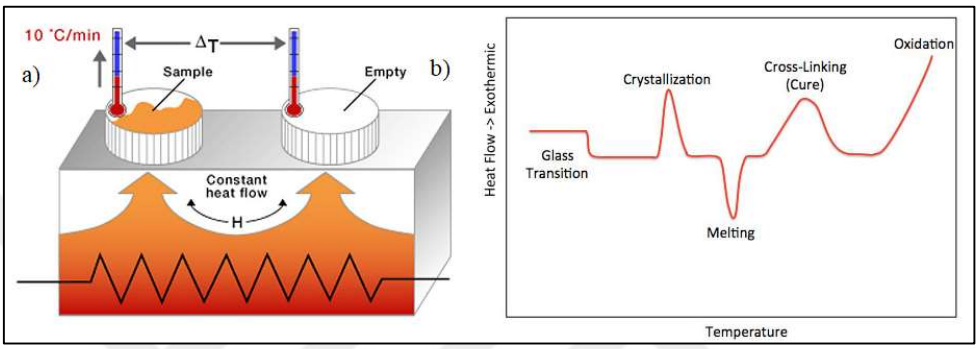

Figure 3.6. A) Working principle of DSC [93] B) A typical thermogram [94]

3.2.2. Scanning Electron Microscopy (SEM)

The scanning electron microscope (SEM) is a device that uses a focused beam of electrons to scan the surface of a sample and make photographs of it. Atoms interact with the beam in diverse ways, providing information on the sample's surface topography and composition. This requires a secondary electron detector which is amplified during the imaging. In Figure 3.7, SEM working principle can be seen.

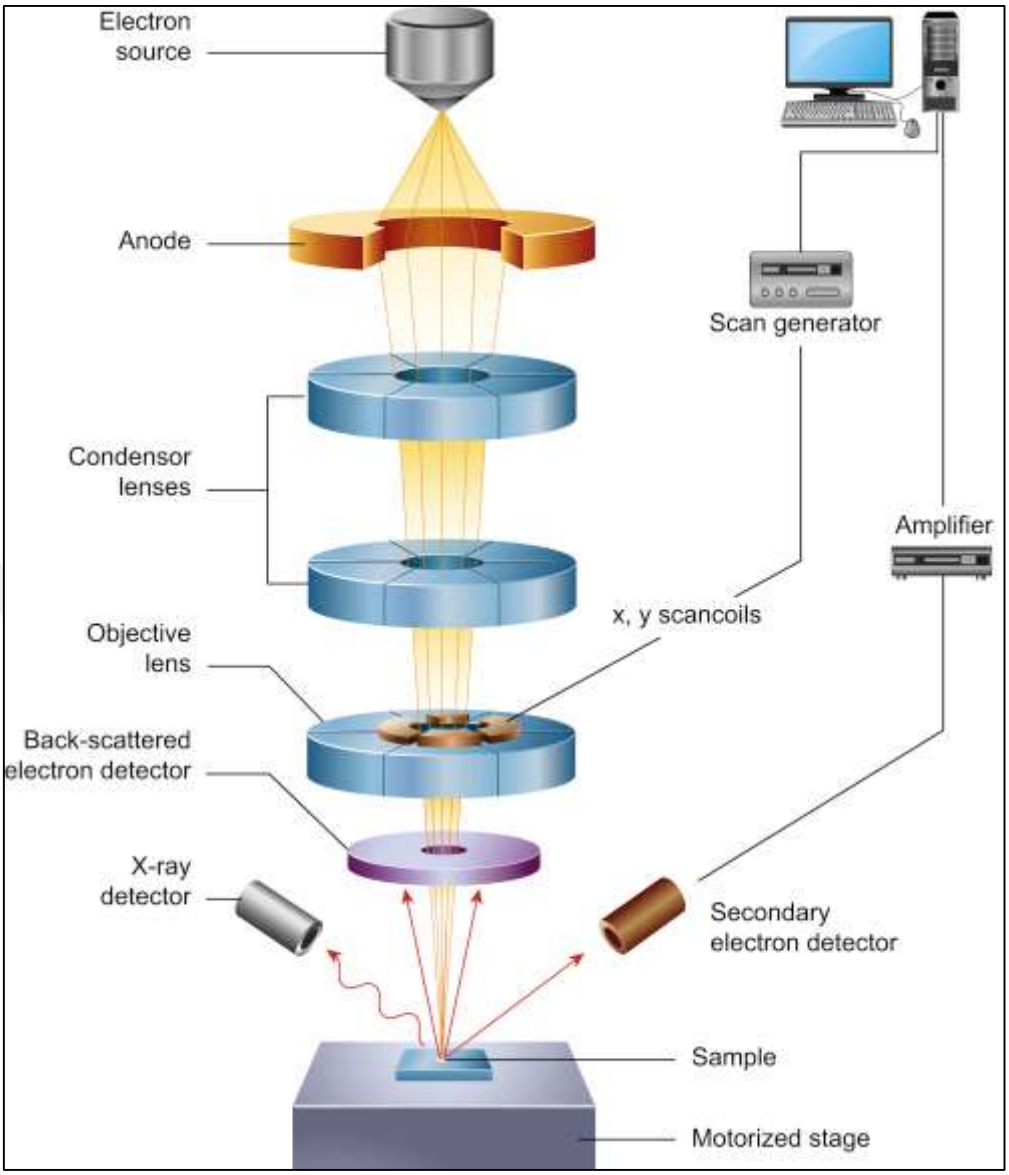

Figure 3.7. Working principle of scanning electron microscope [95]

SEM consists of an electron source which sends electrons to anode. Electron source is a heated filament which releases electrons. Electrons are collimated into a beam by an aperture. Secondary electrons (SE) reflected or back-scattered electrons (BSE), characteristic X-rays and light (cathodoluminescence) (CL), absorbed current (specimen current), and transmitted electrons are some of the signals that can be produced.

Electron beam is focused to the sample with condenser lenses. Focused electron beam is reflected back from the sample and a detector detects the signals and interpret them as height.

3.2.3. Gel Permeation Chromatography (GPC)

Gel permeation chromatography (GPC) is a technique that separates the solution components relative to their size. It is used generally for polymers. Polymers can be characterized according to their average molecular weights and polydispersity index. These all can be calculated via GPC [96].

Porous beads placed in a column are used to separate analytes based on their size. The method of operation is based on the fact that smaller molecules may enter pores more easily and spend more time in them, increasing their retention time. As a result, these smaller molecules will spend more time in the column and elute later. Larger molecules, on the other hand, spend less time in the pores and are eluted more quickly. The molecular weights that various columns can separate are varied.

The porous beads within a column have different pore size. This provides measurement of weight difference between samples. Detection time and peaks are reference for the molecular weight of the sample.

3.2.4. Fourier Transform Infrared Spectroscopy (FT-IR)

The method of obtaining an infrared spectrum of absorption or emission of a solid, liquid, or gas is known as Fourier-transform infrared spectroscopy (FT-IR). The FT-IR spectrometer obtains high-resolution spectral data over a large spectral range at the same time ($400cm^{-1}$- $4000cm^{-1}$).In this method a mathematical process: Fourier transform is required to convert the raw data into the actual spectrum. FT-IR spectroscopy is used to detect different functional groups in PHB.

3.2.5. Proton Nuclear Magnetic Resonance (^{1}H-NMR) Spectroscopy

This method applies nuclear magnetic resonance with respect to proton (Hydrogen-1) within the molecules [97]. This technique can characterize the chemical structure of molecules.

Nuclei in a strong constant magnetic field are agitated by a weak oscillating magnetic field (in the near field) and respond by creating an electromagnetic signal with a frequency characteristic of the magnetic field at the nucleus.

A ^{1}H-NMR spectrometer produces graphs with signal intensity versus chemical shift. Graph can be interpreted from difference on chemical shifts. The exact value of chemical shift is determined by molecule structure, solvent, temperature, magnetic field used to record the spectrum, and other functional groups in the vicinity.

To produce ^{1}H-NMR spectrum, usually deuterated solvents are used. This deuterated solvent also has its characteristic peak due to the proton residues.

3.2.6. High Performance Liquid Chromatography (HPLC)

HPLC is a high-performance version of thin layer chromatography. It relies on passing liquid solution through solid absorbent material. Solid absorbent material passes different molecules with different retention times. With retention time and the peak area, solution composition can be interpreted. In Figure 3.8, HPLC working principle can be seen.

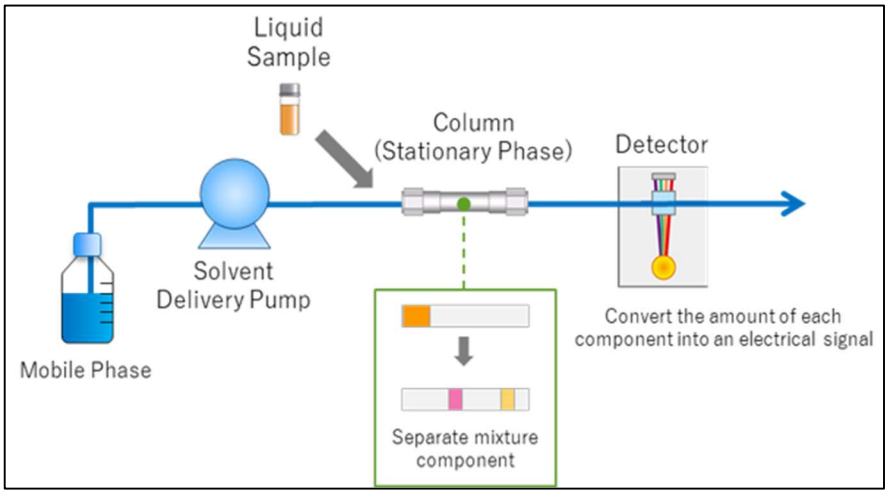

Figure 3.8. Working principle of HPLC [98]

4. EXPERIMENTAL

4.1. SYNTHESIS OF PPF

The traditional synthesis method for the production of PPF utilizes a step growth polymerization of either fumaric acid [72] or diethyl fumarate [99] with propylene glycol (Figure 4.1). In this study, fumaric acid was reacted with an excess of propylene glycol in the presence of p-toluene sulfonic acid as the catalyst and hydroquinone as the radical inhibitor to produce a hydroxyl terminated PPF pre-polymer. Sandarson devised an alternate PPF synthesis process that involved the transesterification of diethyl fumarate and propylene glycol at 250 °C with p-toluene sulfonic acid as the catalyst. Poly(propylene fumarate) diol was synthesized using this approach, with Mn values ranging from 500 to 1200 Da and a molecular mass distribution of 3 to 4.

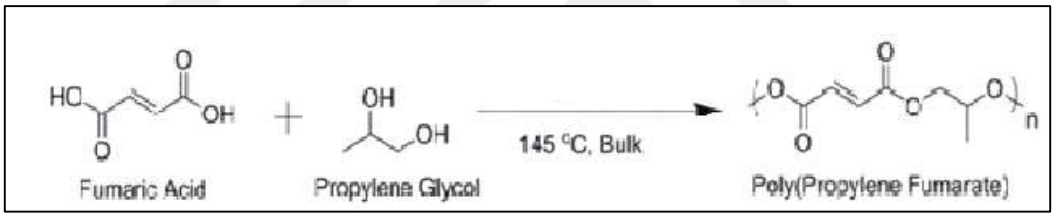

(a)

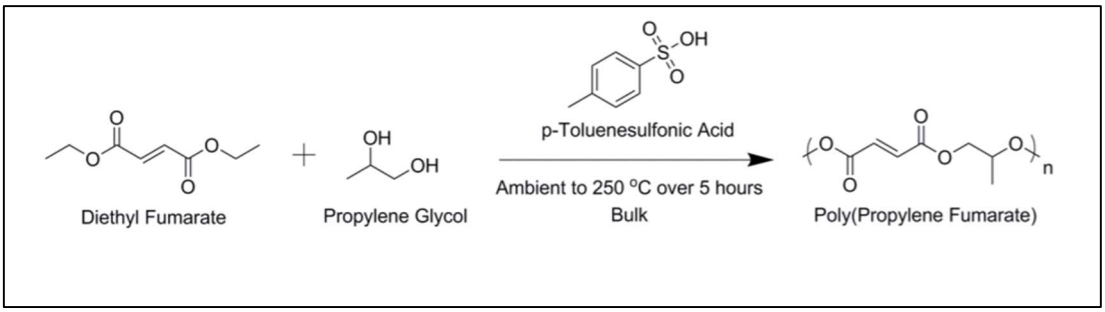

(b)

Figure 4.1. Poly (propylene fumarate synthesis via (a) fumaric acid propylene glycol reaction [72] (b) transesterification of diethyl fumarate and propylene glycol [99]

In this study, for PPF synthesis, 125.5 grams of propylene glycol (PG) and 174.1 grams of fumaric acid (FA) (FA:PG mole ratio=1.5:1.65) were put into a 500 ml round bottom flask equipped with mechanical stirrer, a thermocouple, a nitrogen gas inlet, and a Dean-Stark apparatus connected to a condenser. Then, 1.203 grams of p-toluene sulfonic acid catalyst and 0.290 grams of hydroquinone radical inhibitor were added to the mixture in the flask. The contents of the flask were heated to 145°C using a heating mantle. After heating, solution was stirred at this temperature for 3 hours at 100-150 rpm. At the end of heating for 3 hours at 145°C, the temperature of the reaction medium was increased to 180°C, and the solution was stirred at this temperature for 1 hour. Approximately, 30 ml water was collected as the byproduct of the reaction. At the end of 1 hour at 180°C, the solution was left to cool to room temperature to prevent further polymerization. In Figure 4.2, the polycondensation reaction for PPF synthesis is shown.

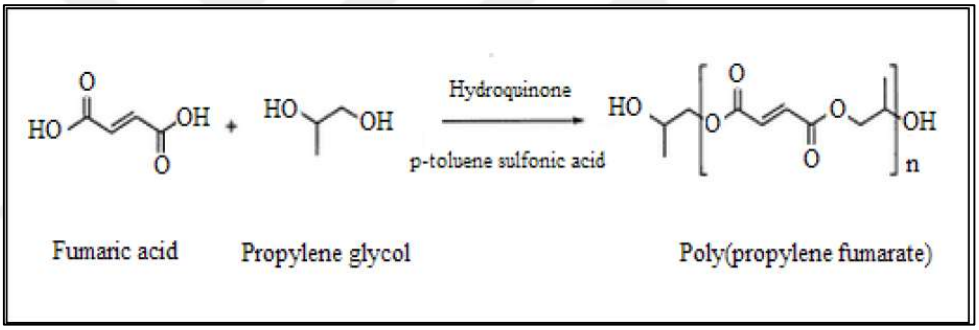

Figure 4.2. Polycondensation reaction for PPF synthesis [72]

For the purification of the poly (propylene fumarate) product, it was first heated in an oven to around 130°C to reduce its viscosity and it was transferred to a beaker. Crude PPF was dissolved in 150 ml of dichloromethane. Vacuum filtration was performed in order to eliminate catalyst and the unreacted fumaric acid. After vacuum filtration, 100 ml of 20:80 ratio of methanol-water solution was prepared and the PPF solution was washed with the methanol-water solution. There was 80 ml water with unreacted propylene glycol at the top phase. PPF in dichloromethane was at the bottom phase. The PPF solution was taken, and the top phase was discarded. Anhydrous calcium chloride ($CaCl_2$) was added to PPF solution in order to eliminate residual water; calcium chloride was added until the solution became totally clear. Vacuum filtration was performed in order to remove calcium chloride. Finally, 150 ml of diethyl ether was added to the PPF solution in dichloromethane and the PPF in the diethyl ether phase was taken. Solution was put into rotary evaporator to evaporate the added

diethyl ether. Finally, the obtained 21.1 grams PPF product was a yellow colored, transparent viscous resin at room temperature.

4.2. PPF/VPA NANOPARTICLE SYNTHESIS

In order to synthesize PPF/VPA nanoparticles, 0.25 grams of SDS was added to 100 mL water, and solution was stirred overnight. 0.38 g. of PPF was dissolved in 5 mL DCM. For the ratio of 70/30: PPF/VPA, 0.163 grams (0,119 mL) of VPA was added to the PPF solution. Afterwards, 0.0002172 grams (0.04wt percent) of Titanium acetyl acetonate and 0.0163 grams of BAPO (3wt percent) were also added to this solution. After dissolving the catalyst and the initiator, 20 mL of SDS solution was poured into the PPF/VPA solution (establishing 9wt percent based on PPF/VPA weight). Solution was then homogenized in a homogenizer for 5 minutes at 1000 rpm. This solution was later irradiated under UV light (365 nm) for 2 hours, with stirring**.** At the end of this time, the solution was centrifuged in order to obtain polymer particles. Polymer particles were then washed with 10 mL water in order to get rid of surfactant. Particles were then put into a freeze dryer for 3 days to remove water. Procedure was repeated for 1 hour of UV cure time and for 5-, 10-, 15- and 30-minutes homogenization time as summarized in Table 4.1. For Paclitaxel loading, 4 mg of Paclitaxel was added to the PPF/VPA solution and homogenized before the addition of the catalyst, initiator and the SDS solution and the same procedure was applied.

Table 4.1. Changed parameters for PPF/VPA particle synthesis

Homogenization time (min)	**UV Cure time (hrs.)**
5, 10, 15, 30	1, 2

4.3. CONJUGATION OF FOLIC ACID TO PPF: PPF-FA SYNTHESIS

To achieve cancer specific targeting abilities, drugs can be prepared with a tumor targeting molecule. To achieve apoptosis of tumor cells a cancer drug must be added to formulation. To achieve stable release and linear profile, stable backbone of polymer is needed. In this study, Paclitaxel is used for the apoptosis of tumor cells and PPF/VPA network polymer is

the stable backbone on this drug formulation. In addition, folic acid was also conjugated to PPF, and particles based on folic acid modified PPF (PPF-FA) and VPA were also prepared. Folic acid is usually delivered into cells via attaching to the folic acid receptor on the cell membrane, which is overexpressed in cancer cells.

For the synthesis of folic acid modified PPF (PPF-FA), DMAP and dehydrant DCC catalytic system were used. DCC/DMAP coupling is a good way to bind tumor-targeting ligands to polymer chains that have hydroxyl groups at the end [3]. Thus PPF-FA conjugation will be obtained by the Steglich esterification reaction between hydroxyl groups of PPF pre-polymer and carboxyl groups of FA. Steglich esterification reaction requires dicyclohexylcarbodiimide as a coupling agent and 4-dimethylaminopyridine as a catalyst. Steglich esterification mechanism can be described as depicted in Figure 4.3 [100];

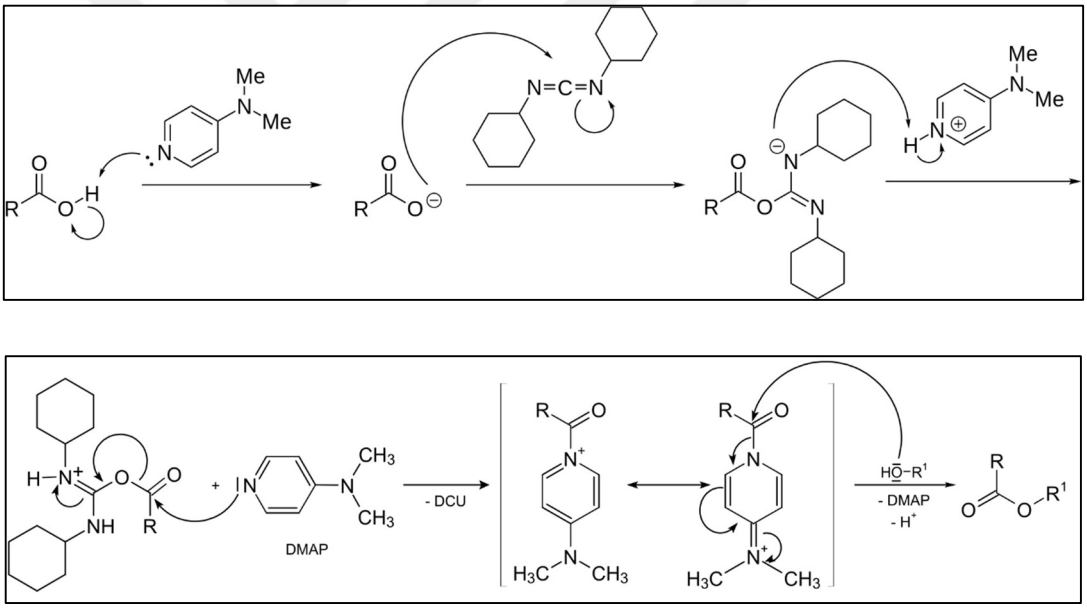

Figure 4.3. Mechanism of the Steglich Esterification [100]

First, the carboxylic acid group of the compound reacts with the DMAP which creates an ion. That ion reacts with the DCC's intermediate carbon to form DCC- conjugated carboxylic acid. Then, the hydrogen in the DMAP reacts with the nitrogen to form NH bond as can be seen at the Figure 4.3. Finally, newly formed compound reacts with the DMAP which forms the ester. In this study, compound with the hydroxyl group is PPF and

conjugation with the carboxylic acid group of FA can be formed with the DMAP and DCC via Steglich esterification reaction.

Approximately 0.5 mmol PPF (0.54575 grams) was added to 0.5 mmol (0,2207 grams) of folic acid along with 3.45 mmol (0.71 g) of dehydrant DCC, 0.4 mmol (50 mg) of catalyst, DMAP in 100 milliliters of anhydrous DMSO. The prepared solution was stirred for 24 hours at room temperature. At the end of this time, solution was filtered by vacuum filtration in order to remove residual unreacted chemicals. Filtrate was then washed and precipitated with 6.25 mL methanol and 93.75 mL of diethyl ether mixture for 5 times to get rid of the unreacted folic acid. Filtrate was put into a vacuum oven at 60 ºC for 48 hours. The dried PPF-FA product was kept at -20 ºC for future use. This procedure was also performed with 0.1 mmol PPF and 0.1 mmol FA along with 0.69 mmol (142 mg) of dehydrant DCC, 0.08 mmol (10 mg) of catalyst DMAP and 20 milliliters of anhydrous DMSO. In addition, the same procedure was also applied changing the PPF: FA mole ratio using 0.1 mmol PPF and 0.2 mmol FA keeping the catalyst concentration and solvent amount constant.

4.4. PPF-FA/VPA NANOPARTICLE SYNTHESIS

The folic acid conjugated PPF product was also polymerized with VPA via UV mini emulsion polymerization to prepare PPF-FA/VPA nanoparticles. First the optimized procedure utilized for PPF/VPA particle synthesis was used for the PPF-FA/VPA particle synthesis. For this purpose, first 0.25 grams of SDS was added to 100 mL water, and this solution was stirred overnight. 0.38 gr PPF-FA was dissolved in 5 mL DCM. For the weight ratio of 70/30: PPF-FA/VPA, 0.163 grams (0.119 mL) of VPA was added to the PPF-FA solution. Afterwards, 0.0002172 grams (0.04wt percent) of Titanium acetyl acetonate (TAA) catalyst and 0.0163 grams of BAPO initiator (3wt percent) were added to this solution. After dissolving the catalyst and the initiator, 20 mL of SDS solution was poured into PPF-FA/VPA solution (establishing 9wt percent SDS based on PPF-FA/VPA weight). Solution was homogenized in a homogenizer for 10 minutes at 1000 rpm. This solution was then irradiated under UV light (365nm) for 2 hours with stirring. At the end of this time, the solution was centrifuged in order to obtain polymer particles. Polymer particles were then washed with 10 mL water in order to get rid of surfactant. Particles were then put into a freeze dryer for 3 days to remove residual water. The UV mini - emulsion polymerization of

PPF-FA with VPA was also carried out with 0.06, 0.1 and 0.2 wt. percent TAA, with 15 and 20 wt. percent surfactant concentrations and 2 weight percent BAPO concentration keeping other conditions of the procedure the same. Initiator, catalyst, and surfactant concentrations used in PPF-FA/VPA particle synthesis are presented in Table 4.2. For Paclitaxel loading, 4 mg of Paclitaxel was added to the PPF-FA/VPA (0.38 g PPF-FA, 0.163 g VPA) solution and homogenized before the addition of the catalyst (0.04wt percent), initiator (3wt percent) and SDS (9wt percent) solution and the same procedure was applied.

Table 4.2. Initiator, catalyst, and surfactant concentrations used in PPF-FA/VPA particle synthesis

PPF-FA/VPA: 70/30 (wt. ratio)		
Surfactant (SDS) Concentration (wt. percent)	**Initiator (BAPO) Concentration (wt. percent)**	**Catalyst (TAA) Concentration (wt. percent)**
9	3	0.04
9	3	0.06
15	3	0.04
15	3	0.06
15	3	0.1
15	3	0.2
15	2	0.04
20	3	0.04

4.5. CHARACTERIZATION PPF AND PPF-FA

4.5.1. FT-IR Spectroscopic Analysis

In this study, FT-IR was used for the structural characterization of folic acid modified PPF (PPF-FA) and PPF/VPA particles. All samples were analyzed with the Thermo Scientific IS50 FT-IR spectrometer. For FT-IR analysis of the PPF-FA pre-polymer, first a background

scan of air was taken. Then, sample taken with a spatula tip and placed in the sample cell was scanned 16 times with a resolution of 4 cm^{-1} in the 400-4000 cm^{-1} range. For the PPF and PPF/VPA polymers, samples were analyzed preparing KBr disc pellets. Approximately 10000 psi pressure was applied when preparing KBr disc pellets. After background scanning of pure KBr pellets, each sample was scanned 16 times in the range of 400-4000 cm^{-1}, with a resolution of 4 cm^{-1}.

4.5.2. ^{1}H-NMR Spectroscopic Analysis

In this study, ^{1}H-NMR was used for the structural characterization of PPF and folic acid modified PPF (PPF-FA) pre-polymers. Samples were prepared dissolving 0,1 grams PPF, PPF-FA or PPF-FA/VPA in 1 ml Deuterated Chloroform. For ^{1}H-NMR spectroscopic analysis, a Bruker AM250 spectrometer with a magnetic field strength of 250MHz was used. A spectral window of 2000Hz, pulse width of 90^{o} with a digital resolution of 0.427 Hz/pt. were used for the measurements which were performed at room temperature (25^{o}C).

4.5.3. GPC Analysis

Gel Permeation Chromatography (GPC) analysis was used to determine the molecular weight of PPF pre-polymer. A Tosoh Ecosec HLC 8320GPC Series model device with flow marker 250 ppm butylated hydroxytoluene was used. The device was equipped with a refractive index detector. Flow speed was set as 0.6 mL/min at 25^{o}C. Tetrahydrofuran (THF) was used as the solvent and the colon used was TSKGel SuperHM-M (6.0 mm I.D. x 15 cm. 3μm). Calibration was performed with linear polystyrene standards having number average molecular weights between 578-427000 g/mol. Samples were analyzed at room temperature (25^{o}C).

4.6. CHARACTERIZATION OF PPF/VPA AND PPF-FA/VPA PARTICLES

4.6.1. Gel Content Analysis

Gel content analysis simply gives a measure of the extent of the cross-linking for the prepared particles. Swelling test was performed to determine the gel content of the synthesized PPF particles. For gel content (wt. % of cross-linked portion) analysis of PPF/VPA and PPF-FA/VPA nanoparticles, first initial weight of the particles ($Weight_{initial}$) were recorded (of about 0.17g) and then nanoparticles were mixed with 3 mL of distilled water and kept in water at room temperature for two days. The swollen crosslinked PPF nanoparticles were dehydrated using a freeze dryer. The particles were subsequently immersed in 3 mL THF and kept in THF for two days. Finally, particles were dried in a vacuum oven at 60℃ for another two days. Experiments were done in triplicates. Dried samples were weighed and weight of sample ($Weight_{final}$) was recorded. Gel content (percent) was calculated according to Equation 4.1.

$$Gel\ content(Percent) = \frac{Weight_{final}}{Weight_{Initial}} x100 \tag{4.1}$$

4.6.2. DSC Analysis

DSC analysis of the UV cured PPF/VPA particles were performed using the "SETARAM DSC 131 Calorimetry and Thermal Analyzer" device. The DSC 131 SETARAM device had a temperature range of -170 to 700 ºC, a resolution of 0.4 µW, crucibles volume between 30 to 100µl and noise RMS of 0.8 µW. For each analysis, approximately 0.17 g. sample was heated from 25°C to 250°C at a rate of 5°C/minute in nitrogen gas atmosphere, with second heating when necessary. For each measurement, heat flow (mW) vs. temperature (°C) graphs were constructed and analyzed. The DSC analysis was primarily used to see if the cure reactions of the PPF/VPA samples were complete or not and also to obtain information about the glass transition temperatures (Tg) of the samples.

4.6.3. SEM Analysis

Scanning electron microscopic analysis was used to determine the morphology and size of crosslinked PPF/VPA and PPF-FA/VPA polymer particles. Surface of the sample coated with Platinum with Polaron SC7640 sputter coater device for a minute. FEI-Philips XL30 ESEM-FEG Scanning Electron Microscopy and Energy-Dispersive X-Ray Analyzer / Image Analysis system was used. SEM device has 10^{-9} torr and better vacuum capacity, area emission electron gun (BC Stability <1 percent /hour, Schottky Emitter), 2-5 nm resolution at spot 2 conditions. It has LFD/ GSED/ ESD detectors and vacuum system assemblies (PLA).

4.6.4. Degradation Analysis via Weight Loss and pH Measurements

Degradation profiles of the prepared polymeric particles were examined via both weight loss and pH measurements. For weight loss measurements, about 0.07 g of PPF/VPA polymer particles was weighed and placed in 10 mL phosphate-buffered saline (PBS) at pH 7.4. Samples were then placed in an orbital shaker (MaxQ Mini 4450) at 37 ℃ at 100 rpm. One sample was removed every week (on weeks 1, 2, 3, 4, 5 and 6) from the PBS solution, washed with water to remove excess PBS and were then freeze-dried and weighed. After lyophilization, difference between the initial and final weight was determined and the weight loss of the polymer particles due to degradation was analyzed as a function of time.

For degradation measurements with pH, first about 0.15 g of the PPF/VPA particles was placed in 10 mL phosphate-buffered saline (PBS) at pH 7.4. Then, samples were placed in an orbital shaker (MaxQ Mini 4450) at 37 ℃ at 100 rpm. The pH values were measured using a WTW inoLab 740 model instrument, every 24 hours for the first 5 days and then weekly. The PBS solution was changed every week. For both weight loss and pH measurements, experiments were done twice.

4.7. ANALYSIS OF DRUG RELEASE FROM PPF PARTICLES VIA HPLC ANALYSIS

PPF/VPA particles with embedded Paclitaxel were washed three times to remove excess Paclitaxel that may reside on the surface of the particle. For drug release studies, about 0.17 grams of the PPF/VPA particles were put in 5 ml PBS at pH=7.4. Right after the initial introduction of the particles in buffer solution, supernatant was immediately removed by centrifugation to determine the initial amount of release. Then 5 mL PBS was added on particles in test tubes and test tubes were placed in an orbital shaker at 37 ℃ operating at 100 rpm. After each predetermined amount of time, supernatant was removed to measure the released amount of Paclitaxel, and a fresh aliquot of PBS was added to the test tubes. The amount of drug release from the particles was measured through 86 days (on days 1, 5, 8, 12, 15, 19, 22, 26, 30, 34, 38, 42, 46, 50, 54, 58, 62, 66, 70, 74, 78, 82, 86). Drug release studies were done in duplicates.

The amount of drug released from the particles to the buffer solution was determined using HPLC. A Shimadzu HPLC system equipped with 2487 UV-Vis detector, 1525 binary pump, 717 autosampler and Degasser was used for drug release studies. The amount of Paclitaxel released was determined as described in relevant studies [21] with some modifications. A X-Bridge C-18 column (150×4.6 mm, particle size 5 μm), was used and the temperature of the column was set to 30 ℃. The mobile phase was composed of solvent X (0.5% H_3PO_4 aqueous solution) and solvent Y (Methanol), and gradient elution conditions were used as listed in Table 4.3 [101]. The flow rate was set to 1.0 ml/min. Injection volume was 50 μL and injections were performed in duplicate. UV absorbance at 227 nm was used for Paclitaxel. In order to construct the calibration curve, Paclitaxel solutions were prepared in 75 percent ethanol solution.

Table 4.3. Gradient elution conditions for HPLC analysis of Paclitaxel

Time (min)	%X	%Y
0.01	94.0	6.0
3.00	94.0	6.0
3.50	35.0	65.0
16.00	35.0	65.0
16.50	94.0	6.0
18.50	94.0	6.0

5. RESULTS AND DISCUSSION

In this study, poly propylene fumarate (PPF) pre-polymer was copolymerized with 30 wt. percent of VPA which may behave differently in different pH mediums to produce PPF/VPA copolymer with a mainly hydrophobic PPF component to form nanoparticles via UV mini-emulsion polymerization. These PPF/VPA nanoparticles which biodegrade over time to nontoxic species were examined as Paclitaxel drug delivery agents. Moreover, preliminary studies on the synthesis folic acid conjugated PPF and its copolymerization with VPA via UV mini-emulsion polymerization to produce PPF-FA/VPA nanoparticles were also carried out to produce nanoparticles that are expected to be selective towards cancer and tumor cells.

First, procedure for PPF/VPA nanoparticle synthesis via UV-mini emulsion polymerization has been optimized. The PPF/VPA particles prepared were characterized by gel content analysis, DSC, and FT-IR spectroscopy. Size and morphology of particles were characterized via SEM, degradation profiles in PBS (pH=7.4) at 37ºC were investigated via weight loss and pH measurements and finally Paclitaxel drug release from PPF/VPA nanoparticles was investigated using HPLC. PPF pre-polymer and folic acid modified PPF (PPF-FA) were characterized with FT-IR and ^{1}H-NMR spectroscopy and molecular weights were determined via GPC. The synthesized PPF-FA/VPA particles were characterized with gel content analysis and DSC, morphology of the particles was analyzed via SEM. The results, analysis and discussions based on the obtained data are presented in the following sections.

5.1. POLY (PROPYLENE FUMARATE) SYNTHESIS

Poly (propylene fumarate) synthesized exhibited a number average of molecular weight of 1091.5 g/mole, weight average molecular weight of 1239.3 g/mole and a polydispersity index of 1.135. The GPC chromatogram for this analysis is presented in Appendix A (Figure A 1). The FT-IR and ^{1}H-NMR spectroscopic analysis of the PPF pre-polymer will be presented in the structural characterization of the folic acid modified PPF product and PPF/VPA particles.

5.2. CHARACTERIZATION OF PPF/VPA NANOPARTICLES

5.2.1. Gel Content Analysis

For the UV mini emulsion polymerization of PPF pre-polymer with VPA, reaction conditions optimized for the UV mini emulsion polymerization of PPF pre-polymer with vinyl pyrrolidone to produce nanoparticles in a related study [101] was used. Thus, for the UV mini emulsion polymerization of PPF pre-polymer with VPA, BAPO was used as a radical initiator in the presence of 9 wt. percent SDS as the surfactant with homogenization of the emulsions in a homogenizer at 1000 rpm. On the other hand, in order to facilitate the UV photo-polymerization of PPF with VPA, titanium acetyl acetonate (TAA) was used as a catalyst at 0.04wt% concentration with 3wt% BAPO initiator based on PPF/VPA total weight using the results of optimization studies for the cure of PPF with VPA in the presence of benzoyl peroxide initiator, N, N-DMT catalyst and TAA co-catalyst (crosslinker) at room temperature [102].

Thus, in the first set of experiments, PPF pre-polymer was photo-polymerized with VPA at a 70:30 weight ratio using 3wt% BAPO initiator, 0.04wt% TAA in the presence of 9 wt. percent SDS as surfactant changing the UV cure time as 1 and 2 hours and homogenization time of the mini emulsions as 5,10,15 and 30 minutes. The gel content of each of the synthesized particles was determined in order to determine the conditions for achieving highest extent of cross-linking. Gel content (weight percent) of the PPF/VPA particles synthesized at different UV mini-emulsion polymerization conditions are given in Table 5.1.

As can be seen from the data presented in Table 5.1, 10 minutes homogenization time resulted in the highest gel content for both 1 and 2 hours of UV cure time. This can be explained with the emulsion polymerization kinetics. The homogenization time must be long enough that emulsions can occur with stability. It may be postulated that, 15- and 30-minutes homogenization time de-stabilize the emulsions while 5 minutes homogenization time is not enough to form stable emulsions. The increase of UV cure time from 1 to 2 hours for 10 minutes homogenization time resulted in an increase in gel content from 85.1 to 87.6 percent whereas the cure time did not affect the gel content for samples prepared with 5,15- and 30-minutes homogenization time. Thus, for the UV mini emulsion polymerization of PPF with VPA, with 3 wt. % BAPO initiator, 0.04 wt. % TAA and 9 wt. percent of SDS surfactant,

10 minutes homogenization time and 2 hours of UV cure time resulted in the highest efficiency of cross-linking.

Table 5.1. Gel content of the PPF/VPA particles synthesized at different UV mini-emulsion polymerization conditions

Homogenization Time (min)	**UV Cure Time (Hrs.)**	
	1	2
	Gel Content (wt.%)	
5	82.32±0.27	83.23±0.14
10	85.14±0.12	87.63±0.17
15	83.12±0.2	83.2±0.21
30	80.23±0.7	79.94±0.51

5.2.2. Results of DSC Analysis

Differential scanning calorimetry (DSC) was also used to analyze the possible post-cure reactions and thermal transitions of the synthesized PPF/VPA particles. Figure 5.1 shows the DSC spectra of PPF/VPA particles prepared via UV emulsion polymerization at different homogenization times (5,10,15,30 min) (a) and that were UV cured for 1, 2 and 3 hours(b). For the DSC thermograms presented the endothermic peaks in the 50-60^{o}C region must correspond to the glass transition temperature (T_g) of these network polymers. In a related study by our group, the T_g of PPF/VPA copolymers that were thermally cured in the presence of 3wt percent benzoyl peroxide (BP) were reported to be 73 ^{o}C as determined from the tan delta maxima via dynamic mechanical analysis (DMA) [72]. Wang et al. [52] also synthesized PPF copolymers which resulted in higher glass transition temperatures than pure PPF polymers that exhibit Tg's in the -30 and 32 ℃ interval [103]. The fact that none of these spectra exhibit major exothermic peaks indicate that the cure reaction of PPF pre-polymer with VPA was nearly complete via the UV cure process of the emulsions.

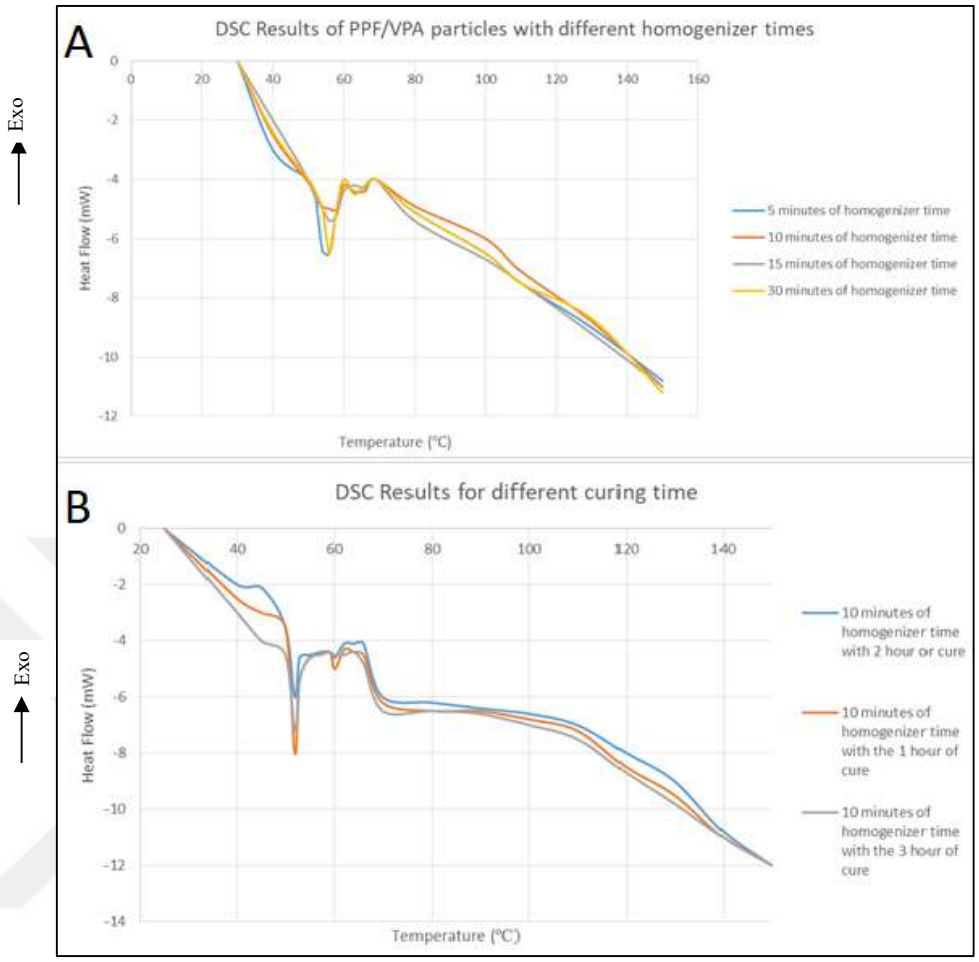

Figure 5.1. DSC thermograms of PPF/VPA particles (a) synthesized with different homogenization times (2 hours UV cure) (b)UV cured for 1,2 and 3 hours.

5.2.3. Fourier Transform Infrared (FT-IR) Spectroscopy Results

PPF/VPA particles prepared via UV mini-emulsion polymerization under the optimized conditions were also characterized via FT-IR spectroscopy. The FT-IR spectra of PPF with PPF/VPA product is presented in Figure 5.2 (a) and that of VPA monomer is presented in Figure 5.2 (b). The major characteristic peaks were identified at 1715 and 1644 cm^{-1} in the spectrum of PPF corresponding to the C=O stretching and C=C stretching bands, respectively. The FT-IR spectrum of VPA showed major characteristic peaks between 2400 and 3000 cm^{-1}, representing the O-H stretch of the phosphonic acid side groups, bands between 1090 and 905 cm^{-1} representing the P-O stretch of the phosphonic acid side group. The peak at around 1614 cm-1 on other hand should correspond to VPA C=C stretching vibrations [104]. After the cross-linking reaction of PPF pre-polymer with VPA, the peak at

1715 cm^{-1} that belongs to C=O stretching should remain constant whereas the peak at 1644 cm^{-1} that belongs to C=C stretching must decrease its absorbance intensity which can be visualized in Figure 5.2 (a). The decrease in the ratio of the absorbance intensity of PPF (C=C) stretching peak at 1644 cm^{-1} to that of carbonyl peak at 1715 cm^{-1} indicated that about 84.8 percent of the fumarate double bond was consumed throughout the UV cure reaction at the end of 120 minutes. The weak band at 1614 cm^{-1} associated with VPA (C=C) stretching seemed to disappear as a result of the radical polymerization whereas the 1086 cm^{-1} peak associated with VPA (P-O) stretching vibration was also present in the spectrum of the PPF/VPA polymer.

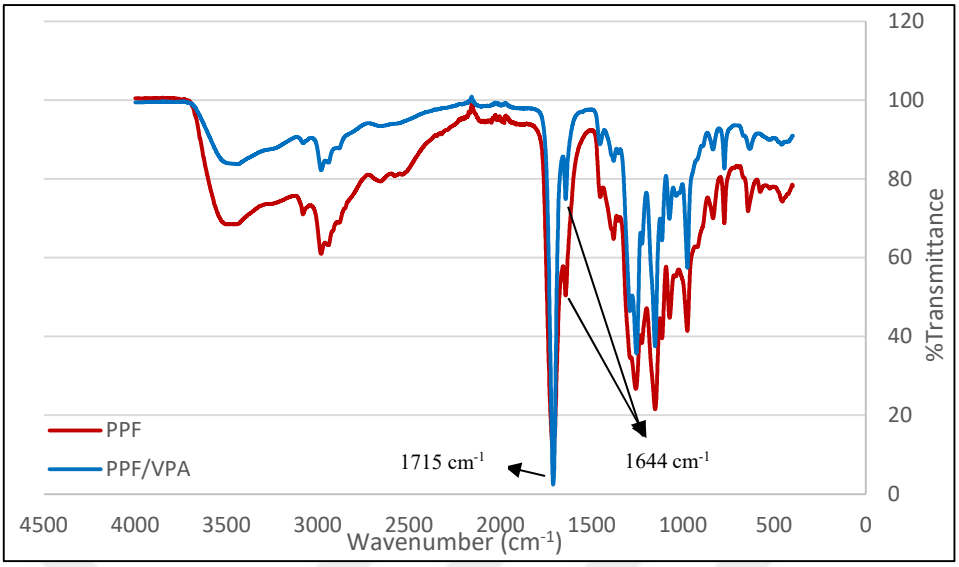

(a)

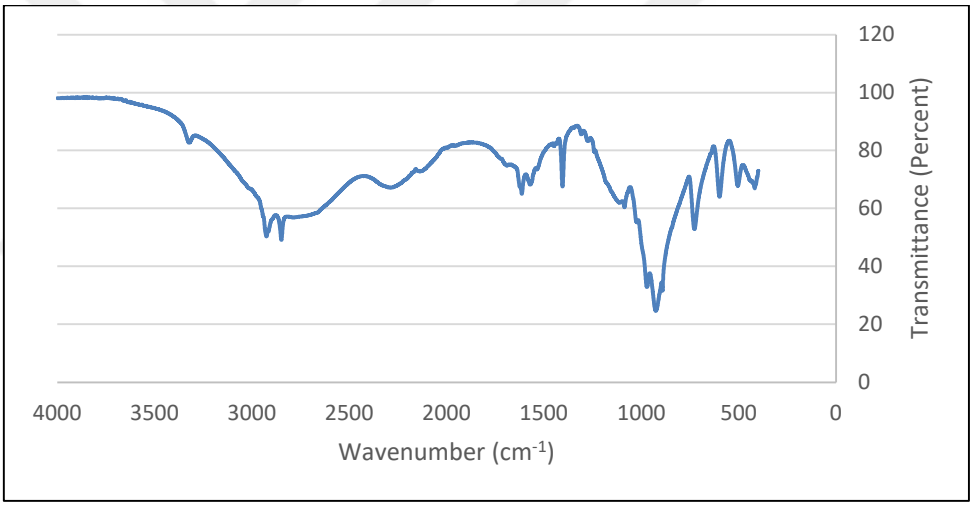

(b)

Figure 5.2. FT-IR spectra of (a) PPF with PPF/VPA and (b) VPA

5.2.4. Scanning Electron Microscopic (SEM) Analysis

In order to analyze the morphology and size of the PPF/VPA particles, scanning electron microscopy was used. Particle formation was observed for all the PPF/VPA particles prepared under the optimized reaction conditions (3wt percent BAPO, 0.04 wt. percent TAA, 9wt percent SDS, 2 hours UV cure) that were homogenized for different periods of time. Figure 5.3 shows the SEM images of PPF/VPA particles prepared with 5 minutes

homogenization time which indicate formation of spherical particles which were not as distinct as those observed with longer homogenization times.

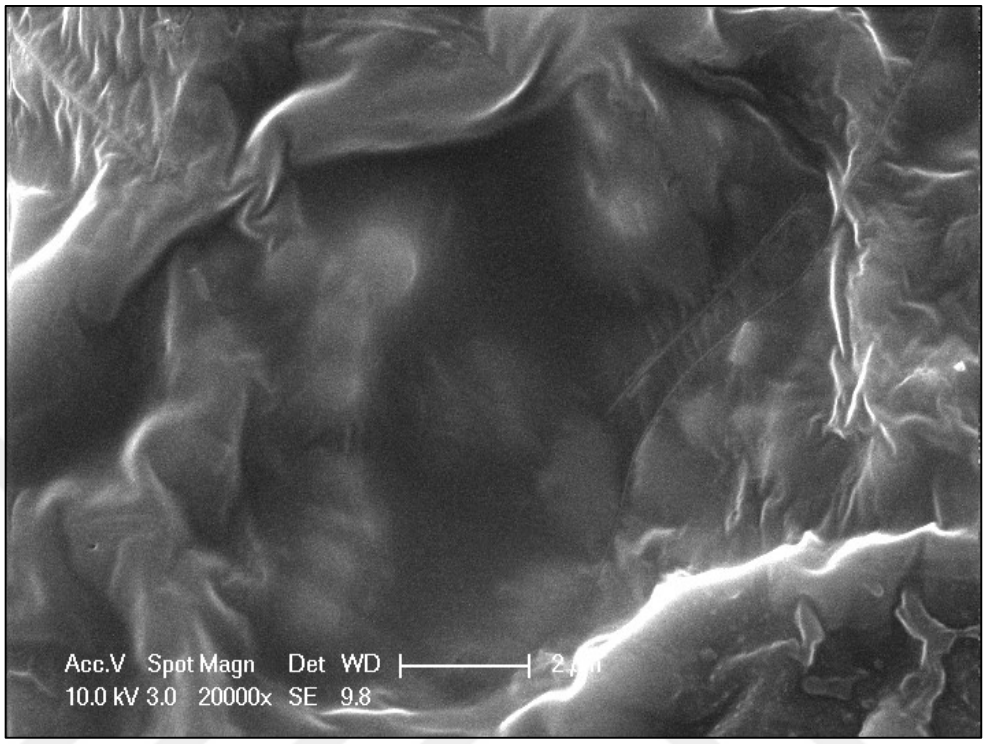

Figure 5.3. SEM image of PPF/VPA particles prepared with 5 minutes homogenization time at 20000x magnification

Figure 5.4 gives a comparison of SEM images of PPF/VPA particles homogenized for 10 minutes and 15 minutes. Figure 5.4 shows a uniform distribution of spherical particles which were more distinct for the 10 minutes homogenized samples whereas particles were more coagulated and exhibited more like rectangular or square shapes rather than spherical shapes for 15 minutes homogenized particles.

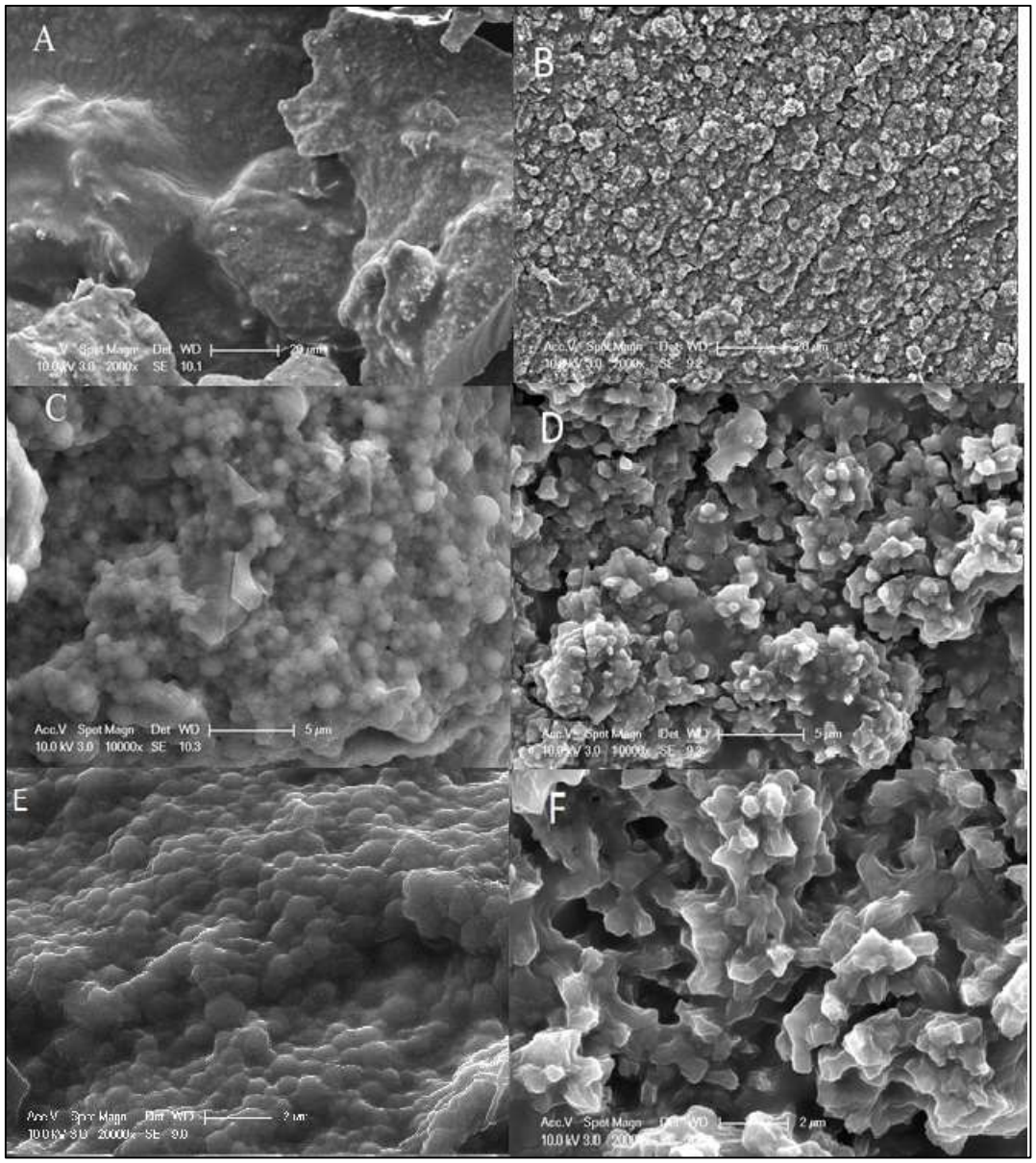

Figure 5.4. SEM Images of 10 and 15 minutes homogenized PPF/VPA nanoparticles. (a) 10 minutes (b) 15 minutes homogenized nanoparticles at 2000 x magnification (c) 10 minutes (d) 15 minutes homogenized nanoparticles at 10000 x magnification (e) 10 minutes (f) 15 minutes homogenized PPF/VPA nanoparticles at 20000 x magnification

Figure 5.5 similarly gives a comparison of SEM images of PPF/VPA particles homogenized for 10 minutes and 30 minutes. Spherical particles can be identified for both 10- and 30-minutes homogenized samples however spherical particles seem to be more distinct for the 10 minutes homogenization time. A size analysis of the PPF/VPA particles homogenized for 10 and 30 minutes are also presented in Figure 5.6. In Figure 5.6 (a), particles with diameters

of 582 nm, 927 nm, 533 nm, 650 nm and 1860nm were labeled for the 10 minutes homogenized particles and the sizes of these particles ranged roughly from 500 nm to 2000 nm. Similarly, in Figure 5.6(b), particles with diameters of 266 nm, 342 nm, 502 nm, 738 nm, 856 nm, and 1153 nm were labeled for the 30 minutes homogenized particles and the sizes of these particles ranged roughly from 250 nm to 1500 nm indicating that 30 minutes homogenization time also resulted in a smaller size of the nanoparticles.

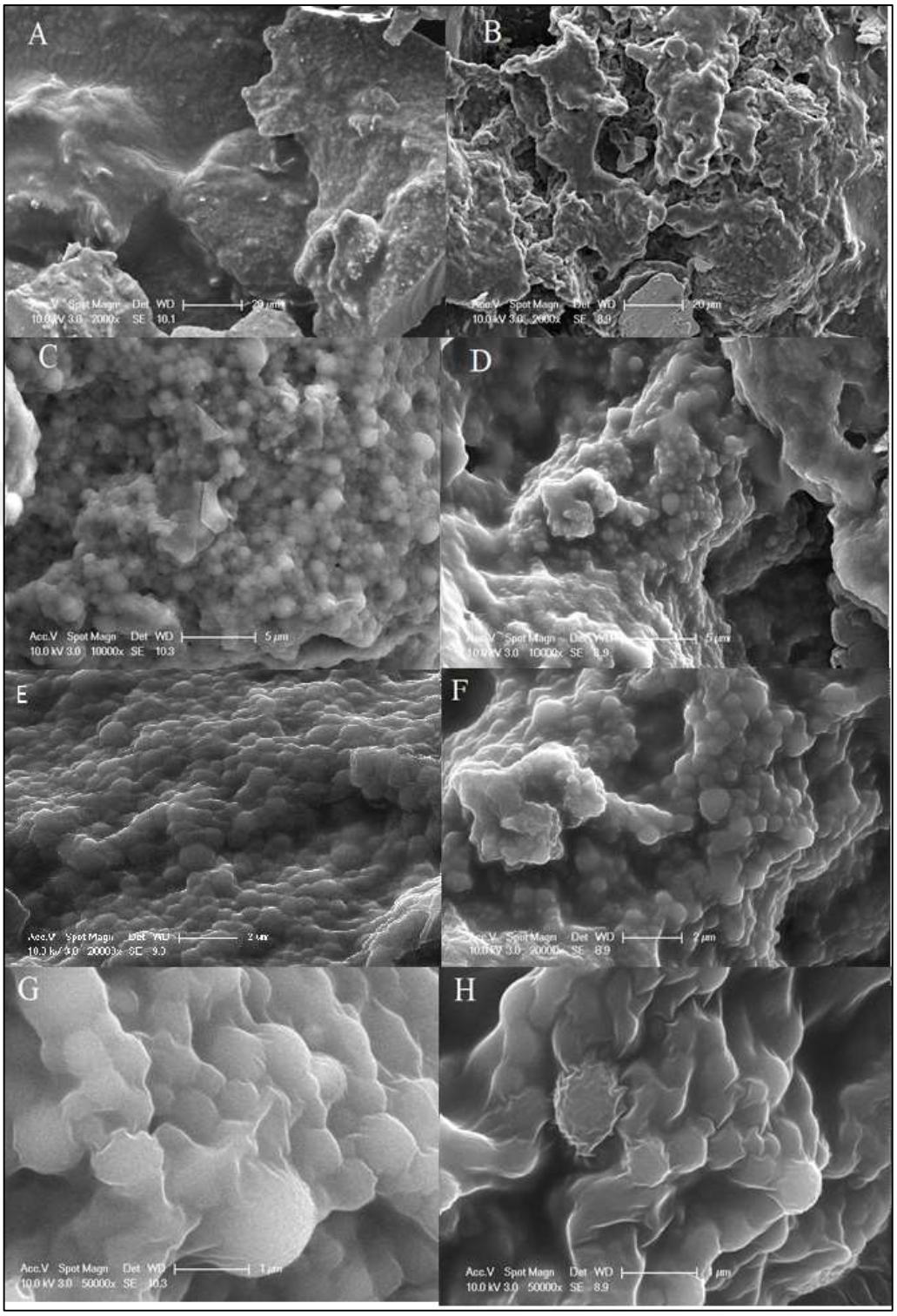

Figure 5.5. SEM Images of 10 and 30 minutes homogenized PPF/VPA nanoparticles (a) 10 minutes (b) 30 minutes homogenized nanoparticles at 2000 x magnification (c) 10 minutes (d) 30 minutes homogenized nanoparticles at 10000 x magnification (e) 10 minutes (f) 30

minutes homogenized nanoparticles at 20000 x magnification (g) 10 minutes (h) 30 minutes homogenized nanoparticles at 50000 x magnification.

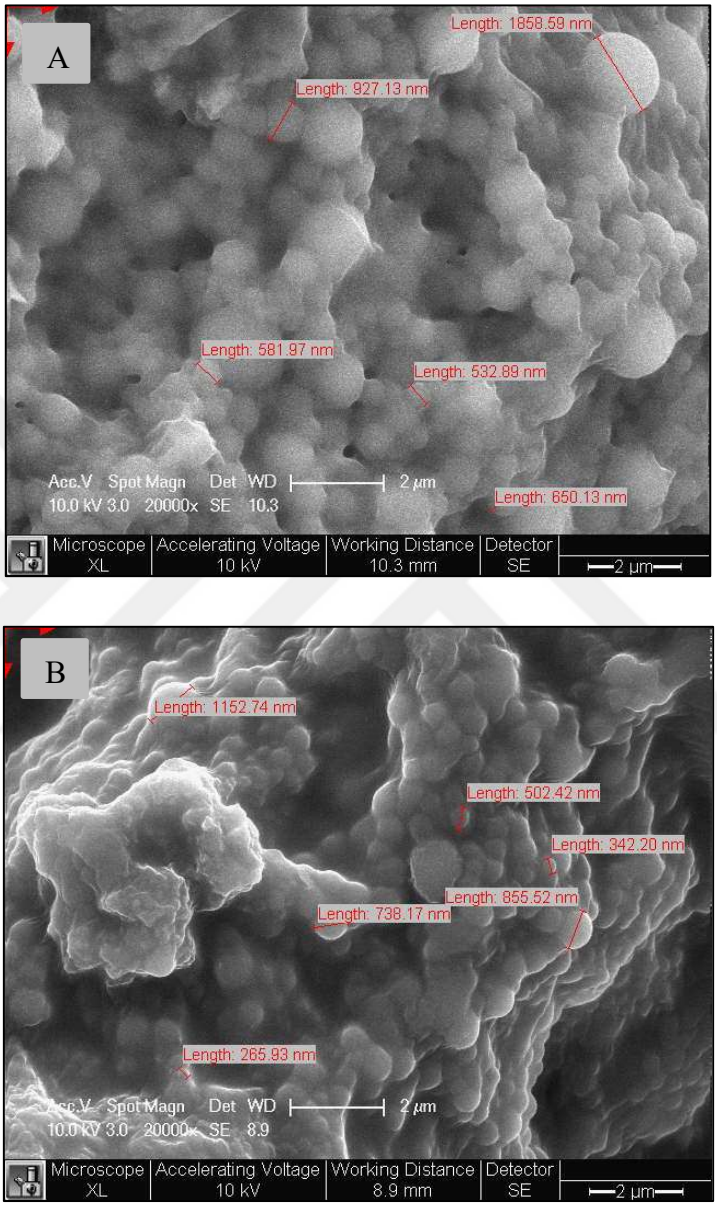

Figure 5.6. Size analysis of (a) 10 and (b) 30 minutes homogenized PPF/VPA nanoparticles at 20000 x magnification

Although as mentioned before, 9 wt. percent surfactant SDS ratio was used as the optimized concentration from a reference study of the same process with PPF/VP particles, PPF/VPA particles prepared with 4.5 and 9 wt. surfactant concentration using 10 minutes homogenization time were also analyzed via SEM as presented in Figure 5.7. SEM images

of the particles at 10000x, 20000x and 50000x magnifications show that the particles are more distinct for the 9-wt. percent surfactant concentration whereas particles seem to be more coagulated for the 4.5 wt. percent surfactant concentration. Thus, in the light of the SEM and gel content analysis results, 10 minutes homogenization time and 9wt percent SDS concentration were used for the preparation of the PPF/VPA particles for further studies.

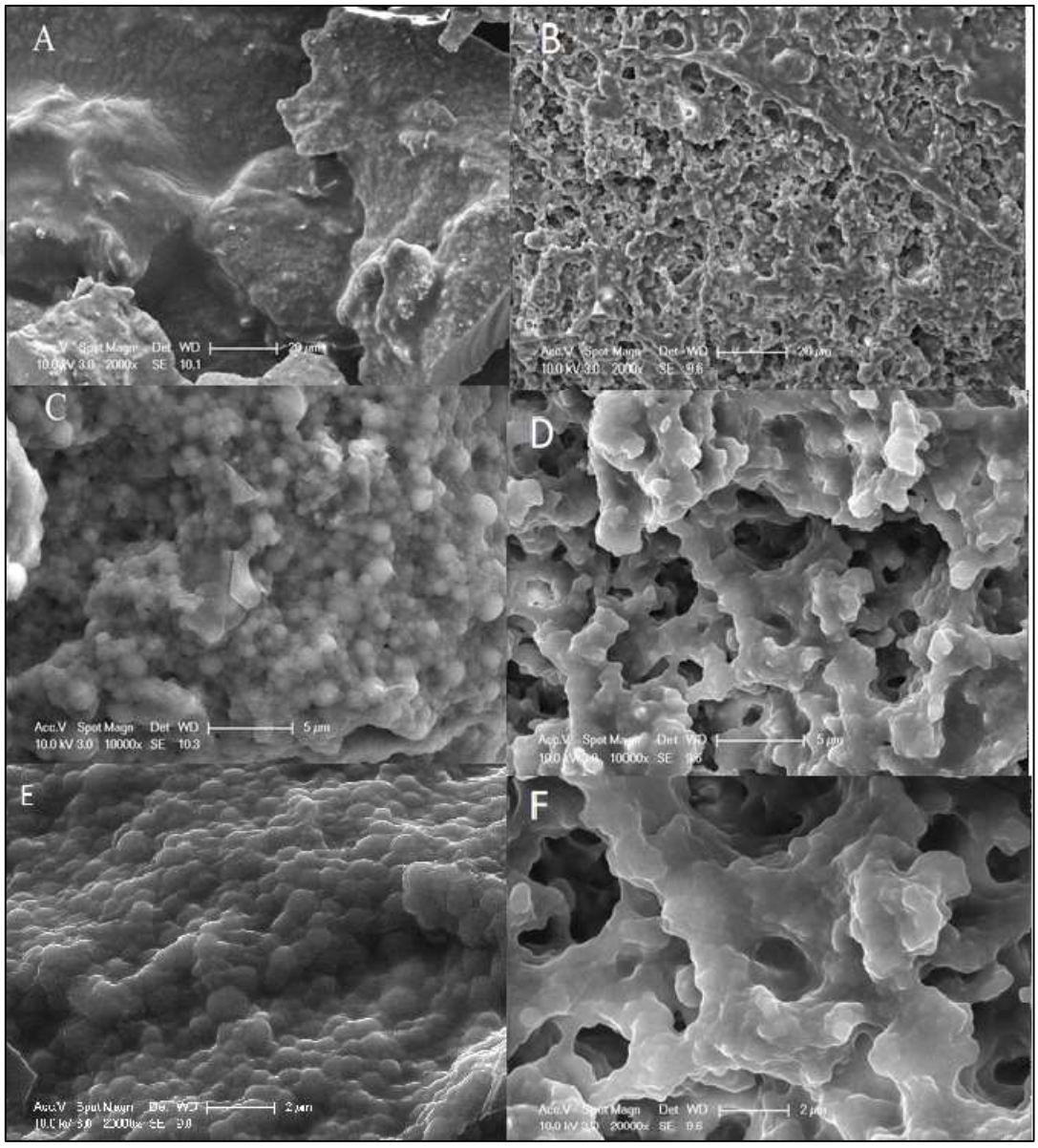

Figure 5.7: SEM Images of 10 minutes homogenized PPF/VPA nanoparticles prepared with 4.5wt% and 9wt%SDS. (a) 9wt% b) 4.5wt% SDS used nanoparticles at 2000 x magnification (c) 9wt% (d) 4.5wt% SDS used nanoparticles at 10000 x magnification (e) 9wt% (f) 4.5wt% SDS used nanoparticles at 20000 x magnification

5.2.5. Degradation Profile of PPF/VPA Particles – pH Analysis

During degradation of the PPF/VPA nanoparticles, acidity increases due to hydrolysis that leads to the formation of fumaric acid and vinyl phosphonic acid therefore, pH should decrease over time as degradation proceeds. pH profiles for the crosslinked PPF/VPA particles prepared with different homogenization times are given in Figure 5.8. The degradation profiles show that particles prepared with 10 minutes of homogenization time exhibit the highest pH values or lowest pH decrease at the end of 89 days indicating a lower rate of degradation, which stems from a higher gel content as determined via swelling studies.

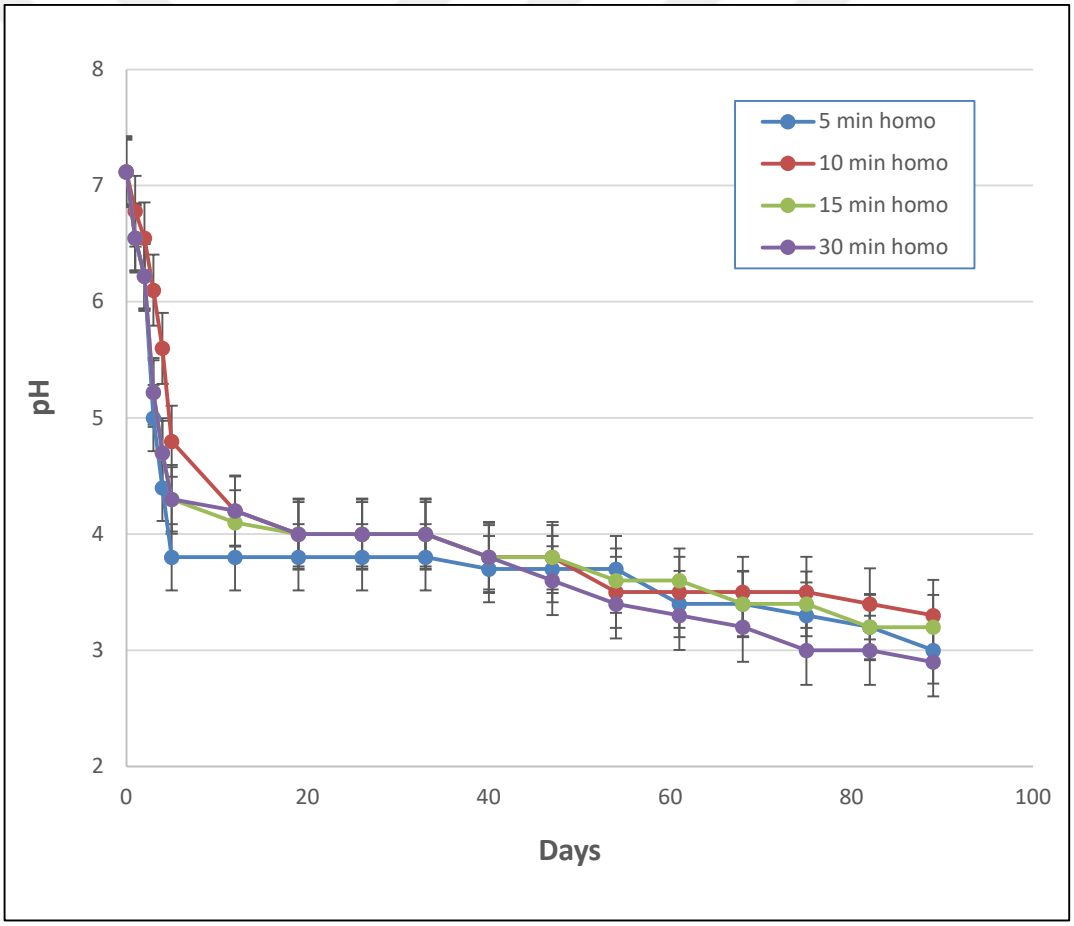

Figure 5.8. pH Degradation profiles of PPF/VPA particles prepared with different homogenization times.

In a previous study by Can et al [72], PPF/VPA polymers at (70/30) composition, prepared via thermal cure in the presence of 3 wt. percent benzoyl peroxide (BP) exhibited similar

degradation profiles which indicated a decrease from pH 7.4 to about 3.5 to 4.0 at the end of 84 days through degradation studies in PBS buffer solution (pH=7.4) where similarly the decrease in pH in the first 5 -7 days was quiet fast and then a lower rate of decrease in pH was observed.

Peter et al. [105] synthesized the poly (propylene fumarate) based β-Tricalcium phosphate (β-TCP) incorporated material. To investigate the degradation behavior of the polymer, Peter et al. placed the samples to 3 ml PBS and tested them mechanically at the end of 1 and 4 days. pH of the samples decreased to 2 percent readily because of the β-Tricalcium phosphate degradation.

Jun et al. [106] investigated the dissolution of β-TCP which indicated a change in pH from 6.3 to 5.4. showing that β-TCP also contributes to the acidity of solution. Degradation of PPF- β-TCP composites resulted in a constant pH value of 4.1 to 4.5 at the end of 30 days which are comparable with our results however, mechanical properties of PPF/β-TCP did not change significantly which was due to the high strength nature of β-TCP filler. In the study of Peter et al., the acidic nature of β-TCP contributed to the acidity whereas in our study VPA comonomer contributed to the acidity in the degradation of PPF polymer.

5.2.6. Degradation Profile of PPF/VPA Particles – Weight Loss Analysis

Another way to track the decomposition of polymers is Weight Loss analysis. Weight loss analysis of crosslinked polymer nanoparticles synthesized with varying homogenization times revealed that roughly 42-55 percent of the particles degraded within 6 weeks. The weight loss percentage versus time plots are shown in Figure 5.9, showing that particles prepared with 10 minutes of homogenization time resulted in the lowest level of weight loss throughout 84 days, which can be attributed to the higher gel content of these particles.

Thus, both pH and weight loss measurements showed that PPF/VPA particles prepared with 10 minutes of homogenization time exhibited the lowest degradation rate in (PBS) buffer solution with pH of 7.4. However, for the weight loss profiles the degradation rate seemed to be roughly constant and a fast degradation in the first 5 to 7 days which seemed to decrease later observed in the pH versus time plots was not applicable for the weight loss profiles.

Timmer et al. [107] investigated the influence of crosslink density and medium pH on the in vitro degradation rate of PPF/PPF-DA (diacrylate) photo-crosslinked networks over a 52-week timeframe. PPF/PPF-DA networks with the lowest crosslink density showed the most degradation, with a weight loss of 17 percent, which was consistent with our findings of a higher degradation rate for lower gel content. For the PPF/VPA cross-linked particles, 88 percent weight loss was observed at the end of 12 weeks as the lowest degradation rate for particles prepared with 10 minutes of homogenization time. PPF-DA networks synthesized in the study of Timmer et al. had high hydrophobicity. Hydrophobicity and lower water uptake have been associated with the lengthy degradation of polyurethanes based on poly (capro lactone) [107]. The more polar and hydrophilic character of VPA and the fact that for nanoparticles a larger surface area is in contact with water should result in a higher degradation rate for the PPF/VPA nanoparticles prepared in our study.

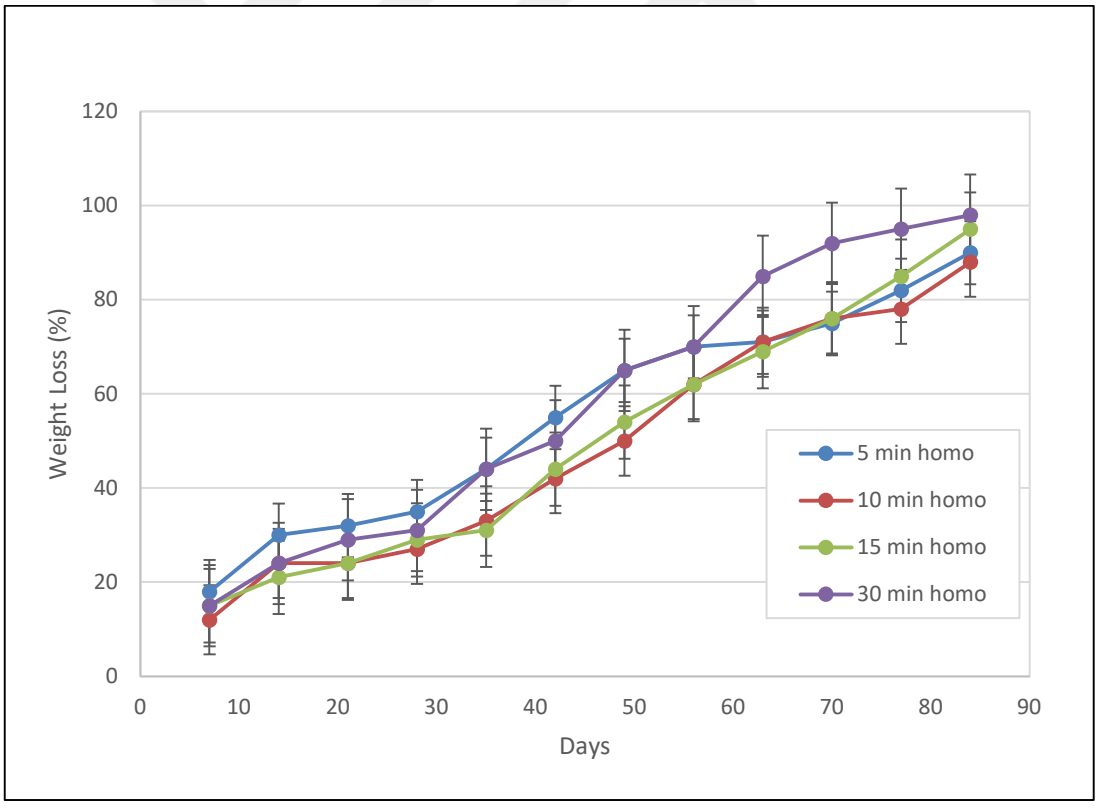

Figure 5.9. Weight loss degradation profiles of PPF/VPA particles prepared with different homogenization times.

Gizem et al. [101] synthesized PPF/Vinyl Pyrrolidone (PPF/VP) (70/30) particles both with and without magnetite through UV emulsion polymerization. In that study, about 54.4 percent weight loss was observed for the PPF/VP particles at the end of 42 days in PBS buffer solution with pH 7.4, whereas in our study the weight loss at the same time period changed from 42 to 55 weight percent for particles prepared with different homogenization times indicating a lower degradation rate for some of the PPF/VPA particles prepared in our work.

5.2.7. Drug Release from PPF/VPA Particles

As described in the experimental section, PPF/VPA particles were prepared in the presence of 4mg Paclitaxel where total weight of the PPF and VPA was 0.543 g corresponding to 0.74 wt. percent of Paclitaxel loading on particles. The drug release from these particles in PBS buffer solution (pH 7.4) was analyzed with HPLC as described in the experimental section. The Paclitaxel (PX) drug release profile from the PPF/VPA particles is presented in Figure 5.10. As can be seen, the cumulative drug release percent versus time plot is linear with an R squared value of 0.9937 and all of the encapsulated drug was released at the end of 82 days. For pharmacokinetics, stable and prolonged release of drug is very important. In the PPF/VPA particles, a sustained linear release profile of the medication was seen, without the normal 'burst effect,' which is crucial for controlled and predictable pharmacokinetics in cancer therapy. Van der Ende [60] synthesized emulsified polyester nanoparticles with drug loading. Drug release with linear profile was also reported in his study.

When the drug release profile of PPF/VPA particles in PBS buffer solution (pH 7.4) is compared with the weight loss profile presented in Figure 5.9, in 84 days about 88 percent of the particles degraded when all the encapsulated drug (100 percent) was released. Thus, it can be proposed that the drug release mechanism is predominantly degradation controlled rather than diffusion controlled. In Gizem et al's [101] study, all the encapsulated Paclitaxel drug was released from the PPF/VP particles at the end of 22 days where the drug release was diffusion controlled rather than degradation controlled. At the 22nd day only 27 percent of the encapsulated drug was released from the PPF/VPA particles, the slower release of Paclitaxel from the PPF/VPA particles as compared to PPF/VP particles can be attributed to both a degradation-controlled release rather than diffusion-controlled release and a higher

gel content of the PPF/VPA particles (87.6 percent) and therefore a more efficient crosslinked system than that of PPF/VP particles (gel content = ~85 percent).

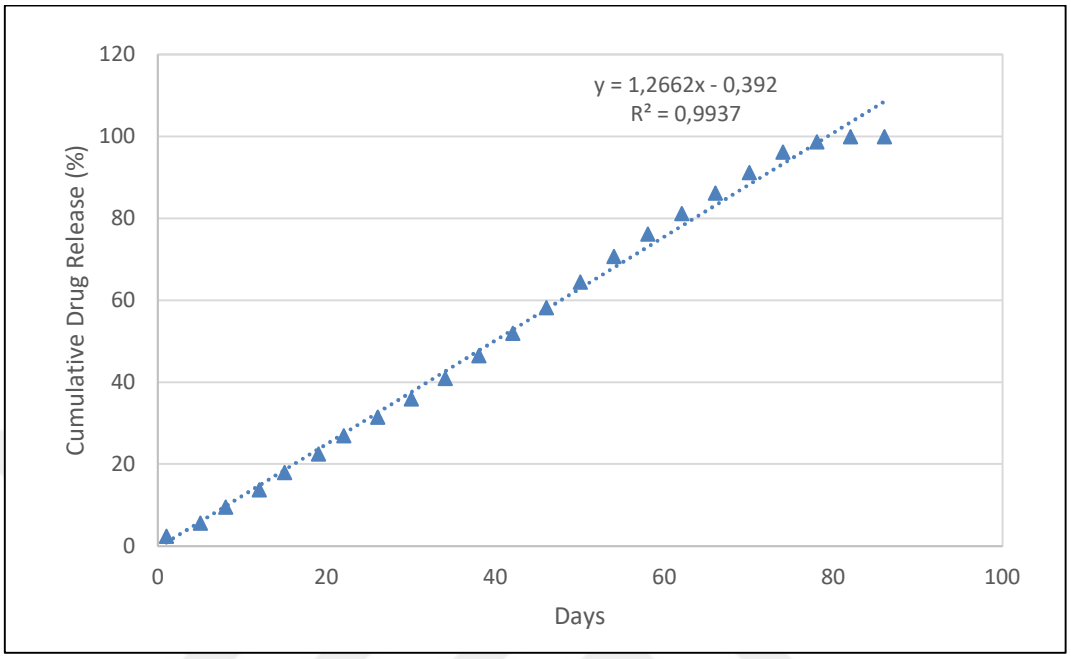

Figure 5.10. Paclitaxel drug release profile of PPF/VPA particles in PBS buffer solution (pH 7.4)

VPA titration curve was investigated by Bahar et al. [108]and it was found that pK_{a1} and pK_{a2} values were 2.74 and 7.34 respectively. As the degradation of PPF/VPA particles decreases the pH of the medium (2.74< pH< 7.34), one can accept only one of the two VPA phosphonic acid groups to be protonated whereas the other one should be deprotonated creating one negative charge on each VPA unit in the network structure which should contribute to the controlled release of the drug from the particles. PPF/VPA polymer particles were not totally negatively charged which could have resulted in a burst release. In addition, tumor microenvironment (TME) is acidic mainly because of high glycolytic rate of tumor cells [109]. Thus, TME for which pH is around ~6.8 will not trigger the deprotonation of both VPA protons. Thus, we can safely predict that PPF/VPA particles will release its drug in a similar manner in the tumor microenvironment.

5.3. CHARACTERIZATION OF FOLIC ACID CONJUGATED PPF (PPF-FA)

In this study, in order to conjugate folic acid to PPF pre-polymer, PPF was reacted with FA (in 1:1 and 1:2 mole ratios) in the presence of DMAP and DCC as the catalyst. The terminal PPF hydroxyl is expected to react with FA carboxylic acid through an esterification reaction as presented in Figure 5.11. The excess folic acid and catalyst were removed from the PPF-FA product as described in the experimental section.

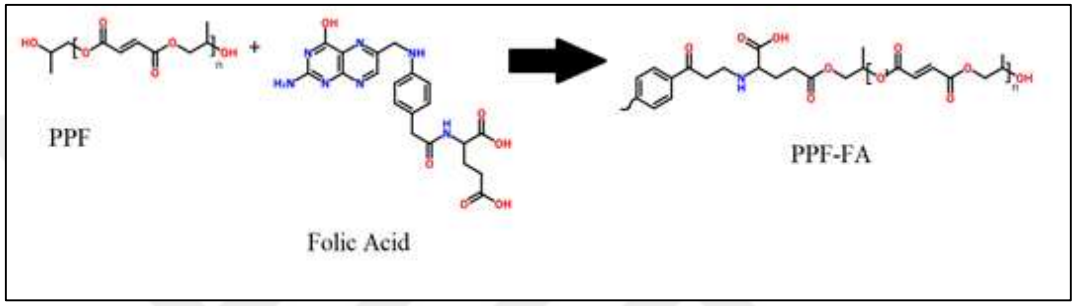

Figure 5.11. The schematic representation of PPF and FA reaction

5.3.1. Fourier Transform Infrared Spectroscopic Analysis of PPF-FA Product

After synthesis of PPF-FA, the product was characterized with FT-IR spectroscopy. In Figure 5.12, the FT-IR spectra of PPF pre-polymer and PPF-FA product are presented. The characteristic peaks of folic acid at around 1602, 1690 and 1481 cm^{-1} that are associated with N-H bending vibration of CONH group, C=O amide stretching of the α- carboxyl group and absorption band of phenyl ring respectively are present in PPF-FA spectra but not in PPF confirming the attachment of FA to PPF. On the other hand, the 1711 cm^{-1} peak representing the ester (C=O stretching) and 1644 cm^{-1} peak showing the (C=C stretching) of PPF are still present in the spectrum of PPF-FA product as expected, since the esterification reaction between PPF and FA creates an additional ester carbonyl group and the fumarate double bonds of PPF are conserved.

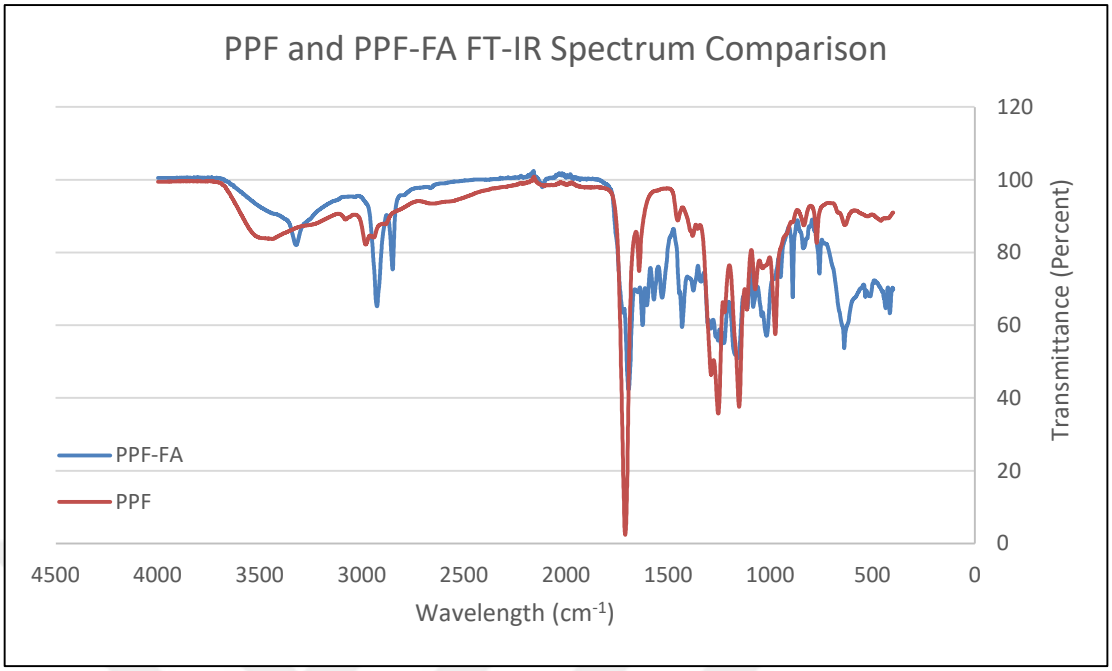

Figure 5.12. FT-IR Spectra of PPF and PPF-FA pre-polymers

5.3.2. ^{1}H-NMR Spectroscopic Analysis of PPF-FA Product

The PPF pre-polymer and the PPF-FA product were also analyzed with ^{1}H-NMR spectroscopy for structural characterization. The ^{1}H-NMR spectrum of the synthesized PPF pre-polymer is presented in Figure 5.13 with the peak assignments for different type of protons on its structure [72].

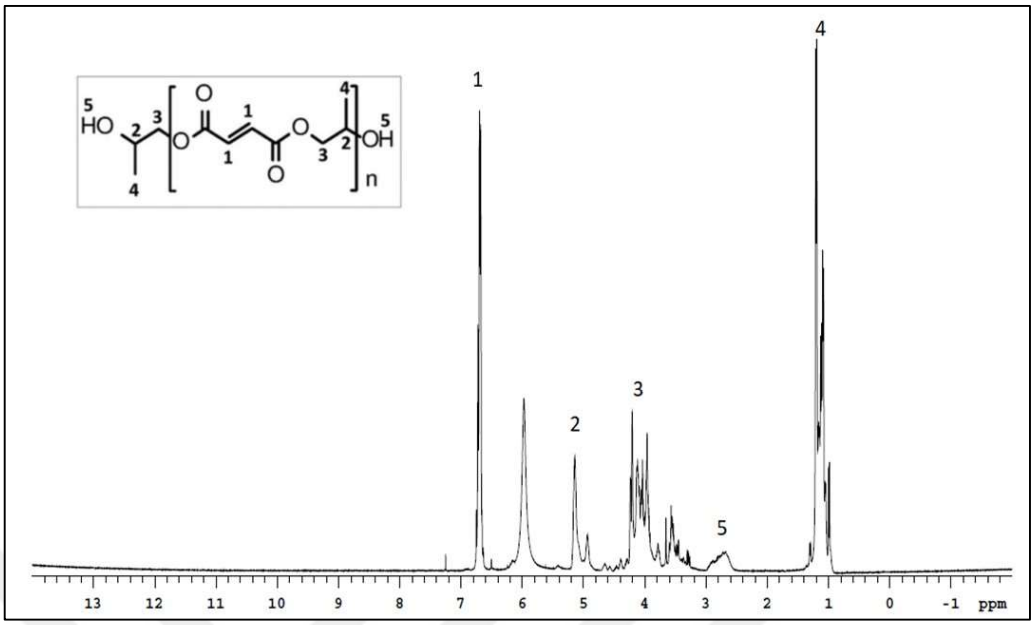

Figure 5.13. ^{1}H-NMR spectrum of the PPF pre-polymer

The ^{1}H-NMR spectrum of the folic acid (FA) is also presented in Figure 5.14 with the corresponding peak assignments for different type of protons on its structure [110].

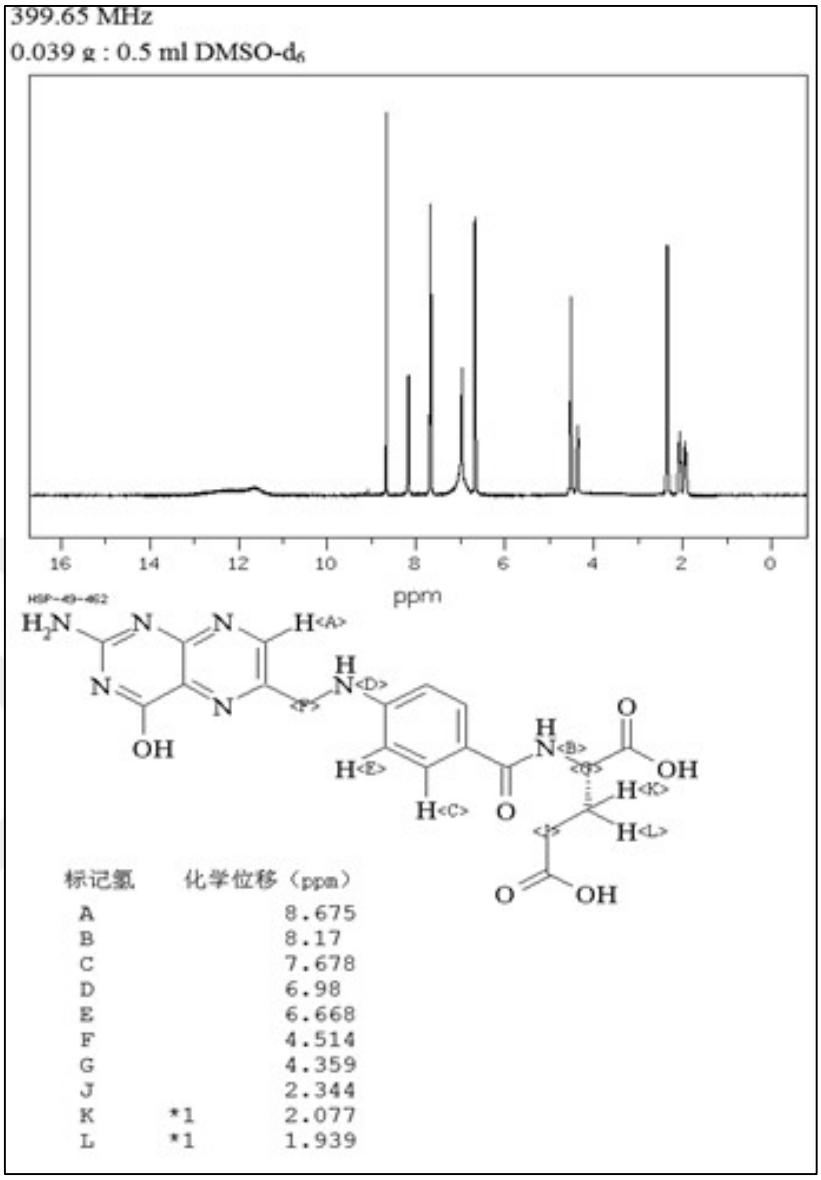

Figure 5.14. [1]H-NMR spectrum of folic acid with peak assignments on different types of protons [110]

Xifeng et al. [3] synthesized PPF-PLGA-PEG self-assembled nanoparticles which were bonded to folic acid for tumor cell-specific response. Xifeng et al. [3] similarly used [1]H-NMR spectroscopy with deuterated chloroform as solvent in order to characterize the polymer-folic acid interface and formation.

Figure 5.15 shows the [1]H-NMR spectrum of the PPF-FA product (0.1:0.1 mol ratio) along with the peak assignments for different type of protons on its structure. PPF protons are shown with white arrows while FA protons are shown with blue arrows. As can be seen from

the figure, the ^{1}H-NMR spectrum of the PPF-FA product carries generally the characteristic peaks associated with protons of both PPF and FA structures. However, use of deuterated chloroform caused chemical shifts to shift right relative to d-DMSO used for FA ^{1}H-NMR spectroscopic analysis presented in Figure 5.15 like the A and B protons of folic acid. The terminal OH protons of PPF which exhibit a broad peak in the 2.5-3.0 ppm region lost intensity in the ^{1}H-NMR spectrum of the PPF-FA without completely being consumed as expected since there should be unreacted OH groups of PPF. In addition, the CH_2-O in the PPF-FA conjugate structure gives a peak in the 3.2 ppm region (3'). The singlet peak at 7.26 ppm on the other hand belongs to residual protons of deuterated chloroform used as a solvent. Thus the ^{1}H-NMR spectroscopic analysis confirmed the addition of FA to PPF through its hydroxyl groups and formation of the PPF-FA product. The ^{1}H-NMR spectroscopic analysis of the PPF-FA (0.1:0.2 mol ratio) product did not show considerable differences in terms of structural analysis and therefore is not presented here.

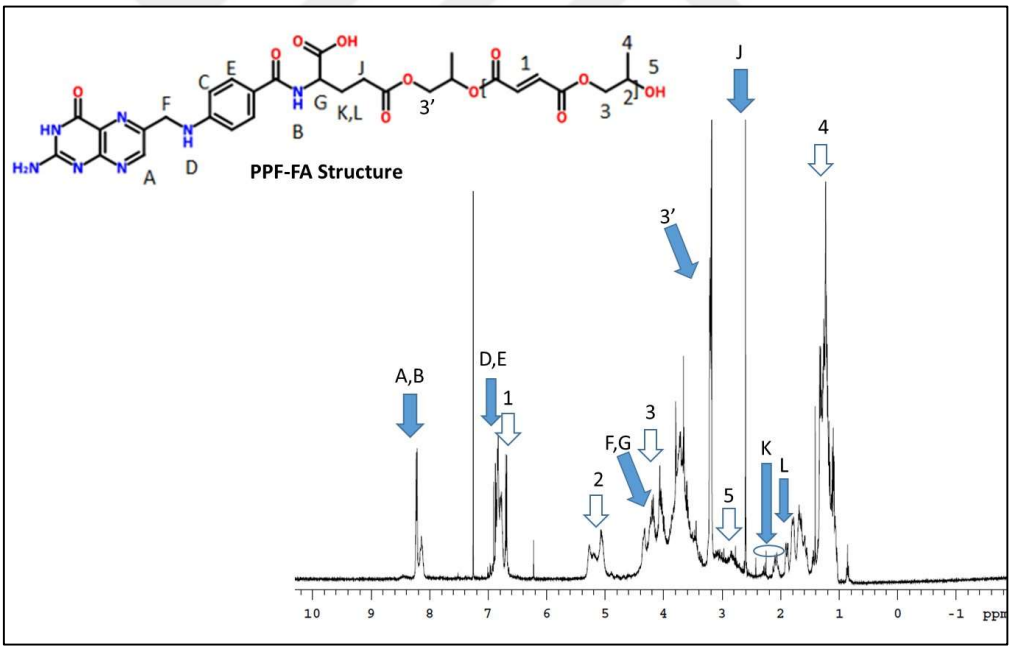

Figure 5.15. ^{1}H-NMR spectrum of the PPF-FA product (0.1:0.1 mol ratio)

5.4. CHARACTERIZATION OF PPF-FA/VPA PARTICLES

As previously described in the Introduction section after the development of the PPF/VPA particles as an anticancer drug delivery agent. For targeting tumor cells preliminary studies on the conjugation of folic acid to PPF and the UV mini-emulsion polymerization of this PPF-FA product with VPA to produce PPF-FA/VPA particles as drug delivery agents were also performed. A schematic representation of the crosslinking of the PPF-FA prepolymer with VPA is presented in Figure 5.16. PPF-FA and VPA polymerization reaction can be controlled and optimized in order to achieve more prolonged drug release and stable nanoparticles.

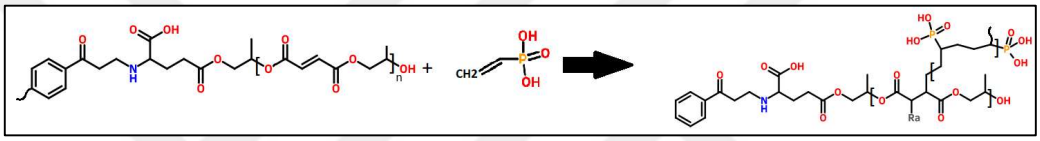

Figure 5.16. Chemical structure of PPF-FA/VPA polymer

5.4.1. Gel Content Analysis

The PPF-FA UV mini emulsion polymerization with VPA was performed changing the surfactant concentration as 9.2 and 15 wt. percent and the TAA co-catalyst (crosslinker) content as 0.06, 0.1 and 0.2 wt. percent in order to optimize particle formation and the gel content of the cross-linked particles. Table 5.2 shows the results.

The PPF-FA/VPA particles synthesized using 0.06 wt. percent TAA, 3 wt. percent BAPO and 9.2 wt. percent SDS at 1000 rpm with 10 min. homogenization time exhibited a maximum gel content value of 88.18±0.16 percent which was close to the gel content value of 87.63±0.17 percent determined for the PPF/VPA particles synthesized under similar conditions. Table 5.2 shows that the increase in TAA co-catalyst concentration results in a decrease in gel content which was not desirable. Stalling of gelling state caused this result. Thus, the use of 0.06 percent TAA was the optimized concentration for crosslinking reaction of PPF-FA polymer with VPA similar to PPF, VPA reaction. According to Table 5.2, PPF-FA/VPA particles synthesized with 9.2 percent surfactant showed slightly higher gel content as compared to those prepared with 15 percent surfactant. However, SEM results showed

that particles synthesized in the presence of 9.2 wt. percent SDS surfactant created different crystal structures rather than spherical particles whereas with the increase of surfactant concentration to 15wt percent, particle formation was observed in addition to crystals as will be discussed in the following section. Particles synthesized with 15 wt. percent surfactant resulted in 83.27 percent gel content with particle formation.

Table 5.2. Gel content of the PPF-FA/VPA particles synthesized at different UV mini-emulsion polymerization conditions

UV mini-emulsion polymerization conditions for PPF-FA/VPA synthesis	**Gel Content (%)**
(0.06% TAA, 3%BAPO, 9.2% SDS) (1000 rpm) (10 min. homogenization time)	88,18±0,16
(0.06% TAA, 3%BAPO, 15% SDS) (1000 rpm) (10 min. homogenization time)	83,27±0,35
(0.06% TAA, 3%BAPO, 15% SDS) (1000 rpm) (10 min. homogenization time) (With Paclitaxel)	87,16±1,2
(0.1% TAA, 3%BAPO, 15% SDS) (1000 rpm) (10 min. homogenization time)	60,66±3,56
(0.2% TAA, 3%BAPO, 15% SDS) (1000 rpm) (10 min. homogenization time)	54,28±5,65

5.4.2. DSC Analysis of PPF-FA/VPA Particles

The synthesized PPF-FA/VPA particles were analyzed via differential scanning calorimetry in order to examine the completion of the cure reaction and the thermal transitions of the polymer. The DSC thermogram of the PPF-FA/VPA polymer is presented together with the PPF/VPA polymer in Figure 5.17. There is no big difference in these thermograms. The endothermic peak at around 50^{o}C region must correspond to the glass transition temperature (T_g) of the PPF-FA/VPA network polymer like the PPF/VPA polymer. The fact that there is no major exothermic peak after the glass transition region indicates that UV cure reaction of PPF-FA with VPA was complete.

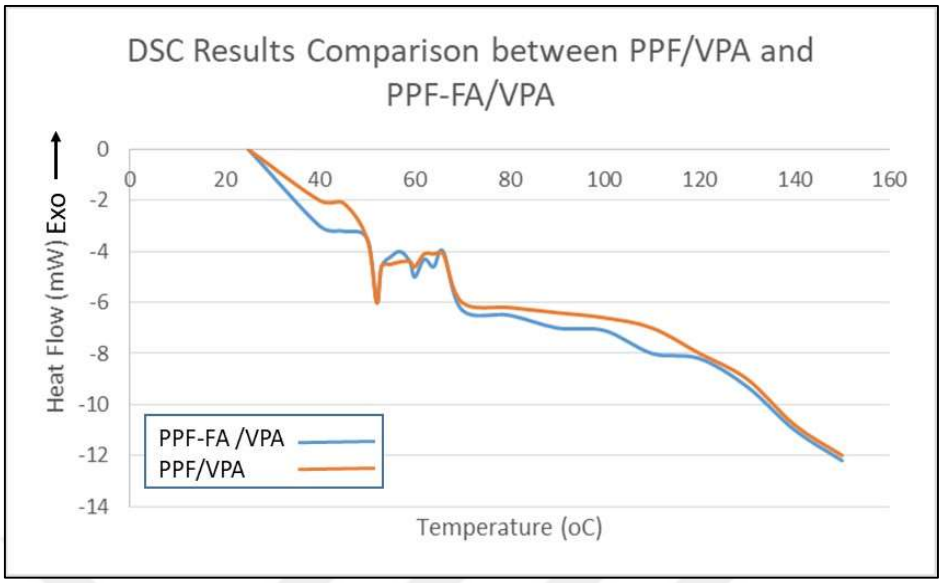

Figure 5.17. DSC thermograms of PPF/VPA and PPF-FA/VPA polymers

5.4.3. SEM Analysis of PPF-FA/VPA Particles

Scanning electron microscopy was used to characterize the morphology of the prepared PPF-FA/VPA particles. When the optimized UV emulsion polymerization conditions used for the synthesis of PPF/VPA particles were used for the synthesis of PPF-FA/VPA particles using 3wt percent BAPO, 0.06wt percent TAA and 9.2wt percent SDS based on PPF-FA and VPA total weight (1000 rpm, 10 min. homogenization time) star-shaped and microplate structures were formed as presented in Figure 5.18. This was an unexpected morphology for the polymer particles produced via mini-emulsion polymerization indicating the use of 9 wt.% SDS was not adequate for the critical micelle concentration (CMC). In order to form spherical particles, the SDS concentration was increased from 9 wt. percent to 15 wt. percent based on PPF-FA and VPA total weight. SEM images of PPF-FA/VPA particles synthesized with 15wt% surfactant at 50000x magnification is presented in Figure 5.19. As can be seen, although rectangular plate shapes are present, nanoparticles with spherical shape have also formed. As particles were formed with increasing concentration of surfactant from 9 to 15 wt. percent, one can assume that the emulsion passed CMC in the presence of 15wt percent SDS.

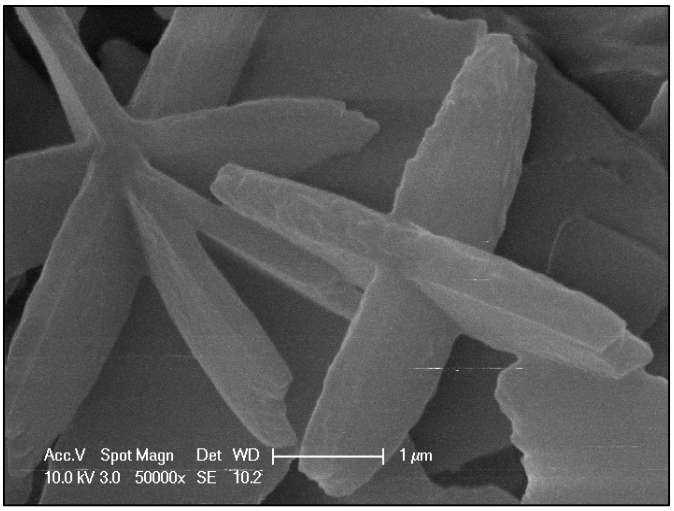

Figure 5.18. SEM image of PPF-FA/VPA product synthesized with 9 wt. % surfactant at 50000x magnification

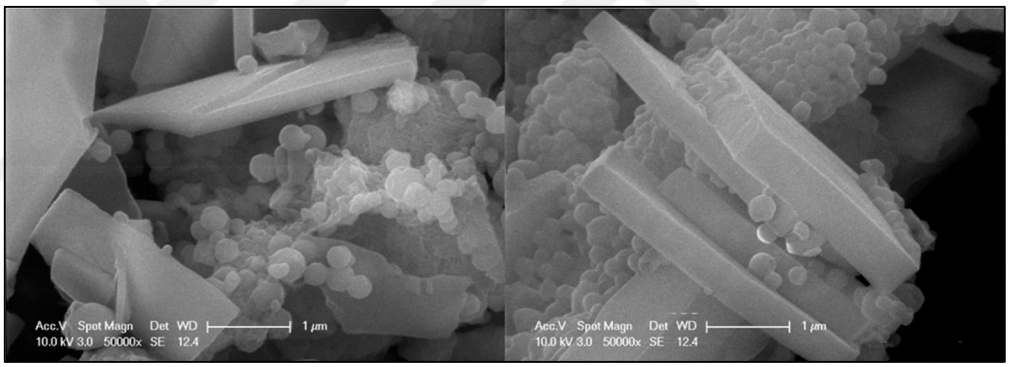

Figure 5.19. SEM images of PPF-FA/VPA product synthesized with 15wt% surfactant at 50000x magnification.

Comparison images for surfactant concentrations of 9 and 15 wt. percent are also presented in Figure 5.20. As can be seen from these images, the increase of surfactant ratio from 9 to 15 weight percent triggered the formation of particles however did not change the micro plate morphology completely.

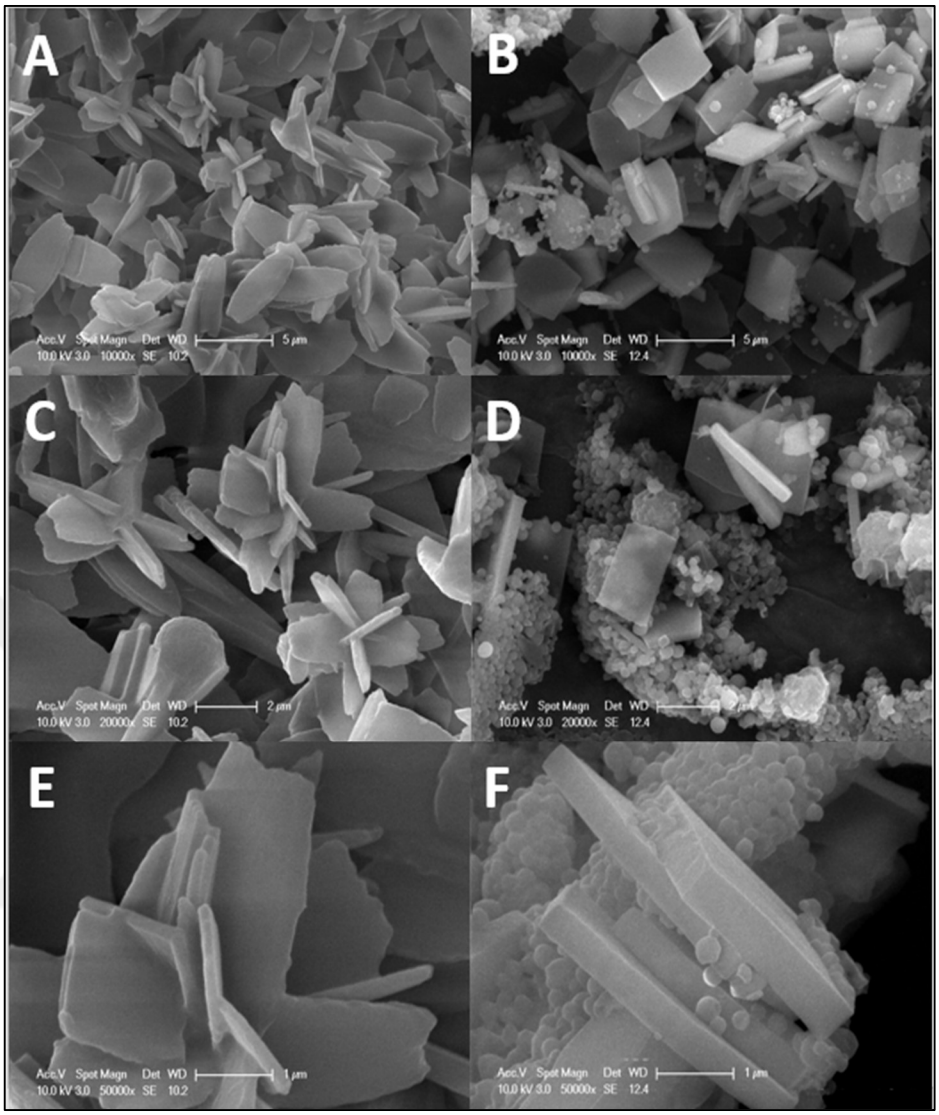

Figure 5.20. SEM image comparisons between 10 minutes homogenized PPF-FA/VPA micro particles for surfactant ratios of 9wt% and 15wt%. A) 9wt% surfactant in 10000x magnification. B) 15wt% surfactant in 10000x magnification. C) 9wt% surfactant in 20000x magnification. D) 15wt% surfactant in 20000x magnification. E) 9wt% surfactant in 50000x magnification. F) 15wt% surfactant in 50000x magnification.

The size of the PPF-FA/VPA particles prepared with 15wt percent surfactant are presented on a SEM image (20000x) in Figure 5.21. As can be seen, particle diameters were in the range of 200 to 600nm whereas the micro plates had lateral dimensions of approximately 2300nm and a thickness of 360 nm. The increase of surfactant concentration from 15 to 20wt percent interestingly resulted in microplate formation without any spherical particle formation.

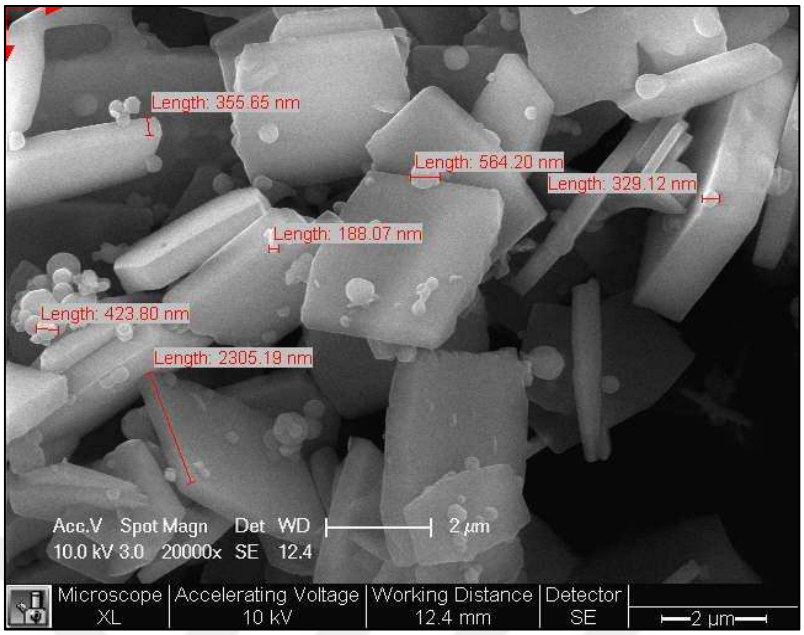

Figure 5.21. Size of PPF-FA/VPA particles prepared with 15wt% surfactant

Homogenizer speed is an important parameter for the particle formation and particle size. Therefore PPF-FA/VPA particles were synthesized with 10 minutes homogenization at 10000 rpm homogenizer speed instead of 1000 rpm keeping other parameters constant (e.g., 15wt percent surfactant). As can be seen in Figure 5.22, the use of 10000 rpm homogenization speed also produced microplates instead of spherical microparticles.

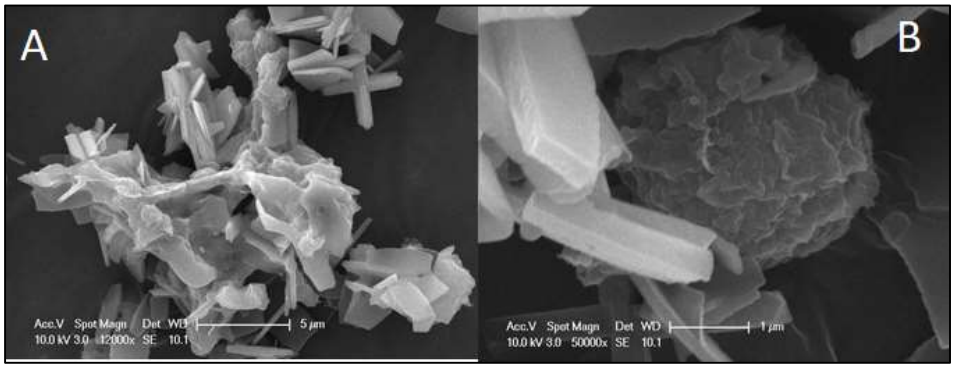

Figure 5.22. PPF-FA/VPA particles homogenized at 10000 rpm for 10 minutes at (a) 12000x (b) 50000x magnification

As the increase of TAA cocatalyst concentration from 0.06wt percent to 0.1 and 0.2 wt. percent decreased the gel content considerably, in an attempt to see the effect of TAA co-

catalyst concentration on particle formation, the PPF-FA/VPA particles were synthesized with 3 wt. percent BAPO, 0.04wt%TAA and 15wt% surfactant. The SEM image of the PPF-FA/VPA particles synthesized with 0.04wt percent TAA is presented in Figure 5.23, showing considerable spherical particle formation along with microplate formation. Figure 5.24 shows a comparison of the SEM images of the PPF-FA/VPA particles synthesized with 0.04 and 0.06 wt. percent TAA. These images indicate that when TAA concentration decreased from 0.06 percent to 0.04 percent, particle concentration increased, and microplate formation decreased.

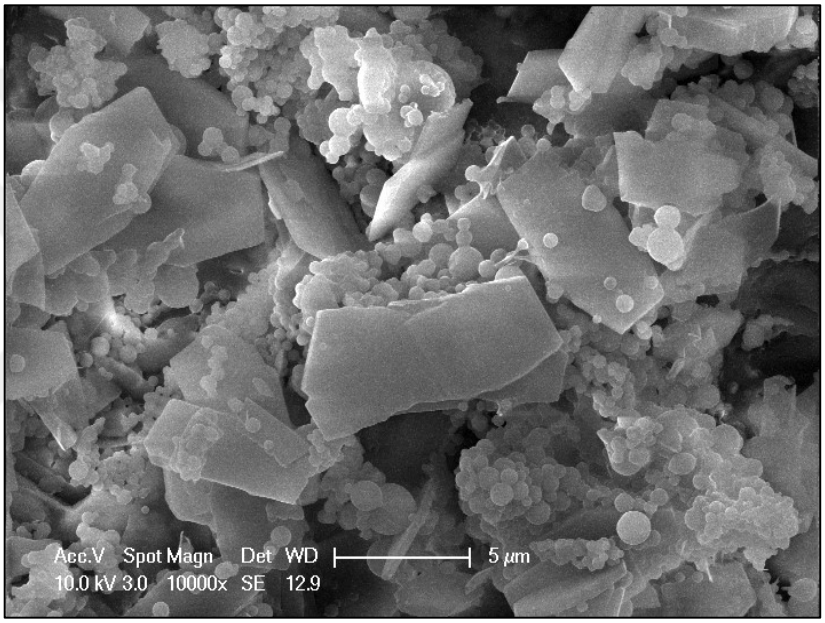

Figure 5.23. SEM image of PPF-FA/VPA particles synthesized with 0.04wt percent TAA

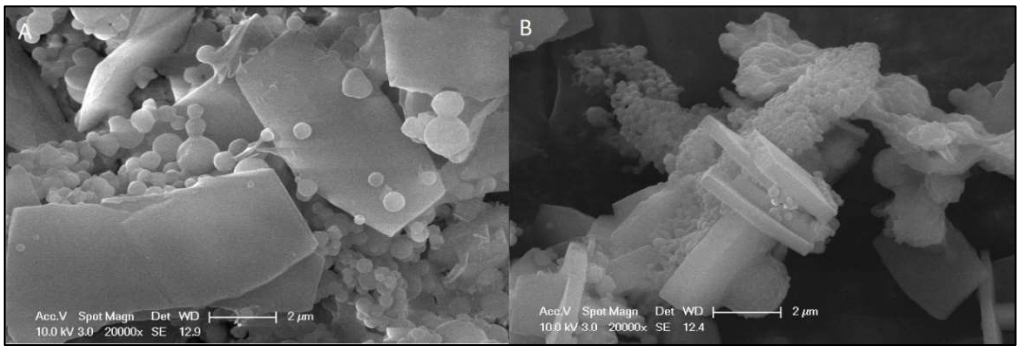

Figure 5.24. Comparison between SEM images of PPF-FA/VPA particles synthesized with (a) 0.06 wt. percent TAA and (b) 0.04 wt. percent TAA

Finally, in order to see the effect of homogenization time on the morphology of the particles, homogenization time was changed from 10 to 15 minutes at 1000 rpm. SEM images of the particles homogenized for 10 and 15 minutes using 15wt percent surfactant are presented in Figure 5.25. As can be seen from this figure, there is no distinguishable difference between 10- and 15-minutes homogenization time, microplate formation can be seen in both.

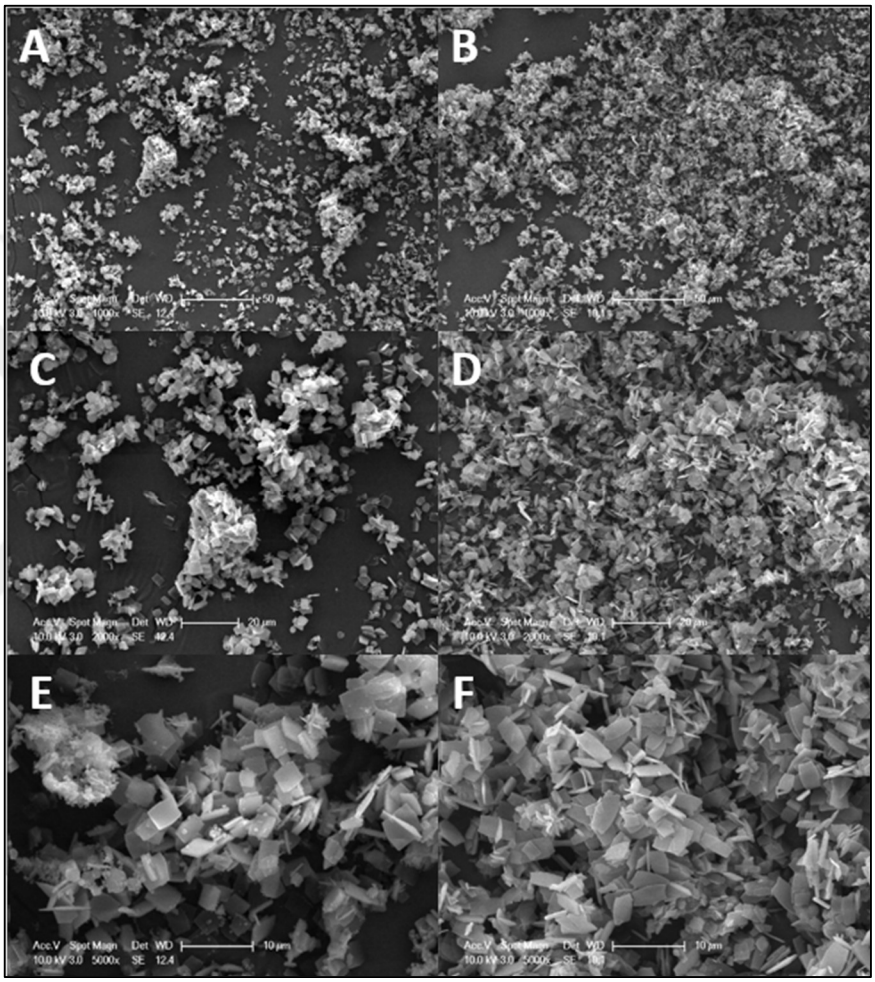

Figure 5.25. SEM images of 10 and 15 minutes homogenized PPF-FA/VPA micro particles for surfactant ratio of 15wt%. (a) 10 minutes homogenization time (b) 15 minutes homogenization time at 1000x magnification (c) 10 minutes homogenization time (d) 15 minutes homogenization time at 2000x magnification. (e) 10 minutes homogenization time (f) 15 minutes homogenization time at 5000x magnification.

Thus, in PPF-FA/VPA UV mini emulsion polymerization, use of 15 wt. percent surfactant (SDS) with 3 wt. percent BAPO and 0.04 wt. percent TAA with 10 minutes of

homogenization time at 1000 rpm seem to be the optimum conditions according to our studies, however further optimization is necessary for a uniform nanoparticle morphology.

6. CONCLUSION

Poly (propylene fumarate) was synthesized through polyesterification of fumaric acid and a slight excess of propylene glycol at defined reaction conditions. Number average and weight average molecular weight of the PPF pre-polymer were determined as 1092 g /mol and 1239 g/mol respectively through GPC analysis. The chemical structure of the PPF pre-polymer was also characterized via FT-IR and ^{1}H-NMR spectroscopic analysis.

PPF pre-polymer was copolymerized with VPA comonomer via UV mini- emulsion polymerization to produce nanoparticles. The optimized reaction conditions using 3wt percent BAPO radical initiator, 0.04wt percent TAA cocatalyst with 9wt percent SDS surfactant and 2 hours of UV cure time with 10 minutes of homogenization time at 1000 rpm resulted in 87.6 percent gel content. SEM analysis indicated that the sizes of these particles ranged roughly from 500 nm to 2000 nm. The PPF copolymerization reaction with VPA through their double bonds via radical polymerization and the formation of the PPF/VPA polymer was also confirmed with FT-IR spectroscopy. The degradation profiles of PPF/VPA particles in PBS buffer solution with pH 7.4 were also obtained via measurements of weight loss and pH. It was found out that depending on the homogenization time of the particles, about 88 to 98 percent of the particles degraded at the end of 84 days. Both pH and weight loss profiles showed that PPF/VPA nanoparticles synthesized with 10 minutes of homogenization time had a lower degradation rate due to a higher gel content as compared to particles prepared with different homogenization times. DSC analysis of the synthesized PPF/VPA particles indicated that the cure of PPF prepolymer with VPA was complete. Most importantly, Paclitaxel drug release from the PPF/VPA particles resulted in linear and prolonged release which is very important for pharmacokinetics and for anti-cancer drugs. The drug release mechanism was found to be degradation controlled rather than diffusion controlled.

The PPF prepolymer was conjugated to folic acid in attempt to prepare PPF-FA/VPA particles through UV miniemulsion polymerization that can be used as anti-cancer drug delivery agents with tumor-specific targeting ability. Both FT-IR and ^{1}H-NMR spectroscopic analysis confirmed the conjugation of FA to PPF.

After PPF-FA synthesis, PPF-FA/VPA nanoparticles were synthesized via UV miniemulsion polymerization. The highest gel content (88.2 percent) was obtained for PPF-FA/VPA nanoparticles synthesized using 3 wt. percent BAPO, 0.06wt percent TAA, 9wt

percent surfactant with 10 minutes of homogenization time at 1000 RPM. DSC analysis of the PPF-FA/VPA particles also indicated the completion of the cure reaction. However, SEM analysis showed that this formulation resulted in the formation of microplates rather than particles. The increase of surfactant concentration from 9 to 15 wt. percent triggered the formation of spherical particles along with microplates. However, PPF-FA/VPA formulation and synthesis must be further optimized for particle formation before these particles can be used as drug delivery agents.

All in all, novel PPF/VPA based nanoparticles with tunable acidic properties were prepared for the first time via UV mini emulsion polymerization [111]. The PPF/VPA nanoparticles exhibited a linear and prolonged release of the encapsulated model anticancer drug Paclitaxel through 84 days showing these particles to be candidates as anticancer drug delivery agents. In addition, FA was conjugated to the PPF prepolymer successfully and the synthesis of the PPF-FA/VPA nanoparticles through UV mini emulsion polymerization gave promising results for their development as drug delivery agents with tumor specific targeting ability.

7. FUTURE WORK

As a future work, PPF and FA reaction can be carried at different mole ratios to ensure the conversion of all PPF hydroxyls to FA esters. In addition, an obvious future work for this study is the optimization of the PPF-FA/VPA synthesis conditions to get a homogenous distribution of spherical particles. Furter studies on the change of surfactant and/or surfactant concentration, BAPO initiator and TAA co-catalyst concentration, VPA comonomer concentration, homogenization and UV light exposure times and homogenization speed can all be performed. In addition, drug release profiles from the PPF/VPA particles at different pH mediums can also be explored as the swelling of the network must change with changing acidity of the medium due to VPA component of the matrix.

REFERENCES

1. D. Han, Z. Lu, S. A. Chester, and H. Lee, “Micro 3D Printing of a Temperature-Responsive Hydrogel Using Projection Micro-Stereolithography,” *Scientific Reports*, vol. 8, no. 1, pp. 1–10, 2018, doi: 10.1038/s41598-018-20385-2.

2. H. Wu, L. Zhu, and V. P. Torchilin, “PH-sensitive poly(histidine)-PEG/DSPE-PEG co-polymer micelles for cytosolic drug delivery,” *Biomaterials*, vol. 34, no. 4, pp. 1213–1222, 2013, doi: 10.1016/j.biomaterials.2012.08.072.

3. X. Liu, A. L. M. II, M. J. Yaszemski, and L. Lu, “Biodegradable and crosslinkable PPF-PLGA-PEG self-assembled nanoparticles dual-decorated with folic acid ligands and rhodamine B fluorescent probes for targeted cancer imaging,” *RSC Advances*, no. 00, pp. 1–3, 2015.

4. G. A. Husseini and W. G. Pitt, “Micelles and nanoparticles for ultrasonic drug and gene delivery,” *Advanced Drug Delivery Reviews*, vol. 60, no. 10, pp. 1137–1152, 2008, doi: 10.1016/j.addr.2008.03.008.

5. Y. H. Yun, B. K. Lee, and K. Park, “Controlled Drug Delivery: Historical perspective for the next generation HHS Public Access,” *J Control Release*, vol. 219, pp. 2–7, 2015, doi: 10.1016/j.jconrel.2015.10.005.

6. J.-X. Lee, PI.; Li, *Evolution of oral controlled release dosage forms. In: Wen, H.; Park, K., editors. Oral Controlled Release Formulation Design and Drug Delivery*. 2010.

7. L. Pérez-Álvarez, L. Ruiz-Rubio, B. Artetxe, M. d. M. Vivanco, J. M. Gutiérrez-Zorrilla, and J. L. Vilas-Vilela, “Chitosan nanogels as nanocarriers of polyoxometalates for breast cancer therapies,” *Carbohydrate Polymers*, vol. 213, no. February, pp. 159–167, 2019, doi: 10.1016/j.carbpol.2019.02.091.

8. T. Bose, D. Latawiec, P. P. Mondal, and S. Mandal, “Overview of nano-drugs characteristics for clinical application: The journey from the entry to the exit point,” *Journal of Nanoparticle Research*, vol. 16, no. 8. Kluwer Academic Publishers, 2014. doi: 10.1007/s11051-014-2527-7.

9. M. Salarian *et al.*, “Microfluidic Synthesis and Angiogenic Activity of Ginsenoside Rg1-Loaded PPF Microspheres,” *ACS Biomaterials Science and Engineering*, vol. 2, no. 11, pp. 1872–1882, 2016, doi: 10.1021/acsbiomaterials.6b00222.

10. S. Esfandiarpour-Boroujeni, S. Bagheri-Khoulenjani, H. Mirzadeh, and S. Amanpour, “Fabrication and study of curcumin loaded nanoparticles based on folate-chitosan for breast cancer therapy application,” *Carbohydrate Polymers*, vol. 168, pp. 14–21, 2017, doi: 10.1016/j.carbpol.2017.03.031.

11. Z. Cai, Y. Wan, M. L. Becker, Y. Z. Long, and D. Dean, “Poly(propylene fumarate)-based materials: Synthesis, functionalization, properties, device fabrication and biomedical applications,” *Biomaterials*, vol. 208, no. August 2018, pp. 45–71, 2019, doi: 10.1016/j.biomaterials.2019.03.038.

12. Y.-C. Kim, J.-H. Park, and M. R. Prausnitz, “Microneedles for drug and vaccine delivery,” *Advanced Drug Delivery Reviews*, vol. 64, no. 14, pp. 1547–1568, Nov. 2012, doi: 10.1016/j.addr.2012.04.005.

13. A. K. T. Thulasidasan *et al.*, “Folic acid conjugation improves the bioavailability and chemosensitizing efficacy of curcumin-encapsulated PLGA-PEG nanoparticles towards paclitaxel chemotherapy,” *Oncotarget*, vol. 8, no. 64, pp. 107374–107389, 2017, doi: 10.18632/oncotarget.22376.

14. M. Erdem, S. Yalcin, and U. Gunduz, “Folic acid-conjugated polyethylene glycol-coated magnetic nanoparticles for doxorubicin delivery in cancer chemotherapy: Preparation, characterization and cytotoxicity on HeLa cell line,” *Human and Experimental Toxicology*, vol. 36, no. 8, pp. 833–845, 2017, doi: 10.1177/0960327116672910.

15. T. S. Anirudhan, M. M. Anila, and S. Franklin, “Synthesis characterization and biological evaluation of alginate nanoparticle for the targeted delivery of curcumin,” *Materials Science and Engineering C*, vol. 78, pp. 1125–1134, 2017, doi: 10.1016/j.msec.2017.04.116.

16. Z. Chen *et al.*, “Hierarchical targeted hepatocyte mitochondrial multifunctional chitosan nanoparticles for anticancer drug delivery,” *Biomaterials*, vol. 52, no. 1, pp. 240–250, 2015, doi: 10.1016/j.biomaterials.2015.02.001.

17. S. Gurunathan, M. H. Kang, M. Qasim, and J. H. Kim, “Nanoparticle-mediated combination therapy: Two-in-one approach for cancer,” *International Journal of Molecular Sciences*, vol. 19, no. 10. MDPI AG, Oct. 20, 2018. doi: 10.3390/ijms19103264.

18. T. Zhong *et al.*, “Imaging the Pore Structure in Geomaterials Using Rhodamine B Covalently Decorated Magnetic Nanoparticles”, doi: 10.1021/acsearthspacechem.9b00071.

19. Dr. N. Kampan, M. Madondo, O. McNally, M. Quinn, and M. Plebanski, “Paclitaxel and Its Evolving Role in the Management of Ovarian Cancer,” *BioMed Research International*, vol. 2015, pp. 1–21, Jul. 2015, doi: 10.1155/2015/413076.

20. M. W. Glasscott, A. D. Pendergast, M. H. Choudhury, and J. E. Dick, “Advanced Characterization Techniques for Evaluating Porosity, Nanopore Tortuosity, and Electrical Connectivity at the Single-Nanoparticle Level,” *ACS Applied Nano Materials*, vol. 2, no. 2, pp. 819–830, 2018, doi: 10.1021/acsanm.8b02051.

21. A. N. M. B. El-hoshoudy, “Emulsion Polymerization Mechanism,” *InTechOpen*, 2018.

22. Y. HB., Emulsion polymerization: effects of polymerization variables on the properties of vinyl acetate based emulsion polymers. 2013.

23. K. Phiwdang, S. Suphankij, W. Mekprasart, and W. Pecharapa, “Selection and peer-review under responsibility of COE of Sustainalble Energy System Synthesis of CuO Nanoparticles by Precipitation Method Using Different Precursors Selection and/or peer-review under responsibility of COE of Sustainable Energy System, Rajamangala University of Technology Thanyaburi(RMUTT),” *Energy Procedia*, vol. 34, pp. 740–745, 2013, doi: 10.1016/j.egypro.2013.06.808.

24. W. Jiang, X. Hua, Q. Han, X. Yang, L. Lu, and X. Wang, “Preparation of lamellar magnesium hydroxide nanoparticles via precipitation method,” *Powder Technology*, vol. 191, no. 3, pp. 227–230, Apr. 2009, doi: 10.1016/j.powtec.2008.10.023.

25. S. Suwanboon, P. Amornpitoksuk, A. Haidoux, and J. C. Tedenac, “Structural and optical properties of undoped and aluminium doped zinc oxide nanoparticles via

precipitation method at low temperature," *Journal of Alloys and Compounds*, vol. 462, no. 1–2, pp. 335–339, Aug. 2008, doi: 10.1016/j.jallcom.2007.08.048.

26. M. Riaz *et al.*, "Surface Functionalization and Targeting Strategies of Liposomes in Solid Tumor Therapy: A Review," *International Journal of Molecular Sciences*, vol. 19, no. 1, p. 195, Jan. 2018, doi: 10.3390/ijms19010195.

27. R. P. Feynman, "There's plenty of room at the bottom," *Micromechanics and MEMS: Classic and Seminal Papers to 1990*, pp. 2–9, 1997, doi: 10.1109/9780470545263.sect1.

28. "Polymer matrix drug delivery apparatus," Aug. 1994.

29. "Different types of nanoparticles commonly used for biomedical... | Download Scientific Diagram." https://www.researchgate.net/figure/Different-types-of-nanoparticles-commonly-used-for-biomedical-applications-and-which_fig2_269182214 (accessed Dec. 01, 2019).

30. P. Korangath *et al.*, "Nanoparticle interactions with immune cells dominate tumor retention and induce T cell–mediated tumor suppression in models of breast cancer," *Science Advances*, vol. 6, no. 13, p. eaay1601, Mar. 2020, doi: 10.1126/sciadv.aay1601.

31. C. Huang, X. Chen, Z. Xue, and T. Wang, "Effect of structure: A new insight into nanoparticle assemblies from inanimate to animate," *Science Advances*, vol. 6, no. 20, p. eaba1321, May 2020, doi: 10.1126/sciadv.aba1321.

32. V. V. Mody, A. Cox, S. Shah, A. Singh, W. Bevins, and H. Parihar, "Magnetic nanoparticle drug delivery systems for targeting tumor," *Applied Nanoscience (Switzerland)*, vol. 4, no. 4, pp. 385–392, 2014, doi: 10.1007/s13204-013-0216-y.

33. B. R. Schroeder *et al.*, "The Disaccharide Moiety of Bleomycin Facilitates Uptake by Cancer Cells," *J Am Chem Soc*, vol. 136, no. 39, pp. 13641–13656, Oct. 2014, doi: 10.1021/ja507255g.

34. Z. Yu *et al.*, "Selective Tumor Cell Targeting by the Disaccharide Moiety of Bleomycin," *J Am Chem Soc*, vol. 135, no. 8, pp. 2883–2886, Feb. 2013, doi: 10.1021/ja311090e.

35. Q. Chen, J. Zheng, X. Yuan, J. Wang, and L. Zhang, “Folic acid grafted and tertiary amino based pH-responsive pentablock polymeric micelles for targeting anticancer drug delivery,” *Materials Science and Engineering C*, vol. 82, no. July 2017, pp. 1–9, 2018, doi: 10.1016/j.msec.2017.08.026.

36. G. Devanand Venkatasubbua S.Ramasamya G.S.Avadhanib V.Ramakrishnanc J.Kumara, “Surface modification and paclitaxel drug delivery of folic acid modified polyethylene glycol functionalized hydroxyapatite nanoparticles,” *Powder Technology*, pp. 437–442, 2013.

37. T. VP, “Structure and design of polymeric surfactant-based drug delivery systems,” *Adv Drug Deliv Rev*, vol. 64, no. 9, pp. 836–851, 2012.

38. G. Seetharaman, A. R. Kallar, V. M. Vijayan, J. Muthu, and S. Selvam, “Design, preparation and characterization of pH-responsive prodrug micelles with hydrolyzable anhydride linkages for controlled drug delivery,” *Journal of Colloid and Interface Science*, vol. 492, no. January 2018, pp. 61–72, 2017, doi: 10.1016/j.jcis.2016.12.070.

39. D. H. R. Kempen *et al.*, “Controlled drug release from a novel injectable biodegradable microsphere/scaffold composite based on poly(propylene fumarate),” *Journal of Biomedical Materials Research - Part A*, vol. 77, no. 1, pp. 103–111, 2006, doi: 10.1002/jbm.a.30336.

40. E. L. Hedberg, A. Tang, R. S. Crowther, D. H. Carney, and A. G. Mikos, “Controlled release of an osteogenic peptide from injectable biodegradable polymeric composites,” *Journal of Controlled Release*, vol. 84, no. 3, pp. 137–150, 2002, doi: 10.1016/S0168-3659(02)00261-4.

41. X. He, J. Ma, and E. Jabbari, “Effect of grafting RGD and BMP-2 protein-derived peptides to a hydrogel substrate on osteogenic differentiation of marrow stromal cells,” *Langmuir*, vol. 24, no. 21, pp. 12508–12516, 2008, doi: 10.1021/la802447v.

42. D. H. R. Kempen *et al.*, “Development of biodegradable poly(propylene fumarate)/poly(lactic-co- glycolic acid) blend microspheres. II. Controlled drug release and microsphere degradation,” *Journal of Biomedical Materials Research - Part A*, vol. 70, no. 2, pp. 293–302, 2004, doi: 10.1002/jbm.a.30080.

43. J. W. Lee, K. S. Kang, S. H. Lee, J. Y. Kim, B. K. Lee, and D. W. Cho, “Bone regeneration using a microstereolithography-produced customized poly(propylene fumarate)/diethyl fumarate photopolymer 3D scaffold incorporating BMP-2 loaded PLGA microspheres,” *Biomaterials*, vol. 32, no. 3, pp. 744–752, 2011, doi: 10.1016/j.biomaterials.2010.09.035.

44. A. Smith and lan M. Hunneyball, “Evaluation of poly(lactic acid) as a biodegradable drug delivery system for parenteral administration,” *International Journal of Pharmaceutics*, vol. 30, no. 2–3, pp. 215–220, Jun. 1986, doi: 10.1016/0378-5173(86)90081-5.

45. A. P. Johari, S. Mohanty, S. K. Kurmvanshi, and S. K. Nayak, “Influence of Different Treated Cellulose Fibers on the Mechanical and Thermal Properties of Poly(lactic acid),” *ACS Sustainable Chemistry and Engineering*, vol. 4, no. 3, pp. 1619–1629, 2016, doi: 10.1021/acssuschemeng.5b01563.

46. P. Grossen, D. Witzigmann, S. Sieber, and J. Huwyler, “PEG-PCL-based nanomedicines: A biodegradable drug delivery system and its application,” *Journal of Controlled Release*, vol. 260, pp. 46–60, Aug. 2017, doi: 10.1016/J.JCONREL.2017.05.028.

47. C. Y. Gong *et al.*, “Biodegradable in situ gel-forming controlled drug delivery system based on thermosensitive PCL–PEG–PCL hydrogel. Part 2: Sol–gel–sol transition and drug delivery behavior,” *Acta Biomaterialia*, vol. 5, no. 9, pp. 3358–3370, Nov. 2009, doi: 10.1016/J.ACTBIO.2009.05.025.

48. J. Che, C. I. Okeke, Z.-B. Hu, and J. Xu, “DSPE-PEG: A Distinctive Component in Drug Delivery System”.

49. Q. Hou, D. W. Grijpma, and J. Feijen, “Porous polymeric structures for tissue engineering prepared by a coagulation, compression moulding and salt leaching technique,” *Biomaterials*, vol. 24, no. 11, pp. 1937–1947, May 2003, doi: 10.1016/S0142-9612(02)00562-8.

50. L. Elomaa, S. Teixeira, R. Hakala, H. Korhonen, D. W. Grijpma, and J. V. Seppälä, “Preparation of poly(ε-caprolactone)-based tissue engineering scaffolds by

stereolithography," *Acta Biomaterialia*, vol. 7, no. 11, pp. 3850–3856, 2011, doi: 10.1016/j.actbio.2011.06.039.

51. S. H. Chang, H. J. Lee, S. Park, Y. Kim, and B. Jeong, "Fast Degradable Polycaprolactone for Drug Delivery," *Biomacromolecules*, vol. 19, no. 6, pp. 2302–2307, Jun. 2018, doi: 10.1021/ACS.BIOMAC.8B00266/SUPPL_FILE/BM8B00266_SI_001.PDF.

52. A. J. Shanfeng Wang, Diederik H. Kempen, Narendra K. Simha, Jack L. Lewis and and L. L. Windebank, Michael J. Yaszemski, "Photo-crosslinked Hybrid Polymer Networks Consisting of Poly (propylene fumarate) (PPF) and Poly(caprolactone fumarate) (PCLF): Controlled Physical Properties and Regulated Bone and Nerve Cell Responses," *Biomacromolecules*, vol. 9, no. 4, pp. 1229–1241, 2008, doi: 10.1021/bm7012313.

53. R. C. Nagarwal, R. Kumar, M. Dhanawat, and J. K. Pandit, "Modified PLA nano in situ gel: A potential ophthalmic drug delivery system," *Colloids and Surfaces B: Biointerfaces*, vol. 86, no. 1, pp. 28–34, Aug. 2011, doi: 10.1016/J.COLSURFB.2011.03.023.

54. D. Zhu *et al.*, "Docetaxel (DTX)-loaded polydopamine-modified TPGS-PLA nanoparticles as a targeted drug delivery system for the treatment of liver cancer," *Acta Biomaterialia*, vol. 30, pp. 144–154, Jan. 2016, doi: 10.1016/J.ACTBIO.2015.11.031.

55. R. G. Kenny and C. J. Marmion, "Toward Multi-Targeted Platinum and Ruthenium Drugs - A New Paradigm in Cancer Drug Treatment Regimens?," *Chemical Reviews*, vol. 119, pp. 1058–1137, 2019, doi: 10.1021/acs.chemrev.8b00271.

56. J. S. Temenoff and A. G. Mikos, "Injectable biodegradable materials for orthopedic tissue engineering," *Biomaterials*, vol. 21, no. 23, pp. 2405–2412, 2000, doi: 10.1016/S0142-9612(00)00108-3.

57. C. C. Wu, L. H. Hsu, S. Sumi, K. C. Yang, and S. H. Yang, "Injectable and biodegradable composite bone filler composed of poly(propylene fumarate) and calcium phosphate ceramic for vertebral augmentation procedure: An in vivo

porcine study," *Journal of Biomedical Materials Research - Part B Applied Biomaterials*, vol. 105, no. 8, pp. 2232–2243, 2017, doi: 10.1002/jbm.b.33678.

58. M. Salarian, W. Z. Xu, M. C. Biesinger, and P. A. Charpentier, "Synthesis and characterization of novel TiO2-poly(propylene fumarate) nanocomposites for bone cementation," *Journal of Materials Chemistry B*, vol. 2, no. 32, pp. 5145–5156, 2014, doi: 10.1039/c4tb00715h.

59. C. E. Mora-Huertas, H. Fessi, and A. Elaissari, "Polymer-based nanocapsules for drug delivery," *International Journal of Pharmaceutics*, vol. 385, no. 1–2, pp. 113–142, Jan. 2010, doi: 10.1016/J.IJPHARM.2009.10.018.

60. A. E. van der Ende, V. Sathiyakumar, R. Diaz, D. E. Hallahan, and E. Harth, "Linear release nanoparticle devices for advanced targeted cancer therapies with increased efficacy," *Polymer Chemistry*, vol. 1, no. 1, pp. 93–96, Feb. 2010, doi: 10.1039/B9PY00272C.

61. J. L. W. S. R. Sershen,S. L. Westcott,N. J. Halas, "Temperature-sensitive polymer–nanoshell composites for photothermally modulated drug delivery," 2000.

62. S. E. Pechar M, Ulbrich K, Subr V, Seymour LW, "Poly(ethylene glycol) multiblock copolymer as a carrier of anti-cancer drug doxorubicin," *Bioconjugate Chem*, vol. 11, pp. 131–139, 2000.

63. S. Sharma, A. Dua, and A. Malik, "Polyaspartic acid based superabsorbent polymers," *European Polymer Journal*, vol. 59, pp. 363–376, Oct. 2014, doi: 10.1016/J.EURPOLYMJ.2014.07.043.

64. L. JC. Gaucher G, Dufresne MH, Sant VP, Kang N, Maysinger D, "Block copolymer micelles: Preparation, characterization and application in drug delivery," *Journal of Controlled Release*, vol. 109, pp. 169–188, 2005.

65. "Poloxamer 188 structure. | Download Scientific Diagram." https://www.researchgate.net/figure/Poloxamer-188-structure_fig2_7244523 (accessed Dec. 01, 2019).

66. D. H. Zhou, G. Zhang, Q. S. Yu, and Z. H. Gan, "Folic Acid Modified Polymeric Micelles for Intravesical Instilled Chemotherapy," *Chinese Journal of Polymer*

Science (English Edition), vol. 36, no. 4, pp. 479–487, 2018, doi: 10.1007/s10118-018-2009-y.

67. J. Liu, Y. Xiao, and C. Allen, "Polymer–drug compatibility: A guide to the development of delivery systems for the anticancer agent, ellipticine," *Journal of Pharmaceutical Sciences*, vol. 93, no. 1, pp. 132–143, Jan. 2004, doi: 10.1002/jps.10533.

68. J. Choi *et al.*, "MULTIMODAL IMAGING OF SUSTAINED DRUG RELEASE FROM 3-D POLY(PROPYLENE FUMARATE) (PPF) SCAFFOLDS," 2011, doi: 10.1016/j.jconrel.2011.06.035.

69. H. Ueda *et al.*, "Injectable, in situ forming poly(propylene fumarate)-based ocular drug delivery systems," 2007, doi: 10.1002/jbm.a.31226.

70. Y. Lu *et al.*, "Microstereolithography and characterization of poly(propylene fumarate)-based drug-loaded microneedle arrays," *Biofabrication*, vol. 7, no. 4, p. 045001, Sep. 2015, doi: 10.1088/1758-5090/7/4/045001.

71. M. C. Hacker *et al.*, "Biodegradable fumarate-based drug-delivery systems for ophthalmic applications," *Journal of Biomedical Materials Research - Part A*, vol. 88, no. 4, pp. 976–989, Mar. 2009, doi: 10.1002/JBM.A.31942.

72. E. C. Görkem Cemali, Avram Aruh, Gamze Torun Köse, "Biodegradable Polymeric Networks of Poly(propylene fumarate) and Phosphonic Acid Based Monomers," *Polym Int*, vol. 69, pp. 1283–1296, 2020, doi: https://doi.org/10.1002/pi.6077.

73. A. R. Amini, C. T. Laurencin, and S. P. Nukavarapu, "Bone tissue engineering: recent advances and challenges.," *Crit Rev Biomed Eng*, vol. 40, no. 5, pp. 363–408, 2012.

74. T. K. I. Galleries, "Polymeric Scaffolds for Tissue Engineering 2," *Hammond Laboratory*, 2016. https://ki-galleries.mit.edu/2016/hyder-2 (accessed Nov. 14, 2019).

75. C. C.-S. Capek I, *Radical polymerization in direct mini-emulsion systems. New Polymerization Techniques and Synthetic Methodologies*. Springer, 2001.

76. S. R. Abdou L, El-Molla M, Hakeim O, El-Gammal M, “Synthesis of nanoscale binders through mini emulsion polymerization for textile pigment applications.,” *Industrial & Engineering Chemistry Research*, vol. 52, no. 6, pp. 2195–2200, 2013.

77. “Scientific Principles:Polymers.” http://matse1.matse.illinois.edu/polymers/prin.html (accessed Oct. 13, 2019).

78. B. Kriwet, E. Walter, and T. Kissel, “Synthesis of bioadhesive poly(acrylic acid) nano- and microparticles using an inverse emulsion polymerization method for the entrapment of hydrophilic drug candidates,” *Journal of Controlled Release*, vol. 56, no. 1–3, pp. 149–158, Dec. 1998, doi: 10.1016/S0168-3659(98)00078-9.

79. S. C. Abeylath and E. Turos, “Glycosylated polyacrylate nanoparticles by emulsion polymerization,” *Carbohydrate Polymers*, vol. 70, no. 1, pp. 32–37, Aug. 2007, doi: 10.1016/J.CARBPOL.2007.02.027.

80. C. CS., “Emulsion polymerization mechanisms and kinetics.,” *Progress in Polymer Science.*, vol. 31, no. 5, pp. 443–486, 2006.

81. G. R. Silvério Neto W, Thyago Jensen A, Ribeiro Ferreira G, Fonseca Valadares L and et al. Belém Gonçalves S, “A survey on synthesis processes of structured materials for biomedical applications: Iron-based magnetic nanoparticles, polymeric materials and polymerization processes.,” *Current Pharmaceutical Design*, vol. 21, no. 37, pp. 5336–5358, 2015.

82. L. A. Eliseeva VI, Ivanchev S, Kuchanov S, *Emulsion polymerization and its applications in industry.*, vol. 3, no. 24. Springer Science & Business Media, 2012.

83. BASF, “VPA Technical Data Sheet,” 2021.

84. “Vinylphosphonic acid,” *MERCK*. https://www.sigmaaldrich.com/catalog/product/aldrich/396311?lang=en&region=TR

85. F. Kotz, P. Risch, D. Helmer, and B. E. Rapp, “Highly fluorinated methacrylates for optical 3D printing of microfluidic devices,” *Micromachines (Basel)*, vol. 9, no. 3, Mar. 2018, doi: 10.3390/MI9030115.

86. MERCK, “Phenyl-bis (2,4,6-trimethylbenzoyl) Phosphine Oxide (BAPO)”.

87. “File:Sodium dodecyl sulfate.svg - Wikipedia.” https://en.wikipedia.org/wiki/File:Sodium_dodecyl_sulfate.svg (accessed Dec. 22, 2019).

88. “Paclitaxel (Taxol, Onxal) Chemotherapy Drug Information.” http://chemocare.com/chemotherapy/drug-info/Paclitaxel.aspx (accessed Dec. 22, 2019).

89. S. Peltier, J.-M. Oger, F. Lagarce, W. Couet, and J.-P. Benoît, “Enhanced oral paclitaxel bioavailability after administration of paclitaxel-loaded lipid nanocapsules.,” *Pharm Res*, vol. 23, no. 6, pp. 1243–50, Jun. 2006, doi: 10.1007/s11095-006-0022-2.

90. “Folic Acid: Uses, Side Effects, Interactions, Dosage, and Warning.” https://www.webmd.com/vitamins/ai/ingredientmono-1017/folic-acid (accessed Jan. 24, 2020).

91. B. Stella *et al.*, “Design of Folic Acid-Conjugated Nanoparticles for Drug Targeting,” *Journal of Pharmaceutical Sciences*, vol. 89, no. 11, pp. 1452–1464, Nov. 2000, doi: 10.1002/1520-6017(200011)89:11<1452::AID-JPS8>3.0.CO;2-P.

92. “Differential Scanning Calorimetry - an overview | ScienceDirect Topics.” https://www.sciencedirect.com/topics/engineering/differential-scanning-calorimetry (accessed Jun. 06, 2020).

93. “Differential Scanning Calorimetry (DSC) | UL.” https://www.ulttc.com/en/solutions/test-methods/thermal-analysis/differential-scanning-calorimetry-dsc.html (accessed Jan. 12, 2022).

94. “Differential Scanning Calorimetry Based Analysis Service - Creative Proteomics.” https://www.creative-proteomics.com/support/dsc-based-analysis-service.htm (accessed Jan. 12, 2022).

95. B. J. Inkson, “Scanning Electron Microscopy (SEM) and Transmission Electron Microscopy (TEM) for Materials Characterization,” in *Materials Characterization*

Using Nondestructive Evaluation (NDE) Methods, Elsevier Inc., 2016, pp. 17–43. doi: 10.1016/B978-0-08-100040-3.00002-X.

96. "Gel Permeation Chromatography - an overview | ScienceDirect Topics." https://www.sciencedirect.com/topics/materials-science/gel-permeation-chromatography (accessed Jun. 06, 2020).

97. Dr. I. Hunt, "Chapter 13 - H NMR," *University of Calgary*, 2018. http://www.chem.ucalgary.ca/courses/350/Carey5th/Ch13/ch13-hnmr.html (accessed Nov. 27, 2021).

98. "What is HPLC (High Performance Liquid Chromatography) ？: SHIMADZU (Shimadzu Corporation)." https://www.shimadzu.com/an/service-support/technical-support/analysis-basics/basic/what_is_hplc.html (accessed Nov. 27, 2021).

99. A. K. Shung, M. D. Timmer, S. Jo, P. S. Engel, and A. G. Mikos, "Kinetics of poly(propylene fumarate) synthesis by step polymerization of diethyl fumarate and propylene glycol using zinc chloride as a catalyst," *J Biomater Sci Polym Ed*, vol. 13, no. 1, pp. 95–108, 2002, doi: 10.1163/156856202753525963.

100. Wikipedia, "Steglich esterification," 2021. https://en.wikipedia.org/wiki/Steglich_esterification (accessed Apr. 19, 2020).

101. S. B. Gizem Karakas, Erde Can, "Sustained Paclitaxel Release from Magnetic Polymer Nanoparticles," Yeditepe University, 2018.

102. S. B. 'Can, E. 'Alarcin, "Cure Time Optimization and Development of Poly(Propylene Fumarate) (PPF)- Beta- Tricalcium Phosphate Based Composites for Bone Tissue Engineering Applications," 2019.

103. M. J. Y. Shanfeng Wang, Lichun Lu, "Bone-Tissue-Engineering Material Poly(propylene fumarate): Correlation between Molecular Weight, Chain Dimensions, and Physical Properties," *Biomacromolecules*, vol. 7, no. 6, pp. 1976–1982, 2006.

104. R. & W. I. & G. J. & W. D. & B. Peter. Dey, "Poly(vinylphosphonic acid- co - acrylic acid) hydrogels: The effect of copolymer composition on osteoblast adhesion

and proliferation.," *Journal of Biomedical Materials Research Part A.* , vol. 106, 2017.

105. S. J. Peter, S. T. Miller, G. Zhu, A. W. Yasko, and A. G. Mikos, "In vivo degradation of a poly(propylene fumarate)/?-tricalcium phosphate injectable composite scaffold," *Journal of Biomedical Materials Research*, vol. 41, no. 1, pp. 1–7, Jul. 1998, doi: 10.1002/(SICI)1097-4636(199807)41:1<1::AID-JBM1>3.0.CO;2-N.

106. Y. K. Jun, S.-H. Hong, S.-H. Kwon, Y.-K. Jun, and H.-E. Kim, "Synthesis and Dissolution Behavior of β-TCP and HA/β-TCP Composite Powders multiferroics View project Blue phospor for LED View project Synthesis and dissolution behavior of b-TCP and HA/b-TCP composite powders," 2003, doi: 10.1016/S0955-2219(02)00263-7.

107. S. He, M. D. Timmer, M. J. Yaszemski, A. W. Yasko, P. S. Engel, and A. G. Mikos, "Synthesis of biodegradable poly(propylene fumarate) networks with poly(propylene fumarate)-diacrylate macromers as crosslinking agents and characterization of their degradation products," *Polymer (Guildf)*, vol. 42, no. 3, pp. 1251–1260, 2001, doi: 10.1016/S0032-3861(00)00479-1.

108. G. W. Bahar Bingol , Wolfgang H. Meyer, Manfred Wagner, "Synthesis, Microstructure, and Acidity of Poly(vinylphosphonic acid)," *Macromolecular Rapid Communications*, vol. 27, 2006.

109. L. Feng, Z. Dong, D. Tao, Y. Zhang, and Z. Liu, "The acidic tumor microenvironment: a target for smart cancer nano-theranostics," *National Science Review*, vol. 5, pp. 269–286, 2018, doi: 10.1093/nsr/nwx062.

110. WinChembase, "H-NMR of Folic Acid".

111. Başkaya B, Can E. Poli(Propilen Fumarat) - Vinil Fosfonik Asit Bazlı İlaç Salım Sistemleri, *14. Ulusal Kimya Mühendisliği Kongresi*. 2021:229.

APPENDIX A: GPC CHROMATOGRAMS

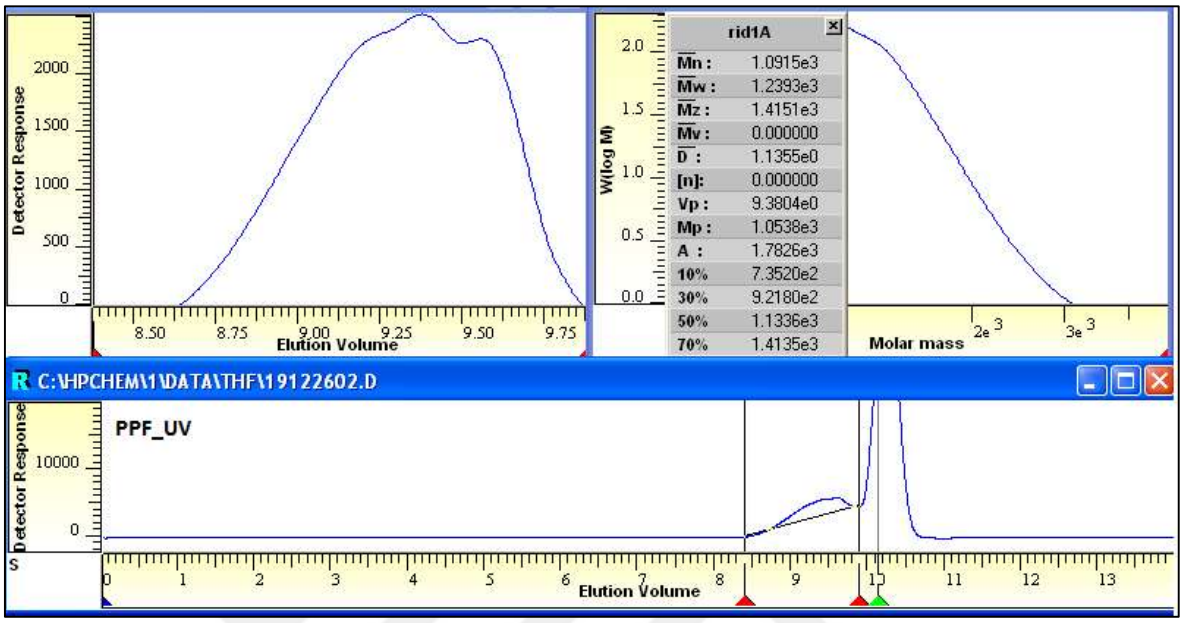

Figure A.1. GPC chromatogram of the synthesized PPF